Title
Spontaneous Activity and Intrinsic Photosensitivity in the Developing Zebrafish Spinal Cord

Author
Friedmann, Drew Robert

Publication Date
2016

Peer reviewed|Thesis/dissertation

Spontaneous Activity and Intrinsic Photosensitivity in the Developing Zebrafish Spinal Cord

By

Drew Robert Friedmann

A dissertation submitted in partial satisfaction of the requirements for the degree of

Doctor of Philosophy

in

Molecular and Cell Biology

in the

Graduate Division

of the

University of California, Berkeley

Committee in charge:

Professor Ehud Isacoff, Chair
Professor Marla Feller
Professor John Ngai
Professor Frederic Theunissen

Spring 2016

Spontaneous Activity and Intrinsic Photosensitivity in the Developing Zebrafish Spinal Cord

Abstract

Spontaneous Activity and Intrinsic Photosensitivity in the Developing Zebrafish Spinal Cord

by

Drew Robert Friedmann

Doctor of Philosophy in Molecular and Cell Biology

University of California, Berkeley

Professor Ehud Isacoff, Chair

The process of perception is one of the most complicated and compelling biological phenomena, capable of inspiring thousands of years of philosophers, physicians, and scientists. One of these researchers, Walter Freeman of Berkeley once stated, “The brain reaches out into the environment and sees something which is then interpreted according to its own past experiences. First you look, then you see.” While the neural computations involved in “seeing” may not be understood for many years to come, we have made much progress in understanding how the brain “looks” into its environment. And by studying animal behavior, we can hope to infer some understanding of the cells that transform these sensory inputs into motor outputs. Working with simple neural circuits—be they in model organisms or at early stages in development—the problem seems more tractable, yet new findings can shift our understanding of perception in unexpected ways.

In this thesis, I present research on motor circuits of the embryonic zebrafish spinal cord. These spinal neurons directly drive the earliest muscle contractions in the fish and are a great model for understanding how activity begins in a nervous system. In the course of these studies, we discovered that the activity within this circuit is strongly inhibited by environmental light at an age before vision and before the spinal cord is connected to brain circuitry. Not all photoreceptors are for sight and there are many examples of deep brain photoreception in invertebrates and basal vertebrates, usually driving circadian and seasonal behaviors. Our finding in zebrafish is surprising due to the direct photodetection by motor neurons in the spinal cord, the developmentally early appearance of this photosensitivity, the possible role for primary cilia in sensing light, and the acute affect on behavior. Additionally, by manipulating spontaneous activity within this circuit, we see effects on the development of neural activity in spinal interneurons. These results change how we think about motor circuits and development. No longer are motor neurons simply passive relay cells, we now can see them as sensory inputs. No longer is development in the spinal cord governed solely by genetic programs, but activity dependent processes can be regulated by the outside world. The existence of this

category of nonvisual photoreceptor across taxa indicates a new way for the brain to "reach out into the environment." Discovering whether and how it alters our perception of the world will hopefully be a focus of future research.

DEDICATION

To Friends, Family, Mountains, and Curiosity,
the four most inspirational forces I know

TABLE OF CONTENTS

ACKNOWLEDGEMENTS

To give a better sense of the duration of a PhD, I like to mention that in my years at Berkeley, my niece has grown from an infant into a kindergartner. Over such an expanse of time, I have interacted with so many people who have all helped me along the way. There's not enough space to thank everyone, but I want to highlight the people whose support was necessary for the work in this thesis and the people who have helped me grow into the scientist I am today.

First, I owe so many thanks to Udi—for taking me into the lab, for encouraging me to develop my own ideas into a project, and for supporting me when I shelved 18 months of work to switch projects. The independence that he has given me is not something offered in every lab and is a testament to his trust in his students. His ability to run a large lab with such a diverse group of people and projects is impressive. I can't count the number of times I've knocked on his door to say, "Udi, quick question...", and received a thoughtful and insightful response on zebrafish behavior, even if he had previously been deep in thought on channel biophysics.

I also need to specifically thank my thesis committee: Marla Feller, John Ngai, and Frederic Theunissen. Marla in particular has been a great role model to me. She was my mentor for my first rotation and since then has always offered amazing advice on project proposals, fellowship applications, and my postdoc search. I have *always* admired her ability to ask direct, sharp, and insightful questions from a position of genuine curiosity. John has also been an important force in shaping my project and the way I think about science. He has always encouraged me to take a step back and think about truly good and interesting biological questions before returning to the details of an experiment. He's also been a great source of career and life advice, in spite of his terrible taste in baseball teams.

The members of the Isacoff lab who have come and gone over the years have all been amazing people for discussing ideas. I especially need to thank my co-authors Adam Hoagland and Shai Berlin. Adam is one of those rare individuals who will put in enormous effort to repair hardware issues and avoid taking credit, humbly stating as an aside, "it's working." Shai has been a great fountain of ideas and never hesitates to tell me when he thinks I'm wrong. He's a rigorous scientist and aspiring to meet his standards make me a better researcher. The fish team has been a fun group to work with—Alden Conner, Carlos Pantoja, Beth Carroll, and Claire Oldfield. You all have made life in the lab a more jovial place and have all contributed suggestions, ideas, and help that have made this project possible. Claire deserves special thanks along with Zach Newman, as my fellow grad students of the same year. We struggled and succeeded together over the years and supported each other along the way. Erica Warp, my rotation mentor, also deserves special thanks for developing the zebrafish spinal cord into a beautiful system for experiments in the lab. She taught me

everything I needed to get this project started and was a truly fantastic and kind person to have as a mentor while getting my feet wet in the lab.

The work presented here also would not have been possible without the support of the individuals who actually keep things running. To the members of the fish facility, especially Mel Boren and Kait Kliman, thank you so much for your dedication to the animals and your constant efforts to keep things afloat. To Hitomi Okada and Cherise Stanley, thank you for your amazing molecular work in the lab. You are two of the most dedicated and reliable people I've met in *any* lab, and we are amazingly lucky to have had your help. Sandra Wiese, thank you for keeping the lab running smoothly—I am nearly certain we are the only lab on campus that is actually up to date with all of our safety forms.

The core facilities at Berkeley also merit a special mention for their contribution to the work in this thesis. Justin Choi of the Functional Genomics Lab and Hector Nolla of the Flow Cytometry Core both were welcoming and helpful with all of my novice questions. Holly Aaron of the Molecular Imaging Center has built and manages an impressive facility. I credit her with teaching me most of what I know about microscopy and the majority of the images in this thesis would not be quite so beautiful without her input.

Thanks also to everyone that I've met along the journey. David Presti, thank you for being an amazing person and an inspiration to remember what amazing things exist beyond the physical brain. Angie Ribera, Kamran Khodakhah Matt Kittelberger, and Claire Wyart, thanks for listening and for teaching—you all have shaped my research with your insights. Tsung-Li Liu and Eric Betzig, thank you for welcoming me to Janelia and for taking amazing images of zebrafish spinal cords.

To my family—my parents, Laurel and Bob, and my sister Heather and her family. Thank you for your support and your understanding over these years. I couldn't have done it without you. To my friends and my climbing and skiing partners, thanks for keeping me sane.

And lastly, I cannot thank my partner Lieselotte enough. Through all of my successes and failures, she has been there. As a grad student herself, she understands how crushing it can be when a crucial experiment doesn't work. But as a partner, she has always provided me so much more—the emotional support to push through the hard times and the wherewithal to listen to me both gripe and boast. Partners of PhD students deserve a degree of their own at the end. I could not have done this without her.

CHAPTER 1

GENERAL INTRODUCTION

Development of sensory modules and motor modules

At its most conceptual level, the purpose of a nervous system is to sense the surrounding environment and translate that information into beneficial motor output. Simple nerve nets in radially symmetric basal organisms are constructed from elemental modules for sensing inputs and generating motor output. For example, box jellyfish and other cnidarians generate movement from coordinated rhythmic activity in groups of pacemaker neurons and use ambient light levels to regulate the output of these motor centers (Garm and Bielecki, 2008). This basic motor module, a pacemaker node with a rhythmic output, is found throughout the animal kingdom. These central pattern generators (CPG) drive the selection between feeding behaviors in aplysia, cycles of digestion in crustaceans, and cardiac rhythmicity in everything from leech to humans (Selverston, 2010). And in each of these examples, the phase and frequency of the neurons in these CPGs is sensitive to sensory modulation. Understanding how environmental inputs such as light can regulate small behavioral modules will be important for drawing connections among photomotor behaviors through evolution—from the swimming behavior of the jellyfish through to non-visual circadian rhythms in humans.

Discovery of motor modules: the spinal central pattern generator

Tracing back our understanding of motor behavior and neural function points to an origin in ancient Greece. Though it wouldn't be realized for centuries, the first discovery of a neural circuit may have materialized in Hippocrates' observation that paralysis occurs in the body contralateral to the site of the head injury. Little progress in the following two thousand years leads to the 17th century, when prevailing theories held that intelligence and the mind were contained in ventricular humor. In spite of this misunderstanding, Descartes suggested that 'threads' would connect the skin to the fluid of the brain and back to muscles in order to pull away from a painful stimulus (Figure 1). Separating these fast automatic responses from purposeful behaviors originating in the mind, Descartes popularized the concept of mind-body dualism. With these ideas, he is credited with identifying the neural origin of reflex theory, a cornerstone in the next two hundred years of behavioral neuroscience. Interestingly, he also placed an extreme importance on the pineal complex, a photosensitive neural structure important in nonvisual circadian behaviors in many vertebrate organisms.

With the introduction of research on model organisms, Robert Whytt (1714-1766) identified the spinal cord as a necessary and sufficient origin for reflexive movement in decapitated frogs. Through into the early 20th century, and in spite of progress in anatomical and electrical understanding of spinal function, there remained a controversy in spinal pathways between two camps. First, those who thought the spinal cord was simply a center for these reflexes and otherwise was under complete control of the brain (Lotze, 1817-1881). And second, those who believed it to possess psychic properties in a continuum with the brain (Pflügger, 1829-1910).

Famously, Sherrington fell into the first camp and through identification of circuitry for reciprocal inhibition in spinal reflex arcs, he pushed the idea that complex motor behavior originated from integration and overlap of chains of sensory reflexes(Sherrington, 1910). Sherrington's own experiments, in addition to those by T.G. Brown (Brown, 1911), used decerebrate cats, which could exhibit a normal gait and pattern of complex motor activity when suspended above a treadmill. The procedure supported the idea of a central pattern circuit within the spinal cord, but did not disprove reflexology as the experiment relied on sensory feedback. More difficult to explain were Brown's results showing persistence of these motor rhythms in the presence of anesthesia doses sufficient to suppress peripheral reflexes (Brown, 1914).

However, it wasn't until research by Coghill that the ideas of Pflügger were revived as his new findings didn't fit with Sherrington's organizing principles (Coghill, 1929). Coghill carefully observed the sequential appearance of behaviors during the embryonic development of the salamander and posited—in contrast to reflex theory—that complex motor behavior is differentiated from generalized behaviors in early development. Importantly, these early intrinsic behaviors were spontaneous, arose before reflexive responses, and grew in complexity with the addition of new cellular connections. Thirty years later, a flurry of new experiments firmly established the existence of motor output generated by intrinsic neural activity within the central nervous system. Invertebrate work demonstrated persistent, rhythmic copulatory behaviors in decapitated mantids (Roeder et al., 1960) and persistent, rhythmic flight patterns in locusts with either sensory nerves severed or heads removed(Wilson, 1961). Experiments by Hamburger, et al. (1961-65) in the chick embryo, like Coghill, also demonstrated spontaneous behaviors (3 days post fertilization) before responses to tactile stimulation (7 dpf) (Hamburger, 1963; Hamburger and Balaban, 1963; Hamburger et al., 1965). The new leap in thinking came from lesion experiments and the observation that spontaneous motor output continued both above and below the lesion site.

These results and others were reviewed by Bullock in 1961 (Bullock, 1961), who acknowledged the stature and importance of reflexology before systematically undermining each of its core assumptions with recent experimental evidence. He summarized his argument, "but central patterning is the necessary and often sufficient condition for determining the main characteristic features of almost all actions, whether stimulus triggered or spontaneous." As such reflex theory now existed in parallel with the new field of central pattern generators.

The vertebrate CPG for locomotion

The neural substrate underlying these central rhythmic modules is commonly described as one of two potential solutions: a pacemaker driven network or one that relies on interneuronal connections and intrinsic properties of those cells (Goulding, 2009). However, it is probable that in some cases, both may exist in the same network (Cowley and Schmidt, 1995; Garm and Bielecki, 2008). Studies of swimming in *Xenopus* tadpoles and the ancestral aquatic lamprey have greatly furthered our

understanding of the neuronal players in a simplified CPG for locomotion. The basic layout is conserved in spinal circuitry from these swimming organisms through to the circuitry for walking in limbed mammals (Kiehn, 2011; Selverston, 2010). In the bilateral organization of most vertebrate spinal circuits, this common arrangement includes connections for propagating and regulating ipsilateral excitation as well as contralateral inhibitory projections for suppressing activity on the opposite side of the body during a wave of activity (Figure 2).

Further evidence supporting evolutionary conservation of this network is the shared transcriptional profile of the key neuronal types owing to common developmental signaling and morphogen responses (eg. Shh, BMP, Nodal, etc.) that result in similar patterning in fish, frog, chick, and mouse (Bullock, 1961; Grillner and Jessell, 2009; Lupo et al., 2006). As such, evaluating swimming CPGs in more basal aquatic organisms is valuable for understanding spinal networks in all vertebrates. In these swim circuits, ipsilateral glutamatergic excitatory interneurons recruit both motor neurons and contralaterally projecting interneurons (Kiehn, 2011; Saint-Amant, 2010). Though the tadpole CPG commissural neurons are only inhibitory, in mammalian, lamprey, and zebrafish spinal cords, there is also evidence for excitatory commissural interneurons (Goulding, 2009; Kiehn, 2011). However, in these swimming organisms, a role isn't yet clear for these glutamatergic interneurons. In contrast to the circuits for limb control, the swimming CPG is distributed more-or-less evenly along the length of the organism. This allows for not just intra-segment contralateral inhibition via glycine, but also delayed ipsilateral propagation to generate the wave-like pattern of muscle contractions for swim (Grillner and Jessell, 2009).

Though inhibitory glycinergic synapses appear to be required for left-right alternation in most CPGs, some of the excitatory drive propagates through gap junctions, especially during embryonic development (Li et al., 2009; Personius et al., 2001; Saint-Amant and Drapeau, 2001). These predominantly passive channels flux ions and small molecules such as cAMP through ipsilaterally coupled neurons, including premotor excitatory interneurons and motor neurons themselves (Kiehn and Tresch, 2002; Song et al., 2016). Though recent evidence points to these gap junctions as a mechanism for motor feedback into the CPG, during embryonic development, electrical coupling is the primary source of excitatory drive to motor neurons (Saint-Amant and Drapeau, 2001). Early electrical coupling is a common feature of developing neural networks, including mammalian retina and cortex in addition to the spinal cord (Blankenship and Feller, 2010; Montoro and Yuste, 2004). The correlated electrical activity that results from passive coupling of cytosolic compartments is believed to play a role in the eventual chemical synapse formation that underlies the majority of the mature network (Park et al., 2011; Todd et al., 2010; Yu et al., 2012).

Activity dependent development in spontaneous networks

The mechanism for gap junctions in circuit formation has been shown to require both the adhesive properties conferred by closed connexin hemichannels

(Elias et al., 2007) as well as the currents they conduct (Yu et al., 2012). This latter finding fits into a larger topic in developmental neuroscience—processes that either require or are regulated by neural activity within the developing network. This phenomenon is widespread in developing brain regions including the retina (Ackman et al., 2012; Penn et al., 1998), cortex (Garaschuk et al., 2000), hippocampus (Ben-Ari et al., 1989; Kleindienst et al., 2011), and spinal cord (Gu et al., 1994; Kastanenka and Landmesser, 2010; Pineda et al., 2006; Plazas et al., 2013).

Activity dependent development, like plasticity in mature networks, falls under two primary mechanisms. The first, homeostatic plasticity, occurs over relatively long timescales (hours-days) and integrates neuronal activity at the cellular and network levels in order to maintain activity within prescribed ranges (Davis, 2013; Turrigiano and Nelson, 2004). The trigger for homeostatic plasticity may be sensing of internal calcium concentration or firing rates in comparison to a predetermined setpoint(Hengen et al., 2013; Mahoney et al., 2014). Mechanisms for return to the homeostatic setpoint include the scaling of synaptic weights across entire cells(Turrigiano et al., 1998), tuning of intrinsic excitability by adding or removing channels(O'Leary et al., 2014), and changing the numbers and patterns of synapses in the circuit(Pozo and Goda, 2010; Turrigiano, 2012). The second major class of neural plasticity is the traditional Hebbian view in which positive feedback strengthens (eg. long term potentiation) or weakens (eg. long term depression) individual synapses to reinforce specifically beneficial circuit connections(Malenka and Bear, 2004).

It is important to distinguish the differences between these two types of plasticity since experimental manipulation (especially silencing) of spontaneously active developing networks also needs to differentiate between global suppression and cell- or synapse-specific suppression. This distinction appears in many systems that rely on interneuronal competition to drive Hebbian processes. For example, the famous cases of reducing multiple innervation at the NMJ (Balice-Gordon and Lichtman, 1994) and the refinement of retinotectal projections (Huberman et al., 2008) both require competition between single cells. In each of these cases, growing projections of motor neurons and retinal ganglion cells overlap in their respective target regions of muscle fibers or in the tectum. Given that the retina and spinal cord both output patterns of spontaneous activity, differences in the timing of these outputs provide the necessary information for Hebbian processes at the retino-tectal synapses (Dhande et al., 2011; Stafford et al., 2009) and at the neuromuscular junction (Buffelli et al., 2002; Busetto et al., 2000). Asynchronous inputs to the same cell that vary by more than 20-25 ms (Favero et al., 2012; Zhang et al., 1998) lead to the elimination of the synapse with its input arriving second. In these systems, total synaptic blockade or complete abrogation of neural activity with TTX can abolish the signal driving Hebbian synaptic competition and prevents refinement of these connections (reviewed by (Favero et al., 2014)).

Similarly, axon pathfinding of a specific class of primary motor neuron within the zebrafish spinal cord also requires silencing of activity in individual cells and proceeds normally under global suppression of activity (Plazas et al., 2013). In

contrast, work in the chick embryo has made great strides connecting global patterns of activity to axon outgrowth. Here, pharmacological blockade of activity in spinal neurons results in dorsal-ventral decision defects in axon outgrowth. The potential mechanism for these defects is altered expression of signaling proteins like EphA4 and NCAM, known to play a role in axonal targeting (Hanson and Landmesser, 2004). Blocking $GABA_A$ receptors with picrotoxin (GABA is excitatory in the chick embryo) reduces activity in the spontaneously active CPG and results in defects in motor axon targeting, but it was initially not possible to link these defects to activity patterns or GABA signaling. By expressing channelrhodopsin in the rostral portion of the spinal cord, the authors were able to restore the natural frequency and pattern of activity in an organism that had been treated with picrotoxin. Rescue of the activity patterns not only rescued the axon targeting defects, but also the expression levels of candidate signaling molecules in growth cones (Kastanenka and Landmesser, 2010).

In addition to axon pathfinding and the refinement of axonal projections, neural activity during development can regulate a number of other important processes (Borodinsky et al., 2012). Activity in the spinal cord plays a role in neural proliferation, differentiation, and maturation from a renewing progenitor pool into interneurons and motor neurons
(Borodinsky et al., 2004; Jablonski and Kalb, 2013; Weissman et al., 2004). Reducing neural activity by imposing a mature chloride gradient on the embryonic spinal cord—and thereby reducing the depolarizing influence of glycine and GABA—reduces the total number of motor neurons(Reynolds et al., 2008). Another form of postmitotic differentiation, the selection of neurotransmitter fate, lies downstream of an activity-sensitive Tlx3 transcriptional program (Marek et al., 2010). Inhibition of spontaneous activity reduces intracellular calcium and leads to increased glutamatergic fate selection whereas over-excitation leads to more expression of inhibitory transmitter phenotypes. Importantly, in these examples, this is independent of the total cell number
(Borodinsky et al., 2004; Guemez-Gamboa et al., 2014).

The zebrafish spinal cord as a model system

As discussed above, the conserved spinal cell types and the shared fundamental CPG circuit make basal vertebrates such as *Xenopus*, the lamprey, and the zebrafish excellent model organisms for studying spinal cord development. The zebrafish in particular has been a useful model system since its introduction in the 1970's by George Streisinger at the University of Oregon and spinal cell types were identified and catalogued by electrical properties and morphology throughout the 1980's (Bernhardt et al., 1990; Mendelson, 1986a; Myers et al., 1986; Streisinger et al., 1981). A genetic screen by Christiane Nüsslein-Volhard and Wolfgang Driever in the early 1990's examined over 1.5 million embryos and identified approximately 1000 mutations affecting development in the zebrafish
(Brockerhoff et al., 1995; Haffter et al., 1996; Schier et al., 1996). A number of neural phenotypes were used as metrics in the screen including the aforementioned retinotectal projections and early embryonic behaviors. In particular, multiple mutants

(later identified to be involved in glycine transport or recognition) abolished contralateral inhibition in the spinal cord and decoupled the left-right pattern of activity giving the mutant the apt gene family name *accordion* (Granato et al., 1996).

With the sequencing of the its genome, begun in 2001, zebrafish took off as a model organism. The promise of hundreds of embryos per week, external development from a single cell to a freely swimming larvae, and the ability to image development through transparent skin makes them an ideal choice for observing CNS development and the onset of spontaneous activity—a difficult process to observe in other model systems.

Zebrafish mating is triggered by sunrise in the wild (and timed lighting in laboratory housing) (Parichy, 2015). Development progresses through stereotyped physical growth sequences at temperature dependent rates with fish age described in "hours post fertilization" (hpf) as determined by morphological features (Kimmel et al., 1995). For example, two embryos, each with 18 muscle segments (somites), are both measured as 18 hpf even if raised at different temperatures for different amounts of time. As such, and within an ecologically relevant temperature range, embryos will be anywhere from 3-10 somites at "sunset" and 18-24 hpf at the following "sunrise" (Figure 3).

The development of motor behaviors in zebrafish

The earliest behavior in the zebrafish embryo appears at approximately 17 hpf and begins as individual contractions of trunk muscles (see Figure 4). Over just the next two hours, and with the extension of the tail bud, these early contractions begin to swing the tail from side to side in a behavior referred to as 'coiling' (Saint-Amant and Drapeau, 1998). Early behavioral studies established a peak coiling frequency of approximately 1 Hz at 19 hpf before it rapidly decreases in frequency to below 0.1 Hz by 26 hpf (Drapeau et al., 2002a; Saint-Amant and Drapeau, 1998). Coiling behavior is very robust, altered by few manipulations; however, of note, dechorionation increases the frequency of contractions via an unknown mechanism. Shortly after peak coiling frequency, the embryo develops a response to touch at approximately 21 hpf (Saint-Amant, 2006). Mechanical deflection or a jet of water directed at the trunk of the embryo results in a contralateral contraction followed by 1-3 alternating contractions of the tail—a primitive version of the C-bend escape response to later develop in the larvae (Pietri et al., 2009). Importantly, both the touch response and the coiling that continues through this early developmental period do not require the brain or hindbrain as both behaviors persist in spinalized preparations (Pietri et al., 2009; Saint-Amant and Drapeau, 1998).

By 24 hpf, the individual, alternating contractions underlying coiling give way to an intermediate behavior where two contractions alternate in quick succession with periods of stillness in between (Knogler et al., 2014). This so-called 'double coiling' precedes the rudimentary swimming behaviors that develop by 26 hpf. 'Swim' behavior in embryos consists of sustained side-to-side contractions at approximately 10 Hz that are capable of propelling the animal forwards (Saint-Amant and Drapeau, 1998). Though embryos do rarely exhibit spontaneous swim events, this behavior is

easily stimulated via the touch response. As with the coiling and early touch behaviors, early swimming also persists in spinalized preparations (Downes and Granato, 2006). Though all of these immature behaviors exist in the embryo, zebrafish do not hatch until ~48 hpf (Kimmel et al., 1995) and these purely spinal circuits develop in relative isolation from many environmental stimuli.

Development of spinal neurons and their cellular properties

Even with 3 decades of papers describing the appearance and morphologies of individual classes of spinal neurons, there still remain many discrepancies in the literature about the timing and function of each type of interneuron. Presented here are the consensus findings that are also in line with my own observations (see Figure 5). The first cells in the spinal cord to extend axons are the primary motor neurons (PMN), which do so at around 16 hpf (Eisen, 1991a). These cholinergic cells extend axons into the neighboring muscle and are recognizable by their lateral position within the ventral spinal cord and their large tear-drop shape. These cells are labeled by the mnx1 transcription factor and individual axonal trajectories differentiate between the classes of PMN (caudal projecting, CaP; rostral RoP; and middle, MiP) (Eisen, 1991b; Zelenchuk and Brusés, 2011). The relevant classes of interneurons which may participate in the coiling circuit and have extended axons by 20 hpf include: the ipsilateral caudal (IC) cells, ventral longitudinal descending (VeLD), commissural primary ascending (CoPA), and possibly the circumferential descending cells (CiD) (Saint-Amant, 2010).

The circuit for coiling, albeit comprising of just a few types of cells and existing in isolation from descending inputs, has still not been fully solved. For over twenty years, there was debate as to the source of excitation—whether it relied on pacemaker neurons or if depolarizing oscillations were a distributed and intrinsic property of cells in the network (Drapeau et al., 1999). Recent work in *Xenopus*, (reviewed in (Li, 2011)) argues for pacemaker properties in ipsilateral excitatory interneurons (*chx10*-positive, analogous to CiDs) as well as motor neurons. A small amount of excitation in the form of NMDA is sufficient to drive these neurons with bistable membrane properties into rhythm generators even in the absence of glycine and GABA. In zebrafish larvae at 3-4 dpf, these hindbrain and rostral spinal cord CiDs are necessary and sufficient for driving swimming behaviors and given their participation in spontaneous network activity in the embryo, one hypothesizes they may drive that activity as well (Kimura, 2006). One year later, in zebrafish, the identification of IC cells as a population of pacemakers in the rostral spinal cord has answered some of the field's open questions (Tong and McDearmid, 2012). These cells reside in somites 1-6 with their somas located in the very ventral portion of the spinal cord and project axons ventrolaterally towards the tail (Mendelson, 1986b; 1986a). ICs make gap junctions with motor neurons and respond to current injection in late-stage embryos (after 26 hpf) with membrane oscillations at 1 Hz whereas current injection in other active cell types elicits spiking (Tong and McDearmid, 2012). In spite of the fact that CiDs do not extend axons until 24 hpf (Higashijima et al., 2004a; Pietri et al., 2009), different labs have suggested in unpublished observations

that CiD neurons drive coiling behavior while yet other groups believe ICs are merely a subclass of *chx10*-postive, CiD-like neurons.

Regardless which cells act as pacemakers or rhythm generators, agreement is unanimous that membrane oscillations are generated by persistent sodium currents and are blocked by TTX and riluzole (Buss et al., 2002; Tong and McDearmid, 2012). Surprisingly, most other pharmacological blockers of individual channels and full synaptic blockade alter but do not abolish spontaneous network activity (Drapeau et al., 2002b). These results suggest a network of neurons coupled solely by electrical synapses. Dye injections show transfer between cells and paired recordings between MNs, VeLDs, ICs, and CiDs reveal transmission of steady state hyperpolarizing current, confirming electrical coupling among ipsilateral neurons (Saint-Amant and Drapeau, 2001). Interestingly, hyperpolarizing current even passes from one MN to another MN in the next muscle segment, presumably via the passing axon of an interneuron (Saint-Amant and Drapeau, 2001). Gap junctions persist in the spinal cord, though it is thought that the addition of ipsilateral excitatory chemical synapses is responsible for quickening the frequency of the CPG as the embryo begins swimming behaviors (Saint-Amant, 2010). Some electrical synapses persist into larval and even adult stages (Kiehn and Tresch, 2002; Kimura, 2006; Song et al., 2016).

Neural activity in the early coiling circuit presents similarly in all active cell types. It begins with periodic depolarizations, or plateau potentials, which reach around -45 mV but do not spike and which proceed at 0.6-1 Hz without pauses between events (Drapeau et al., 1999). A few hours later, plateau potentials become interleaved with volleys of fast synaptic currents and the inter-event membrane potential holds at V_{rest}. Depolarizations (200-500 ms in duration) at this age elicit from one to multiple action potentials, depending on cell type. Bouts of synaptic currents also last 200-400 ms and are blocked by the glycine antagonist strychnine, suggesting that they originate during plateau potentials on the contralateral side of the cord. Though glycine activates chloride currents, the chloride reversal potential in early embryos leads to membrane depolarization and in some cases, action potential firing. However, glycine is still perceived as inhibitory through its shunting of depolarizing inputs via reduction in the input resistance of the postsynaptic cell (Saint-Amant and Drapeau, 2000).

Paired recordings on opposing sides of the cord reveal the correlation between depolarizations and contralateral glycine activity; however, the identity of these glycinergic interneurons remains unknown (Moly et al., 2014; Saint-Amant and Drapeau, 2001). The CoPA interneurons, initially suggested to be responsible (Drapeau et al., 2002b), have since been identified as glutamatergic cells (Higashijima et al., 2004b) that transmit touch responses from the sensory Rohon-Beard neurons to the contralateral CiD neurons and their connected motor network (Pietri et al., 2009). However, there is uncertainty about whether they participate in spontaneous network activity (Knogler et al., 2014; Saint-Amant, 2010). These RB-CoPA-CiD synaptic connections are essential for the touch response as glutamatergic blockade abolishes the touch response but leaves coiling behavior

intact (Pietri et al., 2009). Some CoSA (commissural secondary ascending) neurons are *vglut2*-positive, while others expressing *glyt2* are candidates for contralateral inhibition (Higashijima et al., 2004a). Numerous glyt2 cell bodies are present in the rostral segments of the cord by 20 hpf, but their activity and projections have not been fully characterized (Moly et al., 2014). In particular, the CoSA cell type is "weakly defined" (Higashijima et al., 2004b), and may not extend it's axons in time to mediate early contralateral inhibition. This confusion is understandable, since nearly half of morphologically unidentifiable neurons between 20-24 hpf exhibit spontaneous activity during coiling (Saint-Amant and Drapeau, 2001).

Genetic tools for studying neural function and development

The genetic tools available in zebrafish allow for easy testing of transgenic constructs via DNA and RNA injection at the single-cell stage. Adding RNA for the Tol2 transposase into these injections permits the incorporation of a transgene from a Tol2-compatible plasmid into the genome (Kwan et al., 2007). These F0 'founder' individuals mosaically express the transgene and can be used for experiments or raised to adults where mosaicism in the germ line determines the rate of transmission to the F1 individuals. The most common means for driving overexpression of exogenous proteins in the zebrafish is using the Gal4-UAS expression system (Halpern et al., 2008). Control of the yeast Gal4 transcription factor is governed by either a copy of an endogenous promoter or a minimal promoter reliant on local enhancer activity following random insertion in the genome (Kawakami et al., 2004). In each of these cases, expressing a trans-amplifying transcription factor can not only overcome a weak promoter, but also affords flexibility in selection of target effector molecules. Gal4 recognizes a region called the upstream activating sequence (UAS) that consists of 10 repeats of the binding site and an e1b motif that confers directionality of transcription. Maintaining specific Gal4 drivers and UAS reporters on separate transgenes allows for mix-and-match swapping of expression patterns for fluorescent tags and effector proteins.

In addition to overexpression of exogenous proteins, it is relatively easy to knock down or knock out endogenous molecules within the developing embryo. For many years, zebrafish biologists relied on morpholinos for knocking down gene expression. These small synthetic nucleotides, designed in antisense to the target endogenous RNA, either block the transcription start site or a splice site and can be very effective at blocking translation during the first 3 days of development (Bill et al., 2009). However, recent controversy has undermined their popularity in the field and has complicated their interpretation. Off-target effects and generalized toxicity were always a concern with morpholinos, requiring careful validation and proper controls (Eisen and Smith, 2008). A recent report claimed that up to 80% of morpholino-induced morphant phenotypes are not recapitulated by their null-mutation counterparts (Kok et al., 2015). This assessment was done on a pre-selected list of targets and was biased towards genes that regulate morphogenesis. In spite of this bias, this paper raised enough concern in the zebrafish community as to require genetic nulls as controls for morpholino-based experiments.

In a follow up to these issues, the Stainier lab highlighted one specific morpholino, in which the abnormal phenotype was supposedly due to off target effects. The null mutant for the gene *egfl7* developed normally, yet injection of the supposedly toxic morpholino into these null individuals had no effect. The conclusion drawn is that knockout of a gene can induce mechanisms of compensation that are not evoked by knockdown (Rossi et al., 2015). Experimentally, it also suggests that some morpholinos have been unduly maligned, that some negative phenotypes in null mutants deserve a second look, and that it remains important to compare morphants to nulls in order to use either. Thankfully, the advent of the CRISPR-Cas9 system has simplified the generation of knockouts and greatly reduced the amount of effort required in comparison to TALENs and zinc finger nucleases (Blackburn et al., 2013; Jinek et al., 2012).

Optical tools for observing neural function and development

One of the most significant benefits of the developing zebrafish as a model organism is the relative transparency of the skin and tissues. Great efforts, as described above, have been made to characterize the early spontaneous activity in the spinal cord via electrophysiological recordings from one or two neurons at a time. Using calcium indicators as a proxy for neural depolarization, fast confocal microscopy allows observation of many neurons simultaneously (Fetcho et al., 1998). Improvements in volumetric imaging using variants of light sheet microscopy expand this ability from observing cells in a single optical plane to observing brain regions and even whole brains (Chhetri et al., 2015; Keller and Ahrens, 2015). Calcium enters through voltage gated channels during action potentials—and in the zebrafish embryo, during plateau potentials without spiking (Muto et al., 2011). Cell-permeable, calcium-sensitive dyes have been used for years to visualize this response in all cells, and since the early 2000's, genetically encoded calcium indicators permit specification by cell-type (early work reviewed in (Palmer and Tsien, 2006)). The most famous of these indicators, GCaMP, is a circularly permuted version of GFP linked by a calmodulin domain causing increases in fluorescence upon a calcium-induced conformational change (Nakai et al., 2001; Ohkura et al., 2005). The signal to noise ratio has been improved over the years through evolution of the GCaMP molecule, including versions 1.3, 1.6, 2, 3, and at this point, one lineage of derivatives HS and 7, and a separate lineage to versions 5, and 6—including fast, medium, slow responders and a photoactivatable version (Akerboom et al., 2012; Berlin et al., 2015; Chen et al., 2013; Muto et al., 2011; 2013; Ohkura et al., 2005; Tian et al., 2009).

The relative ease of calcium imaging compared to electrophysiology has spread its adoption, yet there are important distinctions to be made. Calcium rise is slow in comparison to changes in membrane voltage and even with the fastest indicators, it is not possible to distinguish events closer than 50-75 ms (Chen et al., 2013). Similarly, the slow rise time of 100-200 ms to peak GCaMP6f results in an imperfect alignment between calcium events and the underlying neural activity. These properties are greatly improved in the recent GCaMP variants, but to some

extent are simply limitations of using calcium as the starting signal. In this vein, it is also not currently possible to observe subthreshold events in the soma nor possible to observe hyperpolarizing currents or chloride-based shunting depolarizations. Voltage dyes and genetically encoded voltage indicators will be the next-generation tool for gaining this information and there is evidence they work in zebrafish; however, their limitations currently outweigh their benefits (Knöpfel et al., 2015).

Optical tools for manipulating neural function and development

In the past ten years, optogenetics has thoroughly permeated the field of circuit neuroscience (Adamantidis et al., 2015). Co-opting an algal blue-light activated cation channel (channelrhodopsin, CHR) for triggering action potentials in neurons has opened many doors for researchers and has been reviewed many times as the tool evolves and diversifies (Deisseroth, 2011; Wietek and Prigge, 2016). Lagging behind in both functionality and widespread adoption are the light-activated tools for neural silencing. The first, halorhodopsin (NpHR), is a yellow-light sensitive chloride ion pump from *Natronomonas* which can hyperpolarize a cell exposed to the correct wavelength of light (Gradinaru et al., 2008). Archaerhodopsin (Arch), the other early option for inhibiting neurons is a pump that lowers membrane voltage by extruding protons from the cytoplasm (Ihara et al., 1999). Both of these options can silence action potentials in neurons, but may also alter cellular physiology by changing ionic gradients and cellular pH. The newest tool for optical inhibition is the result of directed evolution of channelrhodopsin and retains its photoproperties while changing residues along the pore of the channel to flip from flux of cations to passage of chloride. This tool, IC++, will be of great use in mature circuits, but may lead to confusing results in embryonic systems where chloride channels are depolarizing (Berndt et al., 2014). In zebrafish, channelrhodopsin and halorhodopsin have both been useful in the spinal cord for identification of the necessary and sufficient cell types for the initiation and propagation of signals for swimming activity (Eklof-Ljunggren et al., 2012; Wyart et al., 2009).

Of note for this thesis is another light sensitive toolset that has received more attention than use—the OptoXRs. These chimeric proteins use the core transmembrane helices from bovine rhodopsin, but swap out the intracellular loops to match GPCRs that couple to different intracellular signaling pathways (Airan et al., 2009). In this way, light can be used to trigger G-protein activation and subsequent intracellular cascades of the α1- and β2-adrenergic receptors as well as the 5HT1A receptor. However, these tools are hampered by weak activation and there are still efforts underway to identify native light-sensitive GPCRs in other species (Shimamura et al., 2008).

Though the zebrafish would initially seem to be the ideal organism for using optogenetics to probe behavior, there are a number of important controls that are often overlooked. Most groups control for efficacy of optogenetic treatment by expressing the effector protein, but not exposing the organism to the light treatment. Recent findings and the work outlaid in this thesis argue that light-only controls are also necessary. The most obvious example for this is the confounding influence of

imaging light and optogenetic stimulation on visual behaviors. Vision in the zebrafish starts between 68 and 72 hpf with the onset of the optokinetic and optomotor reflex responses (Easter and Nicola, 1996; Neuhauss et al., 1999). Efforts to observe whole brain activity during these visual behaviors have required new hardware to exclude imaging and photostimulation laser light from the retina of larval fish (Vladimirov et al., 2014). With these tools not available to the majority of researchers, the confounds from inevitable visual stimulation must be considered. However, even blind larvae and individuals younger 68 hpf still exhibit photobehaviors as detailed below.

Nonvisual photoreception

Transparent marine organisms that rely on ambient light for behaviors such as maintaining depth in the water column or avoiding predation do not necessarily require a specialized photoreceptive organ for image formation. Whereas in mammals, enucleation abolishes all known responses to light, in non-mammalian vertebrates and many invertebrates, photoreceptive cells are distributed throughout the body plan (Foster et al., 1991; Foster and Hankins, 2002). Across evolutionary history, most species have retained these nonvisual photoreceptors distributed throughout deep brain regions irrespective of the transparency of the overlying bone and tissue (Porter et al., 2012). These receptors are active in organisms with a transparent phase of their life cycle, like the developing zebrafish, and in species with specialized transparent windows over photoreceptive brain structures (Vigh et al., 2002). Even more surprisingly, recent reports suggest that physiologically relevant light levels reach photosensitive cells in embryonic mice through the abdominal wall of the mother (Rao et al., 2013). As such, many questions remain about the acute functions or developmental roles of nonvisual photoreception.

Evolutionary history of nonvisual opsins

The first molecular cloning of a visual photopigment, bovine rhodopsin, was accomplished by Nathans and Hogness in 1983 (Nathans and Hogness, 1983). Shortly thereafter, Zuker et al. cloned the *Drosophila* rhodopsin in 1985 (Zuker et al., 1985). These two molecules set the tone for the majority of subsequent studies on photoreception. Newly identified opsin molecules were classified as belonging to either the vertebrate family (ciliary [c-type], hyperpolarizing, G_t coupled, photobleaching) or the invertebrate family (rhabdomeric [r-type], depolarizing, G_q coupled, bistable). However, as genome sequencing efforts identified hundreds of homologous opsin sequences across taxa and histological samples, the landscape became more muddled. In addition to ciliary and rhabdomeric groups, separate evolutionary branches are required for cnidarian opsins and retinal GPCRs, neuropsins, and peropsins (Porter et al., 2012). Changes in individual key residues also suggest that even within a group, signaling and photoproperties vary more than previously thought (Sato et al., 2011). Further complicating our understanding, mammalian retinal ganglion cells express melanopsin, a r-type opsin, and the brain of annelid worms contains a c-type opsin (Arendt et al., 2004; Panda et al., 2002).

At the organismal level, photoreceptors have also been identified in non-neural tissues like the skin of *Xenopus* and mammalian kidneys (Figure 6). Representative opsins from all major groups have been identified in multiple tissue types—no evolutionary branch exists solely for vision. In the photoreceptor cells of the retina, opsins localize to highly membranous structures, specialized for maximizing photoreceptive molecules in a small surface area. Interestingly, closely related opsins, when identified in other tissues, do not always appear in cells with clear expansion of membranes. Together, this information suggests we do not have a clear understanding of the purpose for nonvisual photodetection across cell types, species, or evolutionary time.

Function of nonvisual photoreceptors across taxa and brain regions

With accumulating individual contributions to the field of nonvisual photodetection, we can begin to piece together general principles. Examples from invertebrates and eyeless stages of development include the ancient *Ctenophora*, the basal chordate *Ciona*, and also the recently described photoresponse in *Drosophila* larvae (Collin et al., 2009; Inada et al., 2003; Xiang et al., 2010). These examples represent one of the general themes: motor behaviors for place preference guided by ambient light levels. In vertebrates, the best known example is the role for melanopsin in governance of circadian rhythm in mammals (Panda et al., 2002). Expressed in retinal ganglion cells of the retina, melanopsin is a r-type photodetector that does not compartmentalize to a specialized membrane structure. These intrinsically photosensitive ganglion cells (ipRGCs) were identified following the realization that mice and humans lacking rods and cones retained circadian rhythms and the pupilary light reflex. The brain regions responsible for these behaviors, the suprachiasmatic nucleus and the olivary pretectel nucleus respectively, receive projections from these ipRGCs and suggest possible subtype specificity within the ipRGC population (Schmidt et al., 2011).

In non-mammalian vertebrates, circadian rhythm is often entrained by a separate brain region, the pineal complex (Fukada and Okano, 2002). This structure, the one emphasized by Descartes, releases melatonin in daily cycles to help regulate sleep (Cassone, 1998). This is also true in mammals where it is entrained by ipRGCs in the retina, but in birds, fish, and amphibians it has been shown to be directly photosensitive (Korf et al., 1989; Mano et al., 1999; Max et al., 1995). Some species, including catfish, salmon, bullfrog, and anole have a thinning of the skull or even a lens-like structure on the surface of the head for transmitting incident illumination to the pineal and parapineal complexes (Ekström and Meissl, 2003). Specialized cells within the pineal share morphological characteristics with retinal rods and cones, including membranous disks in outer segments and ribbon synapses for transmitter release (Reuss, 2010; Zimmerman and Tso, 1975). Further complicating the story, seasonal reproductive cycles in non-tropical species also rely on measuring the duration of the day-night cycle. Day length is often a trigger for reproductive behavior, and in some birds, a signal driving testicular growth. Interestingly, this behavior persists in enucleated and pinealectomized quail and sparrow (Ono et al., 2009;

Takahashi and Menaker, 1982) and can be triggered by illumination of the mediobasal hypothalamus (Silver et al., 1988). There is evidence for opsin expression in this brain region in quail, pigeon, and chick—including melanopsin (opn4), neuropsin (opn5), and vertebrate ancient opsin (García-Fernández et al., 2015; Halford et al., 2009; Wada et al., 1998). Immunoreactivity for other opsin types in yet more deep brain regions would suggest that there are yet undiscovered photobehaviors.

Nonvisual behaviors in zebrafish

Photoreception in the brain of larval zebrafish also goes beyond the pineal complex. The zebrafish genome hosts 18 nonvisual opsins, most of which have never been characterized beyond their expression pattern. Profiles from RNA in situ hybridization data show various local centers of expression in unidentified brain nuclei (Fernandes et al., 2013). In one recent example of these candidate photoreceptors, melanopsin expression in the brain is identified within a domain defined by the Orthopedia transcription factor, including the preoptic tectum (Fernandes et al., 2012). Ablating these neurons or knocking out melanopsin abolishes a 'dark-photokinesis' response. In this behavior, 4 dpf larvae move more in darkness in an unguided light-seeking pattern reminiscent of the previously described 'place preference' behaviors in nonvisual invertebrates. In younger fish, another recently identified nonvisual photoresponse results in a brief but rapid increase in tail motion in 30 hpf embryos following a flash of light (Kokel et al., 2013). The opsin for this behavior has not been identified, but by restricting the illumination area, the hindbrain was determined to be necessary and sufficient for generating the response. Whether these photosensitive brain regions are merely leftover from an evolutionary timepoint before image forming vision or if they guide undiscovered behaviors or developmental processes will require future research from the molecular to the neuroethological levels.

Scope and specific aims of this thesis

The field of activity dependent development has made great inroads identifying a role for neural activity in processes like proliferation, migration, axon guidance, and synapse refinement. However, it has not yet been a question whether or how spontaneous activity during development is regulated. The appearance, frequency, and patterns of spontaneous activity have long been presumed to be driven by membrane properties under the governance of genetic programs. In this thesis I (1) explore the relationship between frequency of spontaneous network activity and the developing patterns of activity, (2) investigate the influence that environmental inputs, namely light, have as regulators of that developing network, and (3) characterize the mechanism of that regulation.

Figure 1.
Descartes' depiction of a reflexive brain circuit. In this model, physical transformations (eg. heating and expansion) move fluid and pull on tangible connections in order to signal from the skin, to the brain, and back to the muscle again. This mechanical reflex arc would be triggered to retract from painful stimuli.

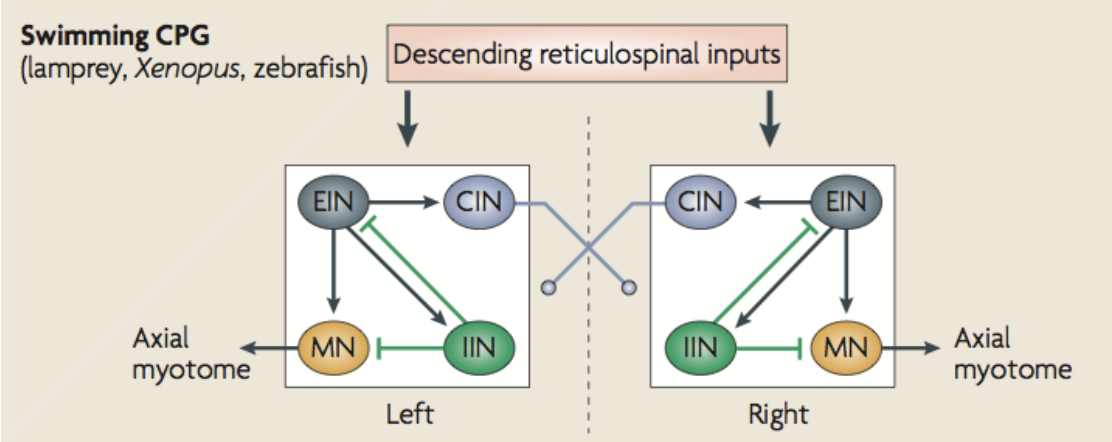

Figure 2.
The basic components of a swimming CPG. This circuit is repeated in each muscle segment of the developing spinal cord. Hindbrain inputs provide tonic drive and this circuit generates left-right alternation. Excitation is propagated along the spinal column by descending ipsilateral excitatory interneurons (EIN). Local regulation is provided by ipsilateral interneurons (IIN) and alternation arises from the participation of contralaterally projecting glycinergic interneurons (CIN). Motor neurons (MN) exit the cord and project into the muscle. (Goulding, 2009)

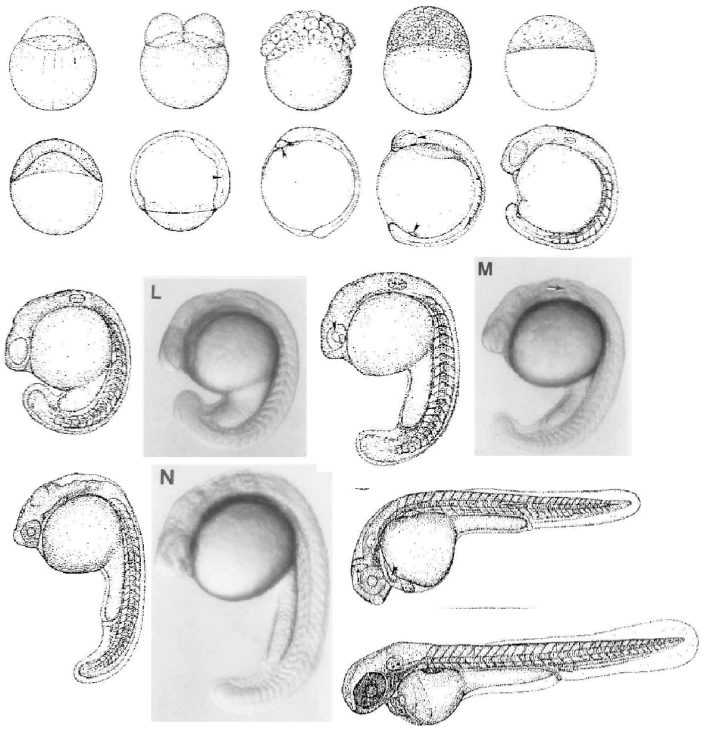

Figure 3.

Selected stages of development in the zebrafish embryo. Top row: 1-cell, 2-cell, 64-cell, high, sphere. Covers 0-4 hpf. Second row: 30% epiboly, 75% epiboly, bud, 6-somite, 14-somite. Covers 4.7-16 hpf. Third row: diagram of 18 hpf, image at 17.5 hpf (L), diagram of 19.5 hpf, image at 19 hpf (M). Bottom row: diagram of 22 hpf, image at 21.5 hpf (N), diagrams of 31 and 48 hpf. Adapted from Kimmel, 1995.

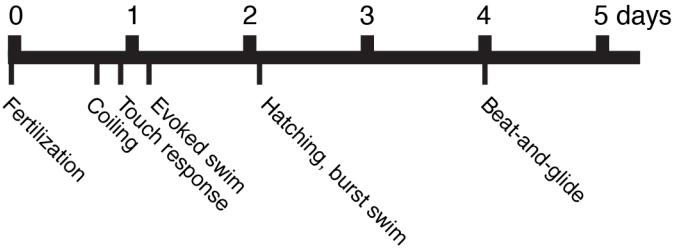

Figure 4.
Developmental progression of distinct motor behaviors in the zebrafish. Adapted from Drapeau, 2002.

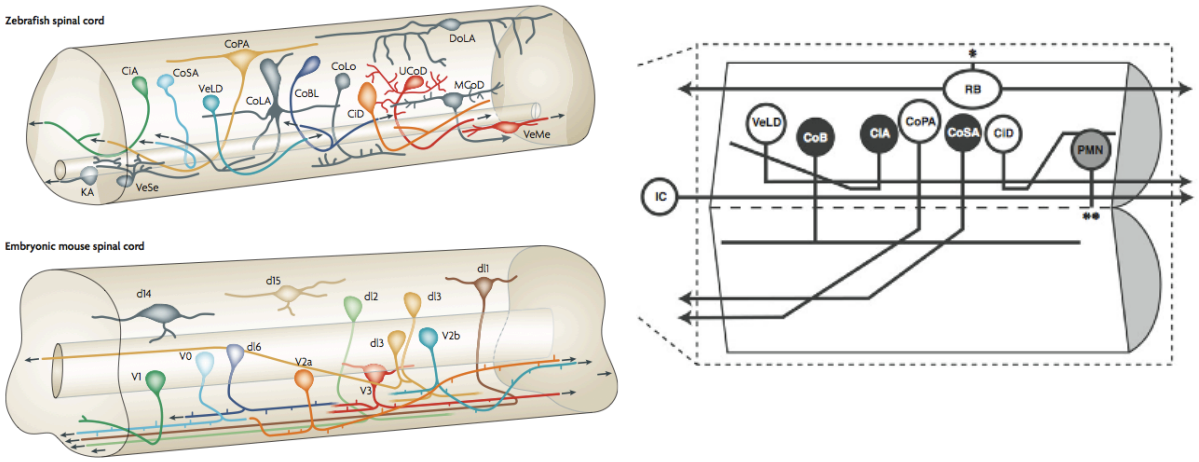

Figure 5.
Left, similarities in circuit layout and cell types of the zebrafish and mouse spinal cord. Cells with similar morphology and transcriptional profiles share the same color scheme. Adapted from Goulding, 2009. Right, layout of the zebrafish spinal cord. Depicted are the somas and axonal trajectories of the 9 classes of cells (~20 cells per hemisegment) with processes at 24 hpf. Excitatory cells are in white, putative glycinergic interneurons in black, and cholinergic motor neurons in grey. Adapted from Saint-Amant, 2010.

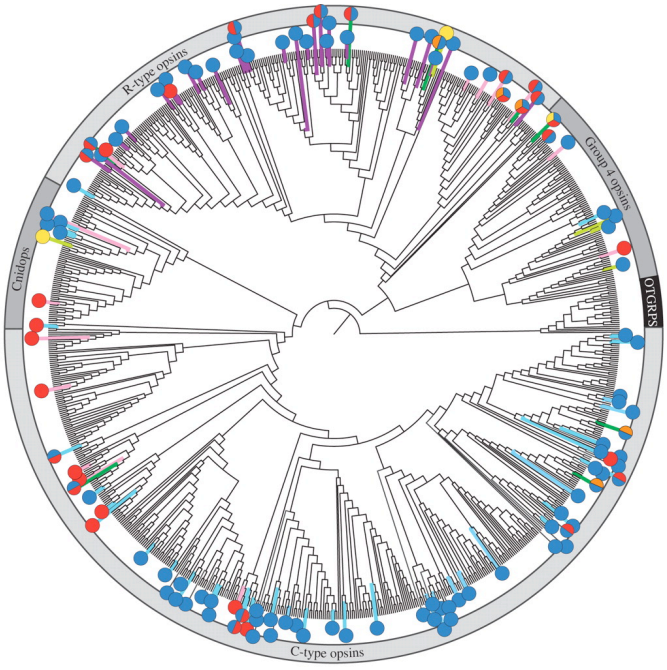

Figure 6.
Maximum likelihood phylogeny of 889 opsins. Individual terminal branches have been color coded based on the tissue of location in which the opsin was identified. Blue: eye, red: brain, orange: skin, yellow: other. Of note, brain expression is seen for R-type, C-type, Cnidops, and Group 4-type clades (identified in the outer circle). From Porter, 2012.

CHAPTER 2

Emergence of Patterned Activity in the Developing Zebrafish Spinal Cord

Current Biology (2012) 22, 93-102

LINKER STATEMENT

The following study was done to observe the formation of the early spinal CPG by imaging neural activity in many cells simultaneously. This would be the first study observing the onset of spinal cord spontaneous activity at the network level *in vivo*. My contributions to this project consist of the chronic inhibition experiments in which we used halorhodopsin to reduce global network activity. I was able to show here that activity patterns in one specific class of neuron, identified in a later chapter, do not mature properly when motor network activity is inhibited.

Emergence of Patterned Activity in the Developing Zebrafish Spinal Cord

Erica Warp,[1] Gautam Agarwal,[1] Claire Wyart,[2] Drew Friedmann,[2] Claire S. Oldfield,[1] Alden Conner,[2] Filippo Del Bene,[3] Aristides B. Arrenberg,[3] Herwig Baier,[3] and Ehud Y. Isacoff1,[2,4]

[1]Helen Wills Neuroscience Graduate Program
[2]Department of Molecular and Cell Biology, University of California, Berkeley, Berkeley, CA 94720, USA
[3]Department of Physiology, Programs in Neuroscience, Genetics, and Developmental Biology, University of California, San Francisco, San Francisco, CA 94158-2722, USA
[4]Physical Bioscience Division, Lawrence Berkeley National Laboratory, Berkeley, CA 94720, USA

Acknowledgements: We thank K. McDaniel, W. Staub, J. Saint-Hillaire, and D. Weinman for fish care; K. McDaniel for assistance with experiment setup; M. Feller for critical reading of the manuscript; and H. Aaron and Intelligent Imaging Innovations for advice and assistance with the optical system. Support for the work was provided by the National Institutes of Health Nanomedicine Development Center for the Optical Control of Biological Function, PN2EY018241 (E.Y.I.), the Human Frontier Science Program, RGP0013/2010 (E.Y.I.), the National Science Foundation (FIBR 0623527) (E.Y.I.), and the National Institute of Health National Research Service Award fellowship (E.W.).

Summary
Background: Developing neural networks display spontaneous and correlated rhythmic bursts of action potentials that are essential for circuit refinement. In the spinal cord, it is poorly understood how correlated activity is acquired and how its emergence relates to the formation of the spinal central pattern generator (CPG), the circuit that mediates rhythmic behaviors like walking and swimming. It is also unknown whether early, uncorrelated activity is necessary for the formation of the coordinated CPG.
Results: Time-lapse imaging in the intact zebrafish embryo with the genetically encoded calcium indicator GCaMP3 revealed a rapid transition from slow, sporadic activity to fast, ipsilaterally correlated, and contralaterally anticorrelated activity, characteristic of the spinal CPG. Ipsilateral correlations were acquired through the coalescence of local microcircuits. Brief optical manipulation of activity with the light-driven pump halorhodopsin revealed that the transition to correlated activity was associated with a strengthening of ipsilateral connections, likely mediated by gap junctions. Contralateral antagonism increased in strength at the same time. The transition to coordinated activity was disrupted by long-term optical inhibition of sporadic activity in motor neurons and ventral longitudinal descending interneurons and resulted in more neurons exhibiting uncoordinated activity patterns at later time points.
Conclusions: These findings show that the CPG in the zebrafish spinal cord emerges directly from a sporadically active network as functional connectivity strengthens between local and then more distal neurons. These results also reveal that early, sporadic activity in a subset of ventral spinal neurons is required for the integration of maturing neurons into the coordinated CPG network.

Introduction

Spontaneous activity is common to developing networks, occurring in the embryo during periods of concentrated axonal growth and synaptogenesis [1]. A hallmark of this activity is correlated population activity. Such correlations are hypothesized to guide the development of neural circuits [2], as demonstrated in the visual system where disruption of correlated retinal waves causes abnormal circuit development in downstream targets [3]. A transition from sporadic, cell-autonomous activity to correlated rhythmic activity has been observed in brain stem [4], cortex [5], and hippocampus [6], reflecting the emergence of connectivity and suggesting that early, sporadic activity may be necessary for the formation of more mature, correlated networks.

Early in the development of the motor system, cell-autonomous spontaneous calcium transients are observed in spinal cord neurons [7] before the maturation of the synaptic network. Later, spinal cord neurons display correlated patterns of spontaneous activity, beginning with bilaterally synchronized bursts of action potentials [8, 9] that convert to alternation between the left and right sides when γ-aminobutyric acid $(GABA)_A$ and glycine receptor signaling switches during development from depolarizing to hyperpolarizing [10]. In vertebrates, manipulation of

correlated spontaneous activity in the spinal cord disrupts axon guidance [11], the balance between excitatory and inhibitory synaptic strength [12], and the formation of the central pattern generator (CPG) [13], which generates oscillatory rhythms for locomotion into adulthood [14]. Though cholinergic activity has been shown to be necessary for the maturation of rhythmic alternation between the two sides of the mammalian spinal cord [13], it is unknown whether activity influences the acquisition of correlations on the same side of the cord and which cell types may mediate this activity dependence.

We investigated the emergence of correlated patterns of spontaneous activity in vivo in the developing zebrafish spinal cord locomotor system using the genetically encoded calcium indicator GCaMP3 [15] to image spontaneous activity noninvasively at single-cell resolution in identified cells. The imaging identified a remarkably rapid transition from sporadic, uncorrelated activity to rhythms characteristic of the locomotor CPG with ipsilateral correlation and contralateral alternation. Acute optical manipulation of activity revealed that the development of functional connectivity underlies the emergence of the coordinated activity. Chronic optical inhibition of activity in motor neurons and ventral longitudinal descending (VeLD) interneurons early in the transition period disrupted the integration of maturing neurons into the correlated network, suggesting that the emergence of the coordinated CPG is activity dependent.

Results

Emergence of Correlated Activity

In vivo calcium imaging with genetically encoded indicators has been used successfully to image neural activity in zebrafish embryos [16] and larvae [17, 18]. We employed GCaMP3 [15, 18] for its high baseline fluorescence and high signal-to-noise ratio [15]. GCaMP3 and the light-gated inhibitory chloride pump halorhodopsin (NpHR) [19, 20], were targeted to neurons of interest using the UAS/Gal4 system.

Spontaneous activity in the zebrafish spinal cord is restricted to ventral neurons of the motor system [21]. We used the Gal4^{s1020t} line developed in an enhancer trap screen [22] to target a subset of these spontaneously active cells (see Figure S1 available online). We have previously characterized this line to contain primary and secondary motor neurons and Kolmer-Agduhr (KA) ascending interneurons in the spinal cord at 5 days post fertilization (dpf) [23]. At 1 dpf, single-cell imaging with Brn3c:GAL4, UAS:mGFP (BGUG) [22] also revealed targeting to descending interneurons (Figures S1C and S1E). The Gal4 insert for this line is near the olig2 gene [23], which exhibits an identical expression pattern and has been shown at 1 dpf to target motor neurons, KA cells, and VeLD interneurons, as well as bromodeoxyuridine (BrdU)-incorporating cells along the midline [24]. We therefore interpret the descending interneurons to be VeLDs.

Single-cell electrophysiological recordings have identified three key neuron types—primary motor neurons, VeLD interneurons, and IC (ipsilateral caudal) descending interneurons—to be always active during spontaneous events in the zebrafish spinal cord at 20–24 hpf [21]. In the Gal4^{s1020t} line, we could image the

population dynamics of spontaneous activity in primary motor neurons and VeLDs, two of the three key neuron types.

During embryonic development, zebrafish display spontaneous bursts of action potentials in the spinal cord that are associated with spontaneous contractions of the tail [25, 26, 21]. We imaged spontaneous calcium activity in UAS: GCaMP3/Gal4^{s1020t} fish at 18 hpf, an hour after the onset of spontaneous behavior [25], and at 20 hpf, when electrophysiological correlation between pairs of spinal neurons has been previously observed [21], and when there is evidence for both electrical and chemical synapse formation in the zebrafish spinal cord [26, 21]. Calcium imaging was performed on embryos paralyzed with α-bungarotoxin to eliminate spontaneous contractions, performed from a dorsal view to simultaneously observe cells on the left and right sides, and centered on somites 5 and 6. Spatial regions corresponding to single active neurons (e.g., regions outlined in Figures 1A and 1D) and intensity traces over time (e.g., time series data in Figure 1B and 1E) were extracted from movies using a semi-automated toolbox [27].

Though activity was present at 18 hpf, it was sporadic, with long-duration events (Figures 1A–1C; Movie S1) that were rarely associated with events in other ipsilateral cells and with no obvious relationship between the left and right sides of the cord. We did observe some correlation between ipsilateral cells at 18 hpf, but this was just between small subsets of nearby cells (e.g., Figure 1B, cells 1 and 2). In contrast, at 20 hpf events were shorter lasting, tightly correlated between nearly all ipsilateral cells, and organized in bursts of alternation between the left and right sides (Figures 1D–1F; Movie S2), as observed previously [16]. The left/right rhythmicity is reminiscent of activity patterns observed during swimming but is significantly slower at this early coiling stage that precedes swimming [28]. We also observed fish that exhibited near-continual alternating bursts (Figure S1F).

Time-lapse calcium imaging was used to characterize the transition between the uncorrelated and correlated network states. Calcium imaging movies of 4 min duration were taken every half hour between 17.5 and 21 hpf. To quantify changes in activity patterns, we calculated the correlation of GCaMP traces for all cell pairs in individual movies. Pairwise correlation matrices of single-cell traces in an example fish (Figure 2A) showed little correlation at early time points, and the few cell pairs that were correlated were weakly so. With time, correlations between ipsilateral neurons became stronger, whereas neurons on opposite sides of the cord became anticorrelated.

Pooled correlation data across fish showed that ipsilateral cells went from weak to strong correlation, reaching a maximum at 20 hpf, 3 hr after the onset of spontaneous behavior [25] (Figures 2B and 2C). During this period, contra-lateral cells became increasingly anticorrelated (Figures 2B and 2C). By 20 hpf, rhythmic oscillations were apparent (Figures 1F and 2B, right), indicating that the components of a CPG are in place. Increases in ipsilateral correlation and decreases in event duration were detected in individual tracked cells that became active early (e.g., starting at 18 hpf, Figure S2A) as well as for cells that became active later (e.g., starting at 19.5 hpf, Figure S2B), suggesting that maturation of the circuit involves the

progressive addition of cells, each of which goes from an initial state of uncorrelated slow activity to network-associated fast activity.

Ipsilateral Synchronization through Coalescence of Local Correlated Groups

Spatiotemporal maps of correlated ensembles in most fish (6/9) at early stages showed multiple nonoverlapping correlated groups on the same side of the cord (Figure 3, 18.5 hpf, left side). With time, the correlations between cells strengthened and the correlated groups increased in size, to eventually include virtually all ipsilateral cells in the field of view (Figure 3, e.g., 20 hpf; Figure S3A). Within these correlated ensembles, cells became more precisely time-locked (i.e., shorter lag times) during this early period of spontaneous activity (Figure S3B). In addition, event amplitude variability decreased during this period (Figure S3C).

In younger embryos (17.5–18.5 hpf), the distance between cells participating in a synchronous event was relatively small, (i.e., correlations were seen between small numbers of neigh-boring cells), whereas temporally coupled cells covered a broader spatial region in older embryos (e.g., 20–21 hpf) (Figure S3D). Conversely, temporal spread was broad at younger stages but tight at later stages as events became more accurately time-locked between ipsilateral cells (Figure S3D). Thus, ipsilateral correlation is accomplished through the coalescence of local correlated groups, which converts small events that are weakly correlated in small groups of cells into large events that occur synchronously on the entire side of the spinal cord. Although the zebrafish spinal cord develops in a rostral to caudal sequence [29], ipsilateral correlations do not emerge in a rostral to caudal pattern, at least in the region of cord that we imaged.

Increased Functional Connectivity Accompanies Emergence of Correlated Activity

Both chemical and electrical synapses have been implicated in mediating spontaneous activity in the spinal cord [9]. Paired recordings have shown that gap junctions play an essential role in the connectivity of the embryonic zebrafish spinal cord [21]. Additionally, uncoupling gap junctions with heptanol or by intracellular acidification eliminates spontaneous activity at 19–24 hpf, whereas blockers of chemical transmission do not [26]. In older embryos (20–20.5 hpf), heptanol eliminated spontaneous activity in all but 3.7% ± 1.6% of cells (n = 11 fish; see Figure S4B for example), whereas 34.7% ± 9.9% of cells remained active in younger embryos (17.5–18 hpf, n = 13 fish; $p = 0.002$, unpaired Student's t test; see Figure S4A for example). Though these results could be due to off-target effects on calcium or potassium channels, they remain consistent with a model in which gap junctions are important for correlated activity at 20 hpf and younger neurons are more electrically cell autonomous.

To examine this apparent emergence of functional connectivity between ipsilateral cells, we manipulated activity in single cells or in groups of cells and examined the effect on neighboring ipsilateral cells. We used the genetically encoded light-driven chloride pump NpHR, which hyperpolarizes neurons in response to yellow light [19]. GCaMP3 and NpHR were genetically targeted to the same population of ventral spinal neurons in $Gal4^{s1020t}$/UAS:GCaMP3/UAS:NpHR-mCherry [20] fish

(Figure S5A). Spatial targeting of NpHR-activating light was accomplished using a digital micromirror device (DMD). Its spatial resolution was tested by photoconversion of the fluorescent protein Kaede, and light could be restricted to single cells (Figure S5E).

Because NpHR-activating 593nm light does not overlap with the excitation or emission spectrum of GCaMP3 [15], calcium events could be imaged simultaneously during NpHR activation. Spontaneous calcium events imaged with GCaMP3 in NpHR-expressing fish were blocked successfully by illumination of 593 nm light at 19 mW/mm^2 (Figures S5B–S5D). As seen earlier, including in other zebrafish neurons [19, 20], light offset triggered rebound excitation (Figures S5C and S5D), al-lowing us to excite as well as inhibit with a single tool.

We observed striking differences in network responses to NpHR activation between younger and older embryos. Illumination of single cells in younger animals (18–18.5 hpf) caused robust inhibition in the illuminated cell and a rebound excitation upon light-off (Figure 4A) but had no effect on other ipsilateral cells, suggesting low connectivity, where individual cells are functionally independent. In contrast, single-cell illumination at 20–20.5 hpf did not significantly affect activity in either the illuminated cell or in other ipsilateral cells (Figure 4B). However, illumination of a group of cells in a region encompassing two hemi-somites strongly suppressed activity during illumination and evoked rebound excitation upon light-off in both the illuminated cells and nonilluminated ipsilateral neighbors (Figure 4C). Connectivity through electrical synapses can explain the ineffectiveness of NpHR single cell manipulation in the older embryo (Figure 4B), because spread to neighbors of chloride current pumped into an individual cell would reduce the efficacy of the hyperpolarization in that cell. The bidirectionality of electrical synapses can also explain why the inhibition and activation spread to nonilluminated cells in both the rostral and caudal directions (Figure 4D) even though the only spontaneously active ipsilaterally projecting interneurons—the VeLD and IC cells—both have descending axons during this period of development [21, 30, 31]. In summary, our data suggest that increased functional connectivity underlies the emergence of ipsilateral correlation observed between 17.5 and 20 hpf (Figure 2C).

Triggered Rhythmic Oscillation with NpHR Reveals Acquisition of Contralateral Antagonism

Supraspinal activation of the spinal CPG is bilateral for forward swimming but triggers an alternating response in downstream spinal targets [32, 28]. This behaviorally relevant coordinated firing relies on robust inhibitory connections between the two sides of the cord [14]. We tested whether the left and right sides of the cord were functionally antagonistic in the embryo by assessing network responses to bilateral stimulation evoked by NpHR rebound excitation that was confined to the neuronal cell types expressing in the $Gal4^{s1020t}$ line. $Gal4^{s1020t}$/UAS:GCaMP3/UAS:NpHR-mCherry embryos were illuminated bilaterally over a four-somite region for 15 s, a duration that reliably triggered rebound excitation at light-off (Figures S5C and S5D; Figures 5A and 5B). At 18 hpf, bilateral rebound activation

triggered calcium events on the left and right sides of the cord with the initial wave of activity occurring nearly simultaneously on the two sides (Figure 5A). In contrast, at 20 hpf, the rebound excitation triggered a wave of activity first on one side and then, after a substantial delay, on the other side (Figure 5B). The firing then alternated back and forth between the two sides, similar to what was seen in spontaneous locomotor-like activity (Figure 1F and 2B, right). The delay between correlated events (two or more cells participating) on the left and right sides following light offset increased significantly between 18 and 21 hpf ($p < 10^{23}$, paired Student's t test, n = 6 fish; Figure 5D), suggesting that contralateral antagonism is strengthened during this period.

Developmental Transition Disrupted by Inhibition of Activity

To determine the influence of uncorrelated spontaneous activity on the formation of the correlated network and the locomotor CPG, we inhibited spontaneous events for 1 hr with NpHR during the period of transition from uncorrelated to correlated activity (18 to 19 hpf), while imaging population activity with GCaMP3 (Figure 6). To prevent cumulative desensitization of NpHR during long-term activation, we applied a 500 msec pulse of blue light (410 nm) every 10 s [33, 19], concurrently with yellow light using a double bandpass filter to prevent rebound stimulation with yellow light off (Figure 6A). Light was applied to the full imaged region covering both sides of the cord and approximately six somites, centered at somites 5 and 6.

Activation of NpHR from 18 to 19 hpf with yellow/blue light resulted in a reduction in the frequency during the 18 to 19 hpf period in NpHR-positive fish as compared to three control groups: (1) NpHR-negative fish without yellow/blue light, (2) NpHR-negative fish with yellow/ blue light, and (3) NpHR-positive fish without yellow/blue light (Figure 6B). NpHR-induced inhibition reduced activity by 66% initially (18 hpf) and by 53% by the end of the illumination period (19 hpf) compared to GCaMP only (group 1) controls (Figure 6B). An intermediate decrease in the frequency of spontaneous events was observed in NpHR-positive fish that did not receive the yellow/blue light protocol (group 3). This effect was attributed to the fact that the 488 nm imaging light overlaps with the NpHR excitation spectrum and activates the pump by approximately 18% [19]. To eliminate potential effects of the imaging light on the frequency of spontaneous events, we imaged the population patterns only at the end of the experiment (22 hpf) for NpHR without yellow/blue light controls.

We observed a substantial reduction in pairwise ipsilateral correlation in the experimental fish (NpHR-positive fish receiving the yellow/blue light protocol) when compared to controls (Figure 6C), though the four groups did not differ at baseline at 18 hpf (ipsilateral correlation one-way analysis of variance [ANOVA], p = 0.22). This reduction in correlation became evident at 20.5 hpf and continued through 22 hpf (Figure 6C). Additionally, the three controls were similar at 22 hpf, indicating that neither NpHR expression alone, possible NpHR constitutive activity alone, nor yellow/blue light alone disrupts the emergence of correlated activity.

An examination of the activity in control and experimental fish showed that by 22 hpf, the experimental fish had a larger proportion of active cells with immature phenotypes (Figure 7B). As shown above (Figures 1–3) and in control fish (Figure 7A), most active cells were part of an ipsilateral, correlated network in the older embryo, with a small minority of the cells showing long-duration, uncorrelated events, and usually residing more medially in the spinal cord (Figures 1D and 1E; Figure 7A, asterisks). In contrast, in experimental fish, approximately 50% of the active cells were uncorrelated, with long-duration events (Figure 7B, asterisks; Figure 7C), displaying the more immature activity pattern that we observed in our single-cell tracking (Figure S2). Associated with this perturbed pattern of activity, we found that in the experimental animals, a larger fraction of the active cells were located closer to the midline of the spinal cord (Figure 7B, asterisks; Figure 7D), where more immature cells, like BrdU-incorporating progenitor cells, have been shown to reside [24]. Groups did not differ in events kinetics (width at half maximum one-way ANOVA, $p = 0.30$) nor the location of active cells (distance to midline one-way ANOVA, $p = 0.28$) at 18 hpf before activity manipulation. The number of active cells per field of view was not significantly different between experimental and control fish (Figure S6), suggesting that the optical inhibition of activity in motor neurons and VeLDs perturbed the developmental transition by reducing the efficiency with which cells that originated at the midline joined the lateral correlated network.

Discussion

Rapid Emergence of Ipsilateral Correlation

Optical measurements of spontaneous activity in genetically selected ventral spinal neurons in live zebrafish revealed a rapid transition from uncorrelated, sporadic slow activity to ipsilaterally correlated fast activity. The transition to correlated activity could be accounted for by the formation of electrical connections, which initially couple nearby neurons into local microcircuits and then merge to include the majority of active ipsilateral neurons into a single coupled network.

Our observations in vivo are consistent with observations made previously. In *Xenopus*, cell-autonomous calcium events are seen in dissociated spinal cultures and in the isolated spinal cord, with short-duration calcium events becoming correlated between small groups of neurons later in development [7]. In isolated spinal cord of rodent [34] and chick [35], spontaneous events, which are correlated between motor neurons and interneurons, propagate between multiple spinal segments [35]. In the zebrafish spinal cord, cell-autonomous calcium events have been detected in axon-less cells of the 19–26 hpf embryo in imaging experiments but likely overlap minimally with the events we detected due to their very slow kinetics [36]. Correlated depolarizations have been observed between pairs of ventral neurons in dual-cell electrophysiological recordings in 20–24 hpf zebrafish embryos [21], which likely correspond to the correlated calcium events we observed with GCaMP. During swimming, waves of activity propagate down the ipsilateral spinal cord, resulting in nearby motor neurons being more correlated than distant ones [14, 28]. A similar, though slower, rostral to caudal propagation is observed in

spontaneously active motor neurons of 24 hpf zebrafish embryos [16]. We observed that nearby spinal neurons became correlated before distant neurons, suggesting that more mature rostral to caudal relationships are established as the first connections are formed between neurons.

The changes in global activity patterns that we observed were associated with a rapid strengthening of functional connectivity between ipsilateral neurons, as seen from the change in the spread of NpHR inhibition and rebound excitation to nonilluminated cells, suggesting that early activity is cell autonomous and later activity depends on network interactions. The initiation of rhythmic spontaneous events in the rodent and chick spinal cord has been shown to depend on recurrent excitation between GABA-, glycine- and glutamatergic interneurons and cholinergic motor neurons [1, 9]. The ipsilateral network interactions that we observed in the zebrafish appear to be mediated via electrical synapses, as shown in previous studies [26, 21], though chemical synapses may also play a role. Gap junctions also appear to play an integral role in the propagation of correlated spontaneous activity in the spinal cord of rodents [9] and chicks [37] and appear to form some of the first connection in the developing retina [38], cortex [39], and hippocampus [6].

Contralateral Antagonism Emerges Concurrently with Ipsilateral Correlation

We found that as the coupled ipsilateral network was established there also emerged a superstructure in which the spontaneous activity alternated from side to side, a fundamental characteristic of the CPG, which has been shown to involve contralateral inhibition through chemical synapses [14]. Earlier lesion studies have indicated that spontaneous activity and left/right alternation in the spinal cord of embryonic zebrafish does not rely on input from the brain [25, 40], suggesting that the network mediating this rhythmic activity is endogenous to the spinal cord. Given that, among the cells expressing in our Gal4 line, only KAs and VeLDs project within the spinal cord, and, of these, only the VeLDs are active in the first day of development; it therefore appears that the VeLDs, and neurons that they drive, can account for a minimal circuit for locomotor-like activity and behavior.

In rats and mice, spontaneous events are at first synchronized between both sides of the spinal cord and begin to alternate between sides around birth when the activation of $GABA_A$ and glycine receptors become hyperpolarizing [8, 9]. We did not observe a period of synchronized spontaneous events between the left and right sides of the spinal cord in the zebrafish. Rather, the first coordinated patterns consisted of both ipsilateral correlation and contralateral alternation (Figures 2B and 2C). We observed similar patterns of alternating activity with bilateral rebound activation with NpHR. The similarity between spontaneous and NpHR rebound-evoked alternation suggests that a bilateral drive may be responsible for triggering the earliest alternating bursts of locomotor-like activity in the embryonic zebrafish.

Activity-Dependent Emergence of the CPG

Inhibition of activity for 1 hr with NpHR during the transition from sporadic to patterned activity disrupted the emergence of correlated, short duration, rhythmic

activity, indicating that early activity is either instructive or permissive for the maturation of the spinal network. In the normal development of the spinal cord, our imaging revealed that cells first display long-duration, uncorrelated events before transitioning to brief, correlated activity as they establish functional connectivity with other neurons. This transition occurred in neurons that became active early (e.g., Figure S2A) and in neurons that matured and integrated into the network at a later stage (e.g., Figure S2B). Light-driven reduction of activity with NpHR reduced the overall ipsilateral correlation by reducing the fraction of cells that made the transition to brief, correlated activity. As seen in control fish experiencing normal activity, the uncorrelated cells tended to be located more medially in the spinal cord, except that in the fish whose activity had been inhibited by light, they went from being a small minority to being roughly half of the active cells (Figure 7).

These effects are striking given that the inhibition of activity is only by approximately half, it lasts for only 1 of the 3 hr of the developmental transition, and it occurs in only a subset of ventral spinal neurons: the VeLD interneurons and motor neurons (the KAs, also targeted in the $Gal4^{s1020t}$ line, have not been shown to display rhythmic spontaneous activity [21]). These observations imply that early spontaneous activity in VeLD interneurons and/or motor neurons, or in neurons that they drive, is required for the integration of less mature neurons into the correlated network and for the acquisition of normal patterns of population activity. The effect that we observe from inhibiting activity between 18 and 19 hpf was not present until 20.5 hpf, suggesting that inhibition of activity in the few cells that are active early likely alters the integration of other neurons that mature later.

Previous studies have shown that calcium fluctuations play an essential role in developmental processes such as cell migration [41], axon guidance [42], and the expression of the membrane proteins that control cell excitability [43]. It is possible that some or all of these mechanisms underlie the effect of activity manipulation that we observe. For example, a lateral position could be required for integration into the correlated network, and blocking migration to this position could subsequently reduce the number of coupled cells. It has recently been shown that endogenous patterns of spontaneous activity are required for the proper development of coordinated patterns of activity in the motor system of an invertebrate [44]. Here we show that early uncorrelated spontaneous activity is required for the formation of coordinated motor circuits in a vertebrate.

Conclusion

Correlated, rhythmic spontaneous activity is a common feature of developing networks and is essential for normal circuit maturation. By applying noninvasive optical tools to image activity, we observed a rapid transition from sporadic, long-duration, uncorrelated activity to fast, correlated, and rhythmic spontaneous activity in the spinal cord of the intact developing zebrafish. Correlated activity between neurons on the same side of the cord was found to emerge through the formation of small local microcircuits and their subsequent coalescence into a single ipsilateral network, at the same time as side-to-side alternation emerged. This transition to

patterned locomotor-like population activity is perturbed by optical inhibition of motor neurons and VeLD interneurons during the transition period, impeding the integration of maturing neurons into the coordinated network. These results indicate that the formation of the spinal CPG is dependent on activity that occurs before functional connectivity is robustly established in the network.

Figure 1. Spontaneous Calcium Activity in Spinal Neurons Progresses from Sporadic to Locomotor-Like During Embryonic Development

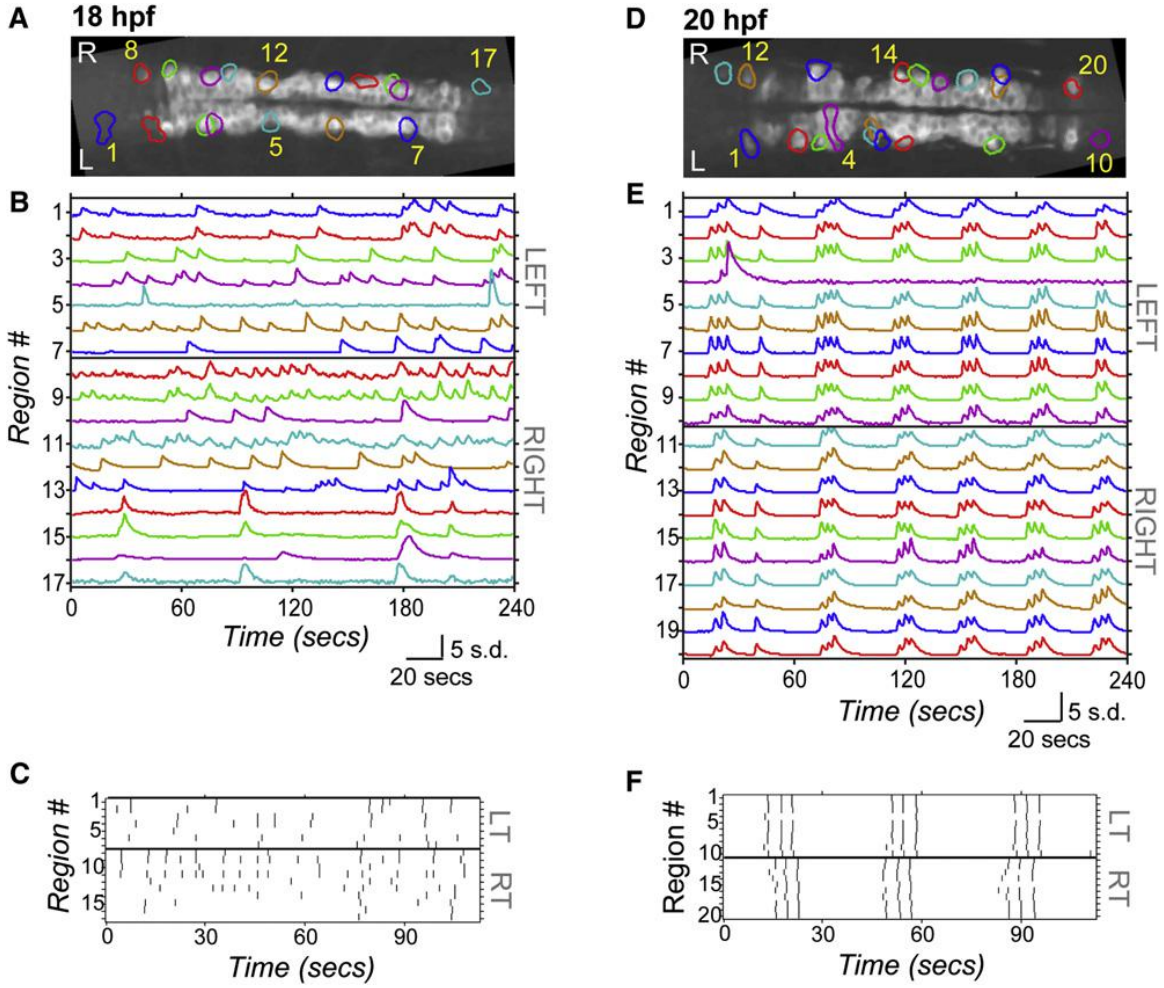

GCaMP3 activity in single neurons in one example embryo at 18 hpf (left) and 20 hpf (right).

A, D. Dorsal views of GCaMP3 baseline fluorescence with active regions circled (rostral left; imaged area somites 4–8). **B,E.** Normalized intensity traces for active regions (identified on y axis) for the left and right sides of the cord, with amplitude corresponding to standard deviations (s.d.) of fluorescence away from baseline. **B.** At 18 hpf, ipsilateral neurons have little correlated firing, though some synchronization is observed (e.g., cells 8 and 9). **E.** At 20 hpf, ipsilateral neurons are tightly synchronized, with few exceptions (e.g., cell 4; note elongated shape extending to the midline). **C,F.** Raster plots of detected events for subsection of data in (B) and (E). **C.** At 18 hpf, population activity is uncoordinated. **F.** By 20 hpf, ipsilateral cells are synchronized, contralateral cells alternate, and a higher order left/right bursting organization is observed. See also Figure S1.

Figure 2. Pairwise Cell Relationships Progress from Independent to Ipsilaterally Correlated and Contralaterally Anticorrelated during a Short Period of Development

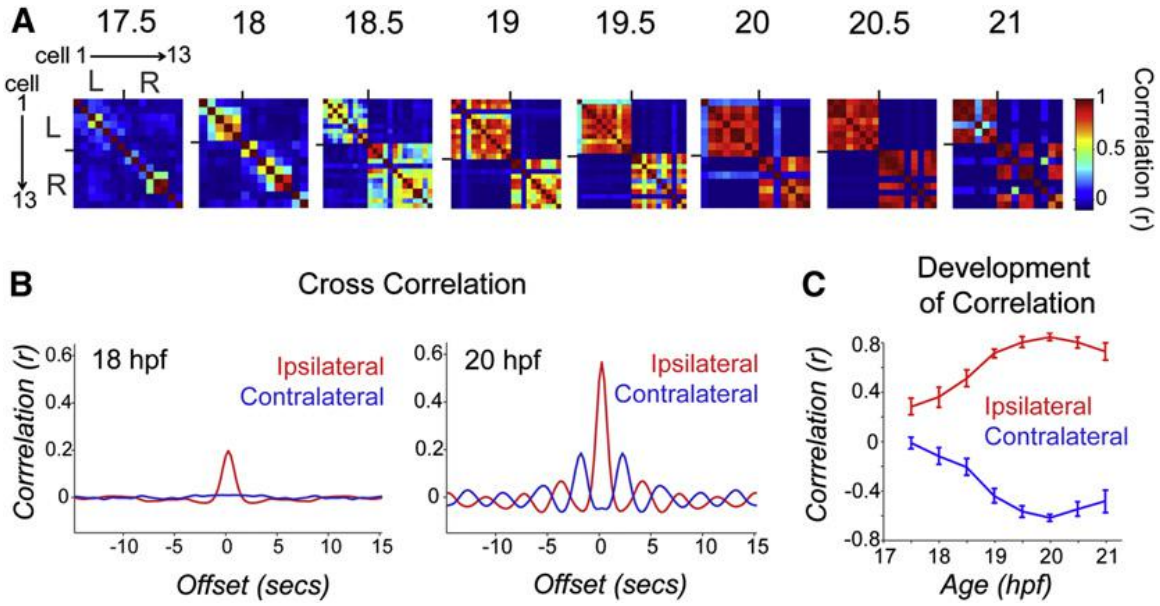

A. Correlation matrices of single-cell traces through the development of an example embryo. Each pixel represents a pairwise comparison between two cells, with high correlation values in red and perfect autocorrelation along the diagonal. Cells are sorted left to right and top to bottom as shown for 17.5 hpf. Ticks mark border between left and right cord and bound a high degree of ipsilateral correlation observed at later time points. **B.** Cross-correlation shows a strengthening of ipsilateral coupling between 18 and 20 hpf and acquisition of oscillatory rhythm by 20 hpf. Cross-correlation was calculated by averaging time-shifted correlation data for all ipsilateral and contralateral cell pairs in individual movies, pooled across nine different fish. **C.** Average pairwise correlations for synchronous events comparing ipsilateral and contralateral cell pairs from individual time-lapse movies acquired from fish ages 17.5 to 21 hpf and pooled across fish. We observed a significant difference between ipsilateral correlations in younger versus older embryos (18 hpf, $r = 0.272 \pm 0.082$; 20 hpf, $r = 0.761 \pm 0.031$; $p < 10^{-3}$, paired Student's t test; n = 9 fish) and a significant increase in the anticorrelation of contralateral cells (18 hpf, $r = 20.207 \pm 0.067$; 20 hpf, $r = 20.710 \pm 0.028$; $p = < 10^{-3}$, paired Student's t test; n = 9 fish). n = 9 fish for 18–21 hpf; n = 4 fish at 17.5 hpf. Error bars = SEM. See also Figure S2.

Figure 3. Ipsilateral Correlation Is Acquired through the Progressive Synchronization of Local Subgroups of Cells

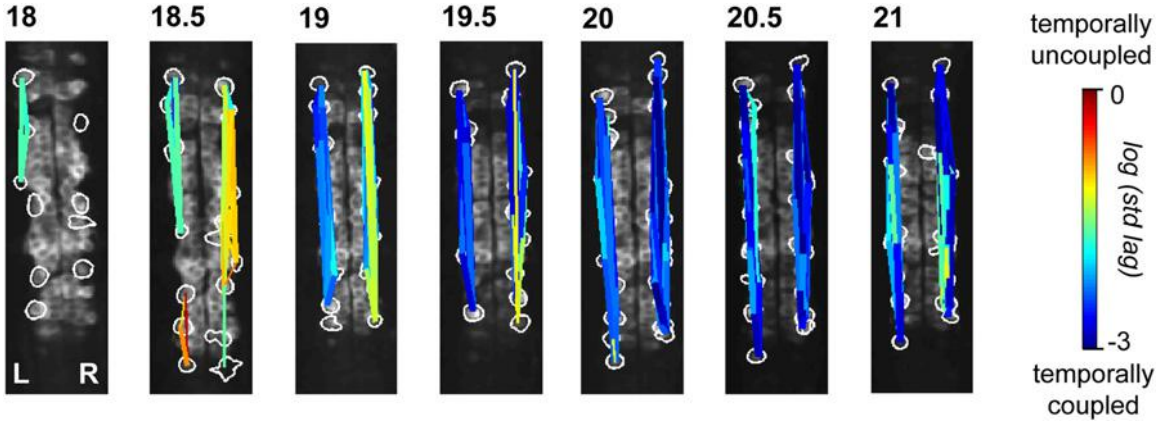

Spatial maps of correlated groups in an example fish from 18 to 21 hpf show small local circuits containing a few cells at 18 and 18.5 hpf that expand into full correlation of each side at later stages. Correlations between all cell pairs were calculated and lines were drawn between cell pairs with correlations greater than 0.2, with thicker lines representing stronger correlation. Line color represents the log of the standard deviation of the lags between event start times of cell pairs and shows an overall increase in temporal precision between ipsilateral pairs as development progresses. See also Figure S3.

Figure 4. Optical Manipulation of Targeted Network Components with NpHR Reveals Changes in Functional Connectivity between Ipsilateral Neurons during Development

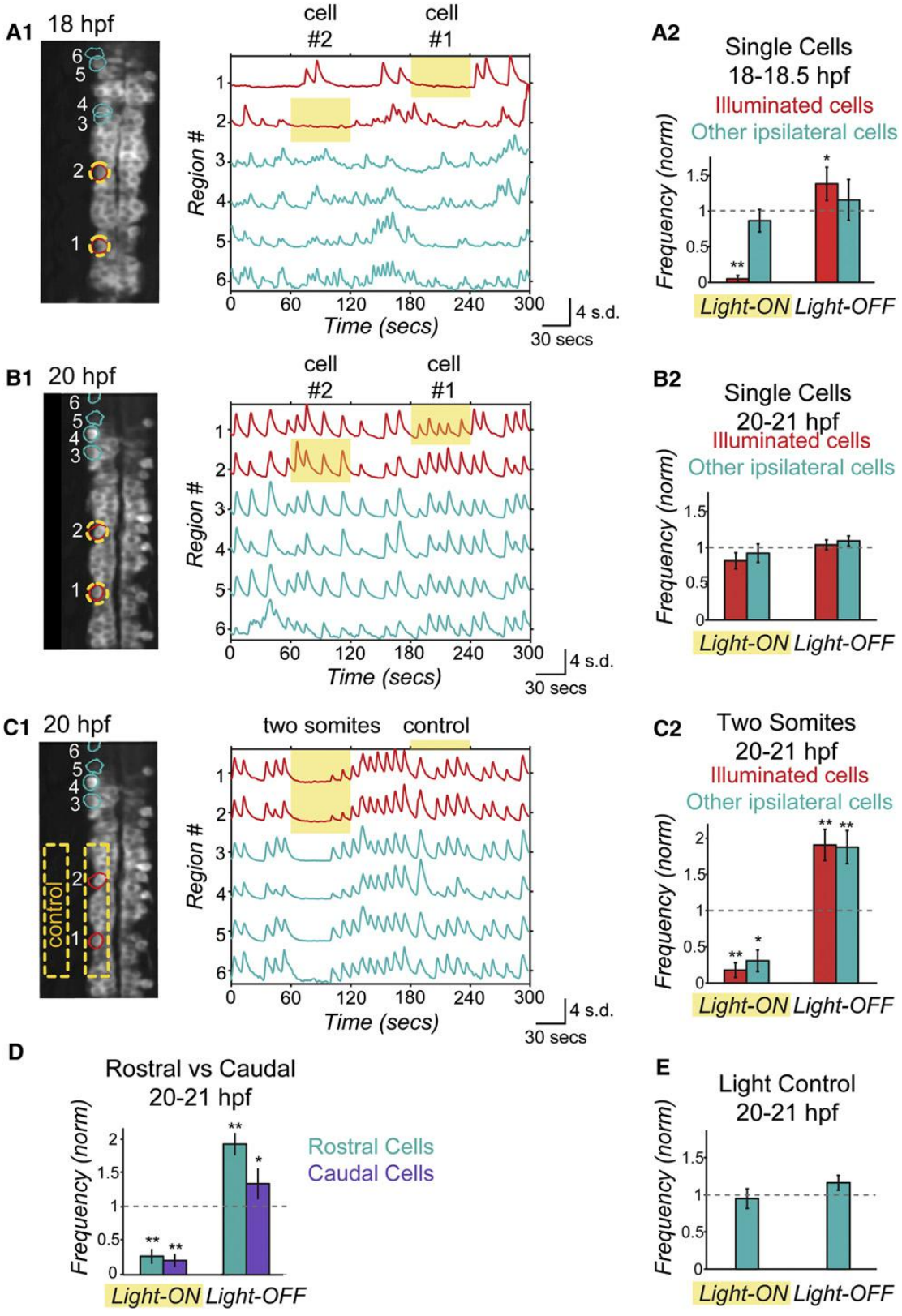

A,B. Single-cell optical manipulation of spontaneous activity with NpHR at 18 hpf (A) and 20 hpf (B). Illumination at 593 nm at 19 mW/mm^2 is targeted successively to two regions outlined in yellow (A1, left), while calcium population activity is simultaneously recorded (A1, right) in the illuminated cells (red) and in the other ipsilateral cells (teal), and here displayed as normalized traces (standard deviation, s.d.) with regions indicated on y axis. **A.** At 18 hpf, application of yellow light to a single cell (during yellow highlight bar) inhibits only the illuminated cell, while other cells remain active. Pooled results (n = 6 embryos) show inhibition during light-ON and activation at light-OFF to be limited to illuminated cells (red bars). **B.** At 20 hpf, single-cell illumination has no effect on activity of either the illuminated or nonilluminated cells (n = 7 embryos). **C.** At 20 hpf, illumination of one side of spinal cord in region spanning two somites (yellow outline in image, left) inhibits and rebound excites both the illuminated cells and other ipsilateral cells (n = 7 embryos). **D.** Reduction of activity and rebound due to NpHR activation at 20 hpf are observed in cells that are both rostral and caudal to the region illuminated. **E.** Control application of light aimed to the side of the cord but within the embryo (C1) does not perturb activity (n = 7 embryos), indicating that effect on unilluminated ipsilateral cells is not due to light scattering, though we acknowledge that light scattering may have different properties in this region. Rostral end points up in fluorescence images. Significance values from paired Student's t-test are *$p < 0.05$ and **$p < 0.01$. See also Figures S4 and S5.

Figure 5. Bilateral Activation with NpHR Rebound Reveals Acquisition of Contralateral Antagonism during Development

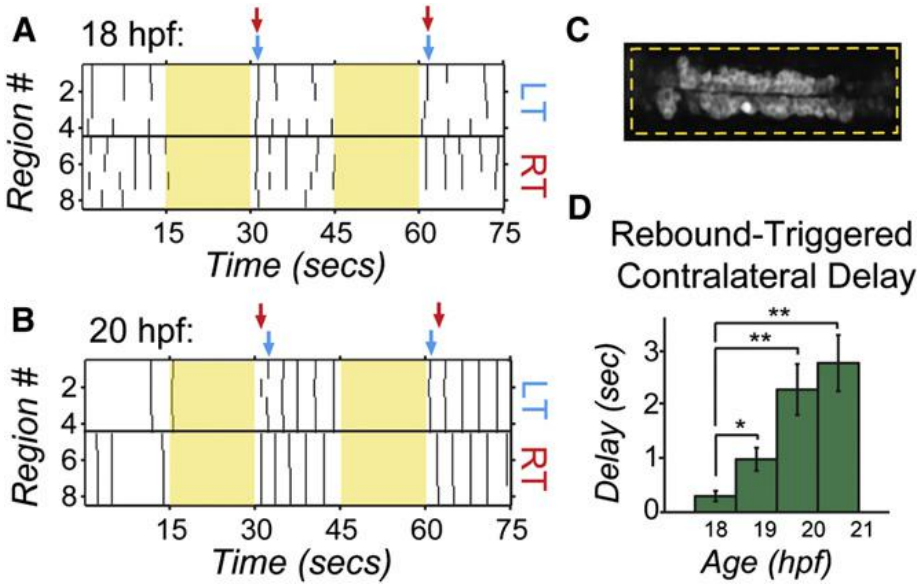

Raster plots of spontaneous events of left and right cells in a single embryo at 18 hpf and 20 hpf during and following bilateral NpHR inhibition with 593 nm light (yellow bars) covering approximately four somites (C).

A. Bilateral activation following NpHR inhibition at 18 hpf results in near simultaneous activation of left (LT) and right (RT) cells following light offset. Arrows indicate the time when two or more cells participate in an event following light offset for one side of the cord (left side, blue; right side, red). **B.** At 20 hpf, activation at light offset of bilateral illumination results in a burst of activity in which one side fires first, followed, after a delay, by firing on the other side and continuing in alternation of firing from side to side. In this example, the right side is active first in trial 1, but the left side is active first in the trial 2. **D.** The delay following offset of bilateral illumination between synchronous events on the left and right sides of the cord (two or more cells participating) increases during development, suggesting an increase in left/right antagonism. n = 5 fish (four trials per fish per condition); *$p < 0.05$; **$p < 0.01$, paired Student's t test. See also Figure S5.

Figure 6. Inhibition of Spontaneous Events with NpHR from 18 to 19 hpf Yields a Subsequent Decrease in Ipsilateral Correlation

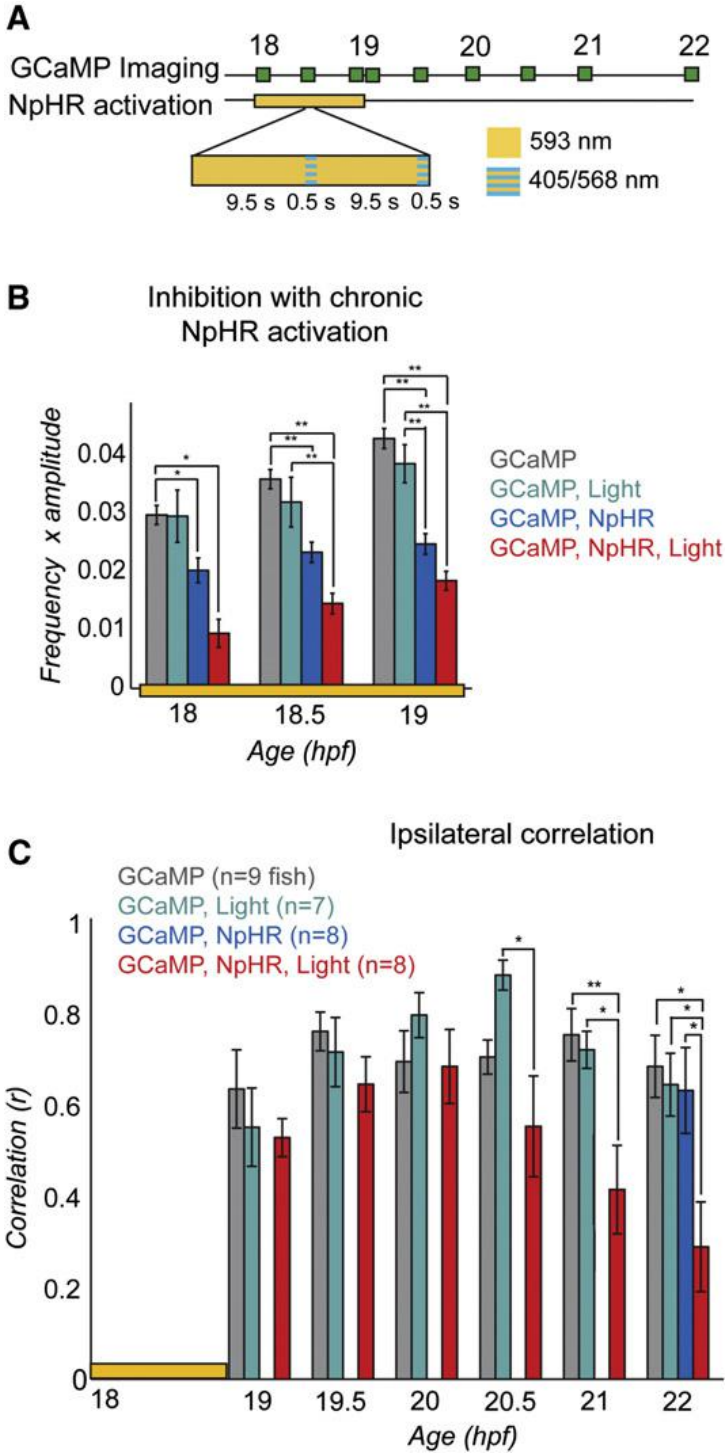

A. Experimental protocol for chronic inhibition experiments. GCaMP movies were acquired during the light manipulation (at 18, 18.5, and 19 hpf) with 488 nm light to determine the effectiveness of the light protocol and at half-hour to hour intervals

thereafter (until 22 hpf) to assess subsequent changes in network dynamics. Stimulation of NpHR was performed from 18 to 19 hpf with continuous 593 nm light at 19 nW/mm^2 interspersed every 10 s with 500 msec long pulses of light simultaneously at two wave-lengths: 405 nm to reduce desensitization of the NpHR and 568 nm to activate it. **B.** The frequency of calcium events from 18 to 19 hpf was quantified for experimental fish expressing NpHR and receiving the yellow light protocol (GCaMP, NpHR, Light) as well as for three kinds of control fish: (1) NpHR-negative fish without yellow/blue light (GCaMP), (2) NpHR-negative fish with yellow/blue light (GCaMP, Light), and (3) NpHR-positive fish without yellow/blue light (GCaMP, NpHR). Means were calculated per cell, n = 13– 385 cells per group. There was a significant effect of group at 18, 18.5, and 19 hpf (one-way ANOVA at each time point, $p < 0.05$), with greatest decreases in the experimental group (red bars; GCaMP, NpHR, Light). The reduction in activity in embryos that expressed NpHR but did not receive the light protocol can be attributed to the activation of NpHR by the 488 nm imaging light. **C.** Average ipsilateral pairwise correlations measured for experimental fish (n = 8) and the three control groups (n = 7 to 9) in movies acquired after the termination of the yellow/blue light protocol reveal a decrease in correlated activity in the experimental fish (GCaMP, NpHR, Light) at later time points compared to all of the controls. There was no difference between groups at 19, 19.5, and 20 hpf (one-way ANOVA at each time point, $p > 0.05$), with significant differences at 20.5, 21, and 22 hpf (one-way ANOVA at each time point, $p < 0.05$). Note that to avoid activation of NpHR in controls without yellow/blue light protocol, GCaMP imaging in this group was only done at 22 hpf. Error bars = SEM. Asterisks in (B) and (C) mark pairwise significance from post hoc comparison with Bonferroni correction (*$p < 0.05$; **$p < 0.01$).

Figure 7. Light Inhibition Decreases the Number of Cells Joining the Correlated Network

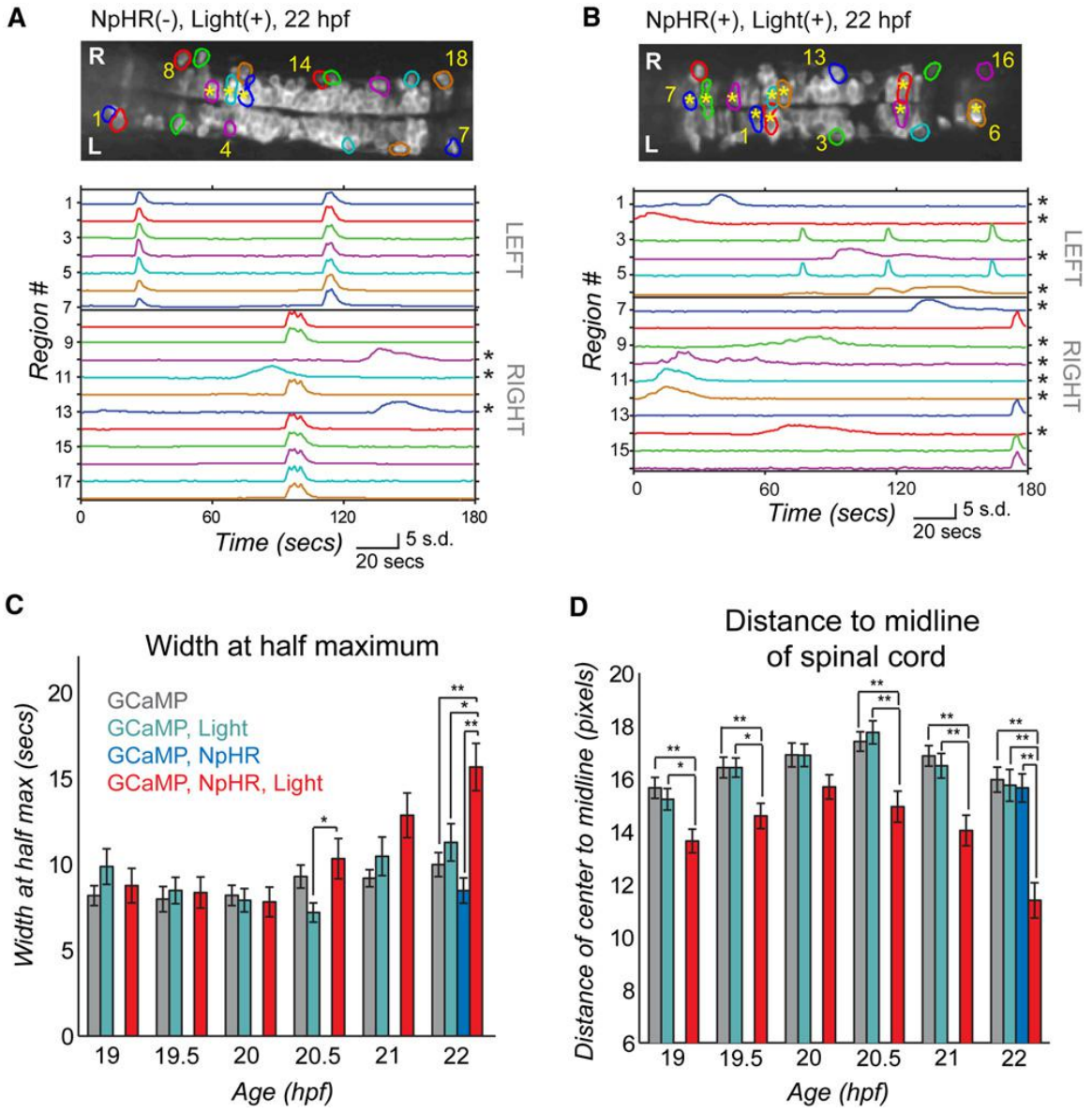

A,B. Baseline GCaMP fluorescence images with active regions circled (top, rostral left) and associated normalized intensity traces (bottom; amplitude plots standard deviation, s.d.) in example control fish (without NpHR but illuminated with yellow/blue light protocol from 18–19 hpf) (A) and experimental fish (with NpHR and illuminated with yellow/blue light protocol from 18–19 hpf) (B) at 22 hpf. Asterisks mark cells with long-duration, uncorrelated events, which increase in number in the experimental fish (B, bottom) and can be seen to reside in the medial spinal cord (B, top). **C.** Average event duration through development was quantified using width at half maximum for experimental fish expressing NpHR and receiving the yellow light protocol (GCaMP, NpHR, Light) and for the three sets of control fish: (1) lacking light and NpHR

expression (GCaMP), (2) lacking NpHR expression (GCaMP, Light) or lacking light (GCaMP, NpHR). There was no difference between groups at 19, 19.5, 20, and 21 hpf (one-way ANOVA at each time point, $p > 0.05$), with significant differences at 20.5 and 22 hpf (one-way ANOVA at each time point, $p < 0.05$), when experimental fish showed increases in event duration. **D.** The distance from the cell center to the midline of the cord for active cells is reduced significantly in the experimental (GCaMP, NpHR, Light) fish compared to the three controls at all ages tested except for 20 hpf (one-way ANOVA at each time point, $p < 0.05$). In (C) and (D), means were calculated per cell (72–137 cells per group). Error bars = SEM. Asterisks in (C) and (D) mark pairwise significance from post hoc comparison with Bonferroni correction ($*p < 0.05$; $**p < 0.01$). See also Figure S6.

References

1. Blankenship, A.G., and Feller, M.B. (2010). Mechanisms underlying spontaneous patterned activity in developing neural circuits. Nat. Rev. Neurosci. *11*, 18–29.
2. Spitzer, N.C. (2004). Coincidence detection enhances appropriate wiring of the nervous system. Proc. Natl. Acad. Sci. USA *101*, 5311– 5312.
3. Torborg, C.L., and Feller, M.B. (2005). Spontaneous patterned retinal activity and the refinement of retinal projections. Prog. Neurobiol. *76*, 213–235.
4. Gust, J., Wright, J.J., Pratt, E.B., and Bosma, M.M. (2003). Development of synchronized activity of cranial motor neurons in the segmented embryonic mouse hindbrain. J. Physiol. *550*, 123–133.
5. Corlew, R., Bosma, M.M., and Moody, W.J. (2004). Spontaneous, synchronous electrical activity in neonatal mouse cortical neurones. J. Physiol. *560*, 377–390.
6. Cre´pel, V., Aronov, D., Jorquera, I., Represa, A., Ben-Ari, Y., and Cossart, R. (2007). A parturition-associated nonsynaptic coherent activity pattern in the developing hippocampus. Neuron *54*, 105–120.
7. Gu, X., Olson, E.C., and Spitzer, N.C. (1994). Spontaneous neuronal calcium spikes and waves during early differentiation. J. Neurosci. *14*, 6325–6335.
8. Nakayama, K., Nishimaru, H., and Kudo, N. (2002). Basis of changes in left-right coordination of rhythmic motor activity during development in the rat spinal cord. J. Neurosci. *22*, 10388–10398.
9. Hanson, M.G., and Landmesser, L.T. (2003). Characterization of the circuits that generate spontaneous episodes of activity in the early embryonic mouse spinal cord. J. Neurosci. *23*, 587–600.
10. Delpy, A., Allain, A.-E., Meyrand, P., and Branchereau, P. (2008). NKCC1 cotransporter inactivation underlies embryonic development of chloride-mediated inhibition in mouse spinal motoneuron. J. Physiol. *586*, 1059–1075.
11. Hanson, M.G., Milner, L.D., and Landmesser, L.T. (2008). Spontaneous rhythmic activity in early chick spinal cord influences distinct motor axon pathfinding decisions. Brain Res. Rev. *57*, 77–85.
12. Gonzalez-Islas, C., and Wenner, P. (2006). Spontaneous network activity in the embryonic spinal cord regulates AMPAergic and GABAergic synaptic strength. Neuron *49*, 563–575.
13. Myers, C.P., Lewcock, J.W., Hanson, M.G., Gosgnach, S., Aimone, J.B., Gage, F.H., Lee, K.F., Landmesser, L.T., and Pfaff, S.L. (2005). Cholinergic input is required during embryonic development to mediate proper assembly of spinal locomotor circuits. Neuron *46*, 37–49.
14. Grillner, S. (2006). Biological pattern generation: the cellular and computational logic of networks in motion. Neuron *52*, 751–766.
15. Tian, L., Hires, S.A., Mao, T., Huber, D., Chiappe, M.E., Chalasani, S.H., Petreanu, L., Akerboom, J., McKinney, S.A., Schreiter, E.R., et al. (2009). Imaging neural activity in worms, flies and mice with improved GCaMP calcium indicators. Nat. Methods *6*, 875–881.

16. Muto, A., Ohkura, M., Kotani, T., Higashijima, S., Nakai, J., and Kawakami, K. (2011). Genetic visualization with an improved GCaMP calcium indicator reveals spatiotemporal activation of the spinal motor neurons in zebrafish. Proc. Natl. Acad. Sci. USA *108*, 5425–5430.
17. Higashijima, S., Masino, M.A., Mandel, G., and Fetcho, J.R. (2003). Imaging neuronal activity during zebrafish behavior with a genetically encoded calcium indicator. J. Neurophysiol. *90*, 3986–3997.
18. Del Bene, F., Wyart, C., Robles, E., Tran, A., Looger, L., Scott, E.K., Isacoff, E.Y., and Baier, H. (2010). Filtering of visual information in the tectum by an identified neural circuit. Science *330*, 669–673.
19. Zhang, F., Wang, L.P., Brauner, M., Liewald, J.F., Kay, K., Watzke, N., Wood, P.G., Bamberg, E., Nagel, G., Gottschalk, A., and Deisseroth, K (2007). Multimodal fast optical interrogation of neural circuitry. Nature *446*, 633–639.
20. Arrenberg, A.B., Del Bene, F., and Baier, H. (2009). Optical control of zebrafish behavior with halorhodopsin. Proc. Natl. Acad. Sci. USA *106*, 17968–17973.
21. Saint-Amant, L., and Drapeau, P. (2001). Synchronization of an embryonic network of identified spinal interneurons solely by electrical coupling. Neuron *31*, 1035–1046.
22. Scott, E.K., Mason, L., Arrenberg, A.B., Ziv, L., Gosse, N.J., Xiao, T., Chi, N.C., Asakawa, K., Kawakami, K., and Baier, H. (2007). Targeting neural circuitry in zebrafish using GAL4 enhancer trapping. Nat. Methods *4*, 323–326.
23. Wyart, C., Del Bene, F., Warp, E., Scott, E.K., Trauner, D., Baier, H., and Isacoff, E.Y. (2009). Optogenetic dissection of a behavioural module in the vertebrate spinal cord. Nature *461*, 407–410.
24. Park, H.-C., Shin, J., and Appel, B. (2004). Spatial and temporal regulation of ventral spinal cord precursor specification by Hedgehog signaling. Development *131*, 5959–5969.
25. Saint-Amant, L., and Drapeau, P. (1998). Time course of the development of motor behaviors in the zebrafish embryo. J. Neurobiol. *37*, 622–632.
26. Saint-Amant, L., and Drapeau, P. (2000). Motoneuron activity patterns related to the earliest behavior of the zebrafish embryo. J. Neurosci. *20*, 3964–3972.
27. Mukamel, E.A., Nimmerjahn, A., and Schnitzer, M.J. (2009). Automated analysis of cellular signals from large-scale calcium imaging data. Neuron *63*, 747–760.
28. Masino, M.A., and Fetcho, J.R. (2005). Fictive swimming motor patterns in wild type and mutant larval zebrafish. J. Neurophysiol. *93*, 3177–3188.
29. Kimmel, C.B., Ballard, W.W., Kimmel, S.R., Ullmann, B., and Schilling, T.F. (1995). Stages of embryonic development of the zebrafish. Dev. Dyn. *203*, 253–310.
30. Bernhardt, R.R., Chitnis, A.B., Lindamer, L., and Kuwada, J.Y. (1990). Identification of spinal neurons in the embryonic and larval zebrafish. J. Comp. Neurol. *302*, 603–616.
31. Kuwada, J.Y., and Bernhardt, R.R. (1990). Axonal outgrowth by identified neurons in the spinal cord of zebrafish embryos. Exp. Neurol. *109*, 29–34.

32. Deliagina, T.G., Zelenin, P.V., and Orlovsky, G.N. (2002). Encoding and decoding of reticulospinal commands. Brain Res. Rev. *40*, 166–177.
33. Hegemann, P., Oesterhelt, D., and Bamberg, E. (1985). The transport activity of the light-driven chloride pump halorhodopsin is regulated by green and blue light. Biochimica et Biophysica Acta (BBA) - Biomembranes *819*, 195–205.
34. Ren, J., and Greer, J.J. (2003). Ontogeny of rhythmic motor patterns generated in the embryonic rat spinal cord. J. Neurophysiol. *89*, 1187– 1195.
35. O'Donovan, M., Ho, S., and Yee, W. (1994). Calcium imaging of rhythmic network activity in the developing spinal cord of the chick embryo. J. Neurosci. *14*, 6354–6369.
36. Ashworth, R., and Bolsover, S.R. (2002). Spontaneous activity-independent intracellular calcium signals in the developing spinal cord of the zebrafish embryo. Dev. Brain Res. *139*, 131–137.
37. Milner, L.D., and Landmesser, L.T. (1999). Cholinergic and GABAergic inputs drive patterned spontaneous motoneuron activity before target contact. J. Neurosci. *19*, 3007–3022.
38. Syed, M.M., Lee, S., Zheng, J., and Zhou, Z.J. (2004). Stage-dependent dynamics and modulation of spontaneous waves in the developing rabbit retina. J. Physiol. *560*, 533–549.
39. Yuste, R., Peinado, A., and Katz, L.C. (1992). Neuronal domains in developing neocortex. Science *257*, 665–669.
40. Downes, G.B., and Granato, M. (2006). Supraspinal input is dispensable to generate glycine-mediated locomotive behaviors in the zebrafish embryo. J. Neurobiol. *66*, 437–451.
41. Komuro, H., and Rakic, P. (1996). Intracellular Ca2+ fluctuations modulate the rate of neuronal migration. Neuron *17*, 275–285.
42. Gu, X., and Spitzer, N.C. (1995). Distinct aspects of neuronal differentiation encoded by frequency of spontaneous Ca2+ transients. Nature *375*, 784–787.
43. Desarmenien, M.G., and Spitzer, N.C. (1991). Role of calcium and protein kinase C in development of the delayed rectifier potassium current in Xenopus spinal neurons. Neuron *7*, 797–805.
44. Crisp, S.J., Evers, J.F., and Bate, M. (2011). Endogenous patterns of activity are required for the maturation of a motor network. J. Neurosci. *31*, 10445–10450.

CHAPTER 3

A Spinal Opsin Controls Early Neural Activity and Drives a Behavioral Light Response

Current Biology (2015) 25, 69-74

LINKER STATEMENT

Of note at this junction are some additional findings observed over the course of the previous study. We believed these to be artifactual at the time, but the work presented in the following chapter explains and builds on the activity dependent effects observed in Chapter 2. For example, the chronic illumination experiments required careful controls and properly calibrated light sources, given that we observed effects from the light itself. Similarly, we often observed a paucity of calcium events during the first 30 seconds of any given 1-photon confocal recording of calcium activity from a dark-adapted fish. At the time, these quirks were unexplained, but we now believe they are downstream of an opsin we've identified in the spinal cord.

In this chapter we outline the discovery of the earliest known photobehavior in the zebrafish—an inhibition of spontaneous coiling behavior. We identify the opsin responsible and determine the sufficiency of the spinal cord for driving the photobehavior. Lastly, we are able to characterize this opsin's ability to couple to the $G\alpha_l$ pathway in a heterologous system.

A Spinal Opsin Controls Early Neural Activity and Drives a Behavioral Light Response

Drew Friedmann,[1] Adam Hoagland,[1] Shai Berlin,[1,2] and Ehud Y. Isacoff[1,2,3]

[1]Department of Molecular and Cell Biology, University of California, Berkeley, Berkeley, CA 94720, USA
[2]Helen Wills Neuroscience Institute, University of California Berkeley, Berkeley, CA 94720, USA
[3]Physical Bioscience Division, Lawrence Berkeley National Laboratory, Berkeley, CA 94720, USA

Acknowledgements: We thank H. Nolla and the Berkeley Flow Cytometry Core for assistance with FACS, Y.G. Choi, J. Ngai, and the Berkeley Functional Genomics Laboratory for assistance and guidance with RNA-seq. This work used the Vincent J. Coates Genomics Sequencing Laboratory at UC Berkeley, supported by NIH S10 Instrumentation Grants S10RR029668 and S10RR027303. We also thank D. Kojima (University of Tokyo, Japan) for providing VALopA cDNA, N. Dascal (Tel Aviv University, Israel) for providing GIRK1, GIRK2, and $G\alpha_{13}$, E. Reuveny (Weizmann Institute, Israel) for providing PTX-S1, and L. Looger (Janelia Farm) for making GCaMP5 available. This work was supported by the NIH Nanomedicine Development Center for the Optical Control of Biological Function (2PN2EY01824) and the Human Frontier Science Program (RGP0013/2010).

Abstract

Non-visual detection of light by the vertebrate hypothalamus, pineal, and retina is known to govern seasonal and circadian behaviors [1]. However, the expression of opsins in multiple other brain structures [2-4] suggests a more expansive repertoire for light-regulation of physiology, behavior, and development. Translucent zebrafish embryos express extra-retinal opsins early on [5, 6], at a time when spontaneous activity in the developing central nervous system plays a role in neuronal maturation and circuit formation [7]. Though the presence of extra-retinal opsins is well documented, the function of direct photoreception by the central nervous system remains largely unknown. Here we show that early activity in the zebrafish spinal central pattern generator (CPG) and the earliest locomotory behavior are dramatically inhibited by physiological levels of environmental light. We find that the photo-sensitivity of this circuit is conferred by vertebrate ancient long opsin (VALopA), which we show to be a $G\alpha_i$-coupled receptor that is expressed in the neurons of the spinal network. Sustained photo-activation of VALopA not only suppresses spontaneous activity but also alters the maturation of time-locked correlated network patterns. These results uncover a novel role for non-visual opsins and a mechanism for environmental regulation of spontaneous motor behavior and neural activity in a circuit previously thought to be governed only by intrinsic developmental programs.

Results and Discussion

During the development of the nervous system, the first incidence of neural activity often occurs before sensory experience [7]. The frequency and pattern of this spontaneously generated activity guide neuronal differentiation, axon pathfinding, and synapse formation in many species and brain regions, including retina [8, 9], cortex [10, 11], hippocampus [12, 13], and spinal cord [14-17]. Since these activity networks are robust and stereotyped, we were surprised to find that spontaneous behavior, exhibited by embryonic zebrafish during the formation of its spinal central pattern generator (CPG), is heavily regulated by an unexpected external stimulus: light. Coiling behavior (Figure 1A and movie S1), a pre-locomotory behavior that is driven by spontaneous CPG activity [18, 19], was dramatically suppressed by illumination with green light (508 nm at 13.2 $\mu W/mm^2$) (Figure 1B). In dark-adapted fish at 22.5 hours post fertilization (hpf), coiling ceased within 1.7 ± 1.4 seconds of the start of illumination and the suppression persisted during a 2-minute period of constant illumination (Figure 1C and 1D, top). The light-induced suppression was also seen several hours later (27 hpf), but was preceded by a brief and transient phase of increased activity, as described recently [20] (Figure 1D, bottom). A systematic examination over early development revealed that photo-inhibition is present as soon as motor activity begins (Figure 1E and S1A).

Coiling was suppressed by light over a broad range of wavelengths, with a behavioral response λ_{max} at 504 nm (Figure 1F) and was inhibited by flashes of light as short as 70 msec (Figure 1G and S1E). The suppression lasted long after the termination of a light pulse, recovering to baseline dark-frequency over minutes ($t_{1/2}$ = 165 ± 21 seconds, n = 96) (Figure S1B). When illumination continued for minutes, the

suppression of coiling partly adapted, relaxing to 43.0 ± 2.5% (n = 96) of the dark-adapted frequency (Figure S1C). Recovery from the light-adapted state also required minutes, similar to the recovery from a brief (2 s) light-exposure (Figure S1C, D), demonstrating that the rate of recovery is independent of the extent of the inhibition and implying that the recovery from different light regimes engages similar signaling cascades. This also shows that the rapid freezing behavior is a genuine light-dependent response, rather than a non-specific reaction to an abrupt contrast change, such as the reversion to darkness following light adaptation (Figure S1C).

Since, at these early ages, zebrafish are blind because photoreceptors and retinal circuitry have not yet developed [21], we wondered if the photo-inhibition of coiling could reflect an intrinsic property of the CPG network. The nascent CPG resides entirely within the spinal cord, requiring putative pacemaker neurons in the most rostral somites, but not the hindbrain [22, 23]. We hypothesized that the calcium activity in the CPG network should therefore also be affected by light. Of the four earliest active cell types—ipsilateral-caudal projecting pacemakers (ICs), primary motor neurons (PMNs), ventral longitudinal descending interneurons (VeLDs), and sensory-driven contralaterally projecting ascending neurons (CoPAs)—the PMNs and VeLDs are contained within the 1020:Gal4 enhancer trap transgenic line [18, 22-26]. We used the genetically encoded calcium indicator GCaMP5 [27] to examine the effect of light on the activity of these cells (Figure 2A, left). To minimize potential photo-inhibition during calcium imaging, we excited GCaMP5 with 2-photon (2P) illumination at 920 nm. Under this condition, we observed spontaneous calcium events in 1020:Gal4^{+} neurons at a frequency of 6.8 ± 0.7 events/min (n = 10 fish) (Figure 2A, black trace). The frequency was reduced by about half when excitation of GCaMP5 was switched to 1-photon (1P) illumination at 488 nm (3.6 ± 0.5 events/min; n = 10 fish) (Figure 2A, gray trace). Akin to the photo-inhibition of coiling behavior, neural activity at the end of the first day of development responded to a 5 second stimulus of 561 nm light with a sustained reduction in the frequency of calcium events (e.g. 24 hpf Figure 2B and 2C), and the inhibition was also induced by the blue-green portion of the visible spectrum (Figure 2D). Interestingly, ipsilateral correlation and contralateral alternation were not affected (Figure 2B and S2A), suggesting that acute light stimulation slows, rather than disrupts, natural behavior.

Detectable photo-inhibition of neural activity became evident at 20.5 hpf, shortly after activity in the network reaches its peak frequency (Figure 2C and S2B). As compared to photo-inhibition of coiling, the effect on neural activity appeared later and of smaller magnitude (compare with Figure 1E and S1A). These differences may arise from the methodological difference between whole-animal illumination, used to study coiling, and very localized illumination, as is done in GCaMP experiments. During Ca^{2+}-imaging, only somites 3-8 received the light stimulus—a fraction of the spinal cord, and missing the most mature, rostral portion of the spinal circuit. Nevertheless the photo-inhibition of neuronal activity by local illumination indicates that somites 3-8 of the spinal cord contain a light sensor that suppresses spontaneous activity.

Between 17 and 20 hpf, newly active neurons join into a circuit formed by ipsilaterally projecting interneurons and switch their pattern of activity from irregular, long, and isolated events to bursts of short events that are correlated among electrically coupled cells on the same side of the cord [18, 26]. By 22 hpf, most active 1020:Gal4$^+$ neurons have joined the CPG network, while a small group of cells display long-duration and uncorrelated activity [17, 26]. Previously, inhibition of early activity was shown to increase the fraction of the uncorrelated cells with long calcium events [26]. We found here that inhibiting activity before 20 hpf via global illumination with green light similarly resulted in a significantly higher percentage of active cells with long-duration, non-correlated calcium events at 22 hpf (Figure 2E, dashed area).

In an effort to identify genes whose protein products are involved in inhibition of the spinal CPG, we used fluorescence-activated cell sorting to purify fluorescent protein-expressing cells labeled by the UAS promoter when crossed to 1020:Gal4$^+$ fish (Figure S3A). Cells from trunk and tail samples of 20 hpf reporter fish were isolated, total RNA extracted, and RNAseq analysis performed [28]. We compared gene expression levels from the 1020:Gal4$^+$ subpopulation of neurons to those labeled in the pan-neuronal HuC:Gal4 line. Among the transcripts whose expression was elevated in 1020:Gal4$^+$ neurons was an extraretinal photoreceptor, namely vertebrate ancient long opsin A (VALopA), an evolutionary intermediate between invertebrate opsins and vertebrate visual photoreceptors [29]. Other genes with elevated expression in 1020:Gal4$^+$ neurons included known ventral spinal cord and motor neuron markers, as well as *olig2*, the genomic insertion site of the 1020:Gal4 enhancer trap [25] (Figure S3B, C). VALopA appeared to be a good candidate photoreceptor for inhibition of the spinal CPG based on its known presence in the spinal cord at 24 hpf and its previously described absorbance spectrum (λ_{max} = 510 nm) [5].

To test the hypothesis that VALopA is the photoreceptor mediating spinal CPG photo-inhibition, we used morpholino knockdown of VALopA expression [20]. The morpholino for VALopA, but not the scrambled control, completely abolished the inhibitory photoresponse in both young and older fish (Figure 3A-C and movie S2). At later ages, when transient photo-excitation preceded photo-inhibition (Figure 3D), VALopA knockdown selectively abrogated the sustained photo-inhibition (Figure 3B). Thus, photo-inhibition develops concurrently with coiling, is elicited by spinal illumination alone, and requires VALopA. Conversely, photo-excitation develops later, is elicited by hindbrain illumination, and is independent of VALopA, in agreement with a recent report [20]. In order to determine whether photo-activation of VALopA in 1020:Gal4$^+$ neurons is sufficient to drive inhibition, we mosaically expressed UAS-VALopA with a cerulean fluorescent marker in 1020:Gal4$^+$ fish whose VALopA expression was knocked down by the splice-blocking morpholino. Photo-inhibition was seen only when the rescue construct was broadly expressed, and the degree of photo-inhibition increased with the expression level of the CFP marker, reporting higher expression levels of VALopA (Figure 3E, F).

To better understand the mechanism of photo-inhibition, we attempted to identify the intracellular signaling pathway that is activated by VALopA. We

heterologously expressed zebrafish VALopA in *Xenopus laevis* oocytes and performed two-electrode voltage clamp recordings. Oocytes had no native light response, nor did injection of cRNA encoding VALopA on its own introduce a detectable light response (Figure 4A). However, co-injection of cRNAs encoding $VALopA_{GFP}$ and the neuronal G-protein activated inward rectifying potassium (GIRK) channel subunits ($GIRK1_{mCherry}$/GIRK2) (Figure S4A), yielded a large photo-current. Increasing external $[K^+]$ from 2 to 24 mM generated an inward current (Figure 4A, B), as is typical of basal activation of GIRK by free native Gβγ in the oocyte [30]. Illumination with 535 nm light evoked an additional increase in current amplitude above basal level (Figure 4A, B and S4B), as is observed with ligand activation of the $G\alpha_i$ class of G protein coupled receptors (GPCRs), such as the acetylcholine-activated muscarinic-2 receptor m2R [31] (Figure S4D-F). Unlike activation of other GPCRs, the combined current persisted without decay for tens of seconds after the light was turned off (Figure 4A and S4B). Inward currents were blocked by the GIRK-channel blocker Ba^{2+}, further confirming that the light-induced currents are GIRK-mediated. These data suggest that VALopA is a $G\alpha_i$-coupled GPCR that turns off very slowly. In support of this, the photo-current was inhibited by expression of the specific $G\alpha_i$-inactivating pertussis toxin (PTX), even when co-expressed with additional wildtype $G\alpha_{i3}$ (Figure 4C, D). Moreover, PTX-insensitive $G\alpha_{i3}$ (C351I) [32] faithfully restored the photo-current in the presence of PTX (Figure 4C, D). As observed with the suppression of coiling behavior in zebrafish, GIRK current in oocytes could be triggered by very brief flashes of light (as short as 5 ms) and, as mentioned above, persisted for minutes afterwards in the dark (Figure S4C). Together, these findings indicate that VALopA couples to the $G\alpha_i$ pathway and suggest that the slow kinetics of this signaling can explain the kinetics of the light-induced inhibition of spontaneous activity and behavior in zebrafish.

Early optogenetics experiments demonstrated the ability of rat rhodopsin to couple to $G\alpha_i$ and inhibit spontaneously active networks in chick spinal cord [33]. We show that in fish, VALopA photo-inhibition similarly influences early activity before the onset of touch, sound, or visual responses, making it the earliest sensory input to the zebrafish spinal cord. At these early ages, spontaneous activity is an important developmental determinant before circuits, synapses, and cell fates are finalized [14-16, 26, 34, 35]. Whereas some activity-dependent processes require competition between neurons, global activity levels were recently shown to regulate transmitter fate in *Xenopus* through the regulation of secreted brain-derived neurotrophic factor [35]. Indeed, we find that global photo-inhibition in early zebrafish affects the distribution of subsequent activity patterns in the locomotory CPG, perhaps reflecting a mechanism by which the light-dark cycle can sculpt early development. It is also conceivable, by analogy to the function of a VALopA homolog in ascidian larvae [36, 37] and an extraretinal photoreceptor in *Drosophila* larvae [38], that VALopA mediates a photo-sensitive avoidance behavior. At sunrise in the wild, embryos will be at varying stages of development depending on spawning time and water temperature [39, 40]. The consistent inhibition by VALopA across these ages could drive a freezing behavior in bright light that eludes predators at a time when the

embryo is trapped in the chorion and before sensory-evoked escape behavior emerges. The uneven timing of development and sunrise could also affect activity-driven processes in an age-dependent fashion, but it is unknown if this would diversify or synchronize the relationship between development and the photoperiod. It will be interesting to see if spontaneously active circuits in other brain regions are similarly flexible to environmental regulation and also if non-visual opsins can acutely control behavior in other vertebrates.

Figure 1. Effect of light on frequency of spontaneous coiling behavior.

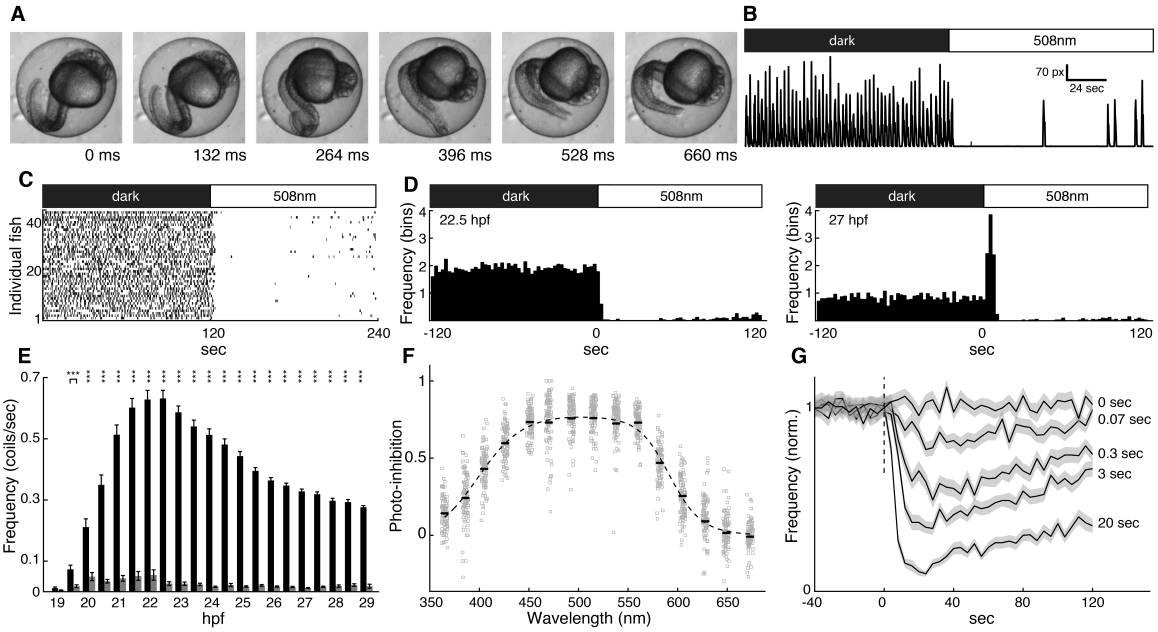

A. Still frames from a movie of a single spontaneous coil in a 27 hpf embryo. **B.** Trace of detected motion (pixel changes) from video of an individual embryo before (dark) and during (508 nm) illumination; peaks represent individual coiling events. **C.** Raster plot of coiling events measured simultaneously in 44 dark-adapted 22.5 hpf embryos under dark and light conditions. **D.** Left, peri-stimulus time histogram of 22.5 hpf embryos from data in (C). Right, histogram of the same fish at 27 hpf. Frequency = mean coils/fish within bins of 2.4 sec. **E.** Mean baseline coiling frequencies (coils/sec) in the dark (black bars) and under green light (gray bars) over developmental time. Two-tailed paired *t* test with Bonferroni adjusted p-values, *** $p < 0.001$; n = 39-75. **F.** Photo-inhibition [$-(Hz_{Light}-Hz_{Dark})/Hz_{Dark}$; coiling measured over 120 sec in each condition] as a function of wavelength. Gray squares are individual responses < 3 s.d. from each mean (black lines). Light power = 133-159 nW/mm^2; n = 96. **G.** Photo-inhibition of coiling frequency by light flashes of indicated durations. Lines indicate normalized mean, bins = 4 sec; s.e.m. in grey; n = 96.

Figure 2. Acute and delayed effects of light on neural activity.

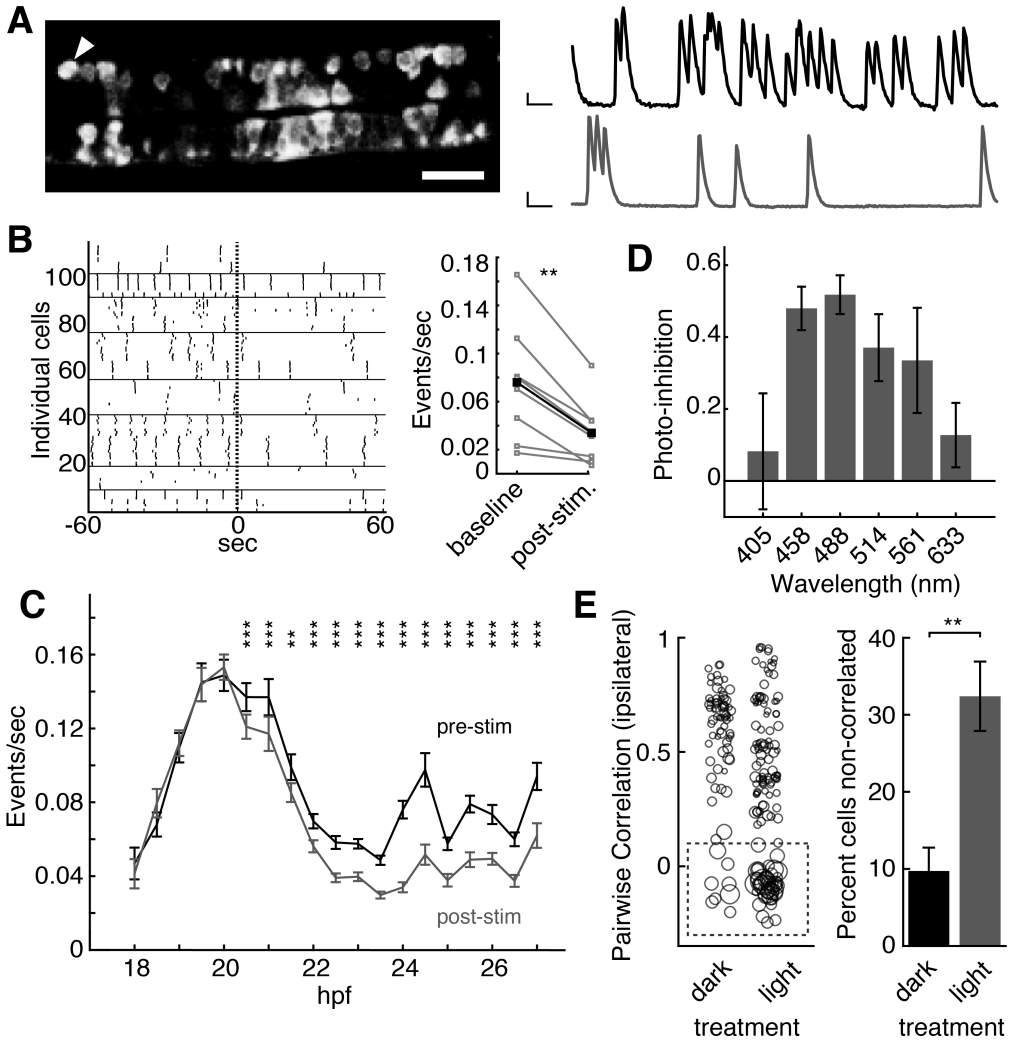

A. Left, image of GCaMP5 fluorescence in ventral spinal cord somites 3-8 of a 1020:Gal4; UAS:GCaMP5 embryo. Scale bar = 20 μm. Right, calcium traces from one cell (arrowhead in image) under 2P (black trace, 920 nm) or subsequent period of 1P (gray trace, 488 nm) excitation, following < 5 sec interval. Axes: 100% ΔF/F, 10 sec. **B.** Left, raster plot of 2P-imaged calcium events in 24 hpf embryos before and after a 5 sec flash (dashed line) with 561 nm light. Measurements from each of 8 fish (horizontal lines delineate individual fish). Right, quantification of calcium event frequency in the 8 fish (grey lines; mean = black line) during a 180 sec period under 2P excitation (baseline) and over 60 sec following the 561 nm light flash (post-stim.). Two-tailed paired *t* test $p < 0.01$. **C.** Frequency of calcium events over 9 hours of development measured under 2P excitation before (pre-stim) and after (post-stim.) a 5 sec 561 nm light flash, as quantified in (B). Two-tailed paired *t* test, Bonferroni adjusted p-values, *** $p < 0.001$, ** $p < 0.01$; *n* = 21-123 cells from 4-8 fish at each age. **D.** Photo-inhibition after illumination with a 5 sec light flash at varying

wavelengths. 103-110 μW/pixel; *n* = 16 cells in 8 fish at each wavelength. **E.** Left, pairwise ipsilateral correlations between cells in 22 hpf embryos following dark or light (508 nm, 13.2 $\mu W/mm^2$) rearing for 2 hours before 20 hpf. Circle size proportional to event width at half max amplitude (range = 1.8-75.7 sec). Dashed box demarcates non-correlated cells. Right, percentage of non-correlated cells (ipsilateral correlation < 0.1) at 22 hpf. Two-tailed unpaired *t* test, p = 0.004. *n* = 6 (dark) and 8 fish (light).

Figure 3. Light inhibition of coiling depends on an extraretinal opsin.

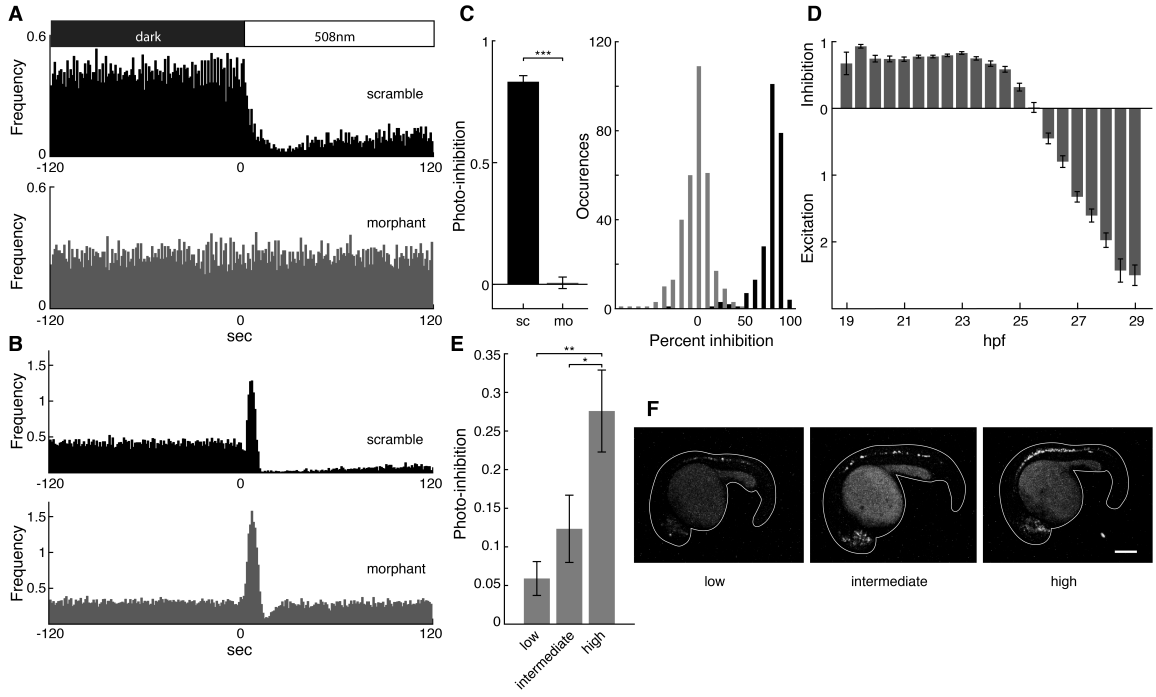

A,B. Representative peri-stimulus time histograms of coiling frequency (events/sec; mean across 6 trials; bin = 1 sec) of embryos at 22-25 hpf (A) or 27-31 hpf (B). Zygotes injected with scrambled control morpholino (*n* = 23 in (A), 34 in (B)) (black) or morpholino against VALopA (*n* = 24 in (A), 41 in (B)) (gray). **C.** Left, mean photo-inhibition of scrambled control morpholino (sc; *n* = 40) and morpholino (mo; *n* = 55) injected 22-25 hpf embryos. Two-tailed unpaired *t* test, $p < 0.001$. Right, frequency distribution of percent photo-inhibition (6 responses per fish) in scrambled control morpholino embryos (black) and morpholino embryos (gray). **D.** Normalized inhibition or excitation of coiling frequency $[-(Hz_{Light}-Hz_{Dark})/Hz_{Dark}]$ in first 12 sec after light onset relative to a 120 sec preceding baseline in darkness (*n* = 39-75). **E.** Mean photo-inhibition (5 responses per fish) of morpholino-injected embryos mosaically expressing low, intermediate, or high levels of a VALopA rescue construct with a mCerulean marker. One-way ANOVA with Tukey *post hoc* analysis, * $p < 0.05$, ** $p < 0.01$; *n* = 59 (low), 18 (intermediate), and 11 (high). **F.** Images of representative embryos expressing low, intermediate, and high levels of mCerulean fluorescence. Scale bar = 200 μm.

Figure 4. VALopA couples to $Ga_{i/o}$ in *Xenopus* oocytes.

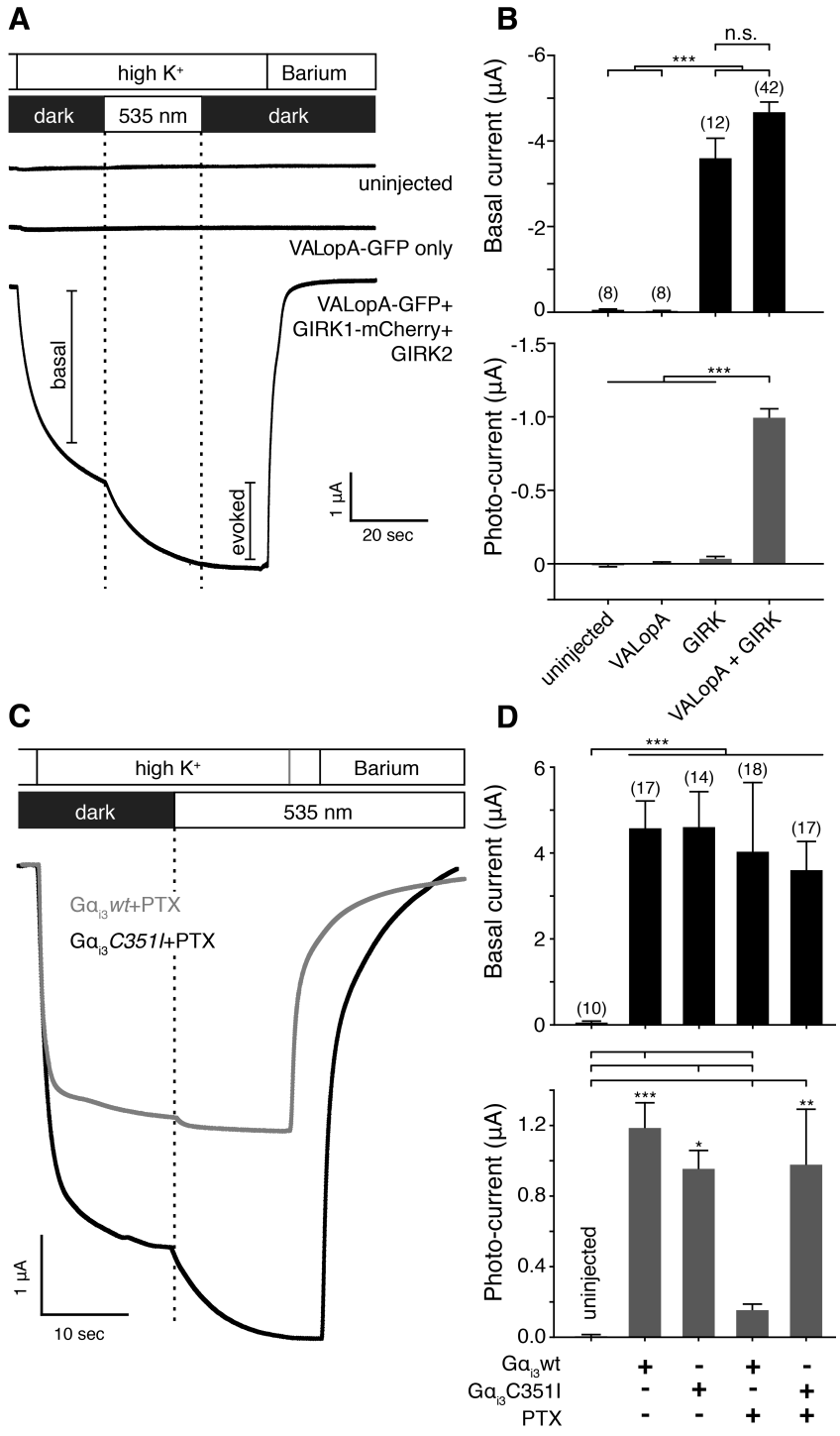

A. Representative voltage clamp currents from an uninjected oocyte (top trace), an oocyte expressing zebrafish $VALopA_{GFP}$ alone (middle trace), or co-expressing $VALopA_{GFP}$ with $GIRK1_{mCherry}$ and GIRK2. Oocytes are initially bathed in ND96, switches to 24 mM K^+ (high K^+), and then 5 mM Ba^{2+} in 24 mM K^+ (Barium).

Illumination through a 535/50 nm bandpass filter (~70 mW/mm^2) is indicated. **B.** Summary for the basal (top) and light-evoked (bottom) GIRK currents as in (A). **C.** Representative currents (protocols as in (A)) from oocytes expressing VALopA$_{GFP}$, GIRK1$_{mCherry}$ and GIRK2 with the catalytic subunit of pertussis toxin, (PTX-S1) and either PTX-sensitive Gα_{i3}-*wt* (gray) or PTX-insensitive C351I mutant Gα_{i3} (black). **D.** Summary for the basal (top) and light-evoked (bottom) GIRK currents in oocytes expressing combinations of Gα_{i3}-*wt*, Gα_{i3}-C351I, and PTX. One-way ANOVA with Tukey *post hoc* analysis * $p < 0.05$, ** $p < 0.01$, *** $p < 0.001$; *n* is indicated above bars.

Figure S1. Effect of light on frequency of spontaneous coiling behavior.

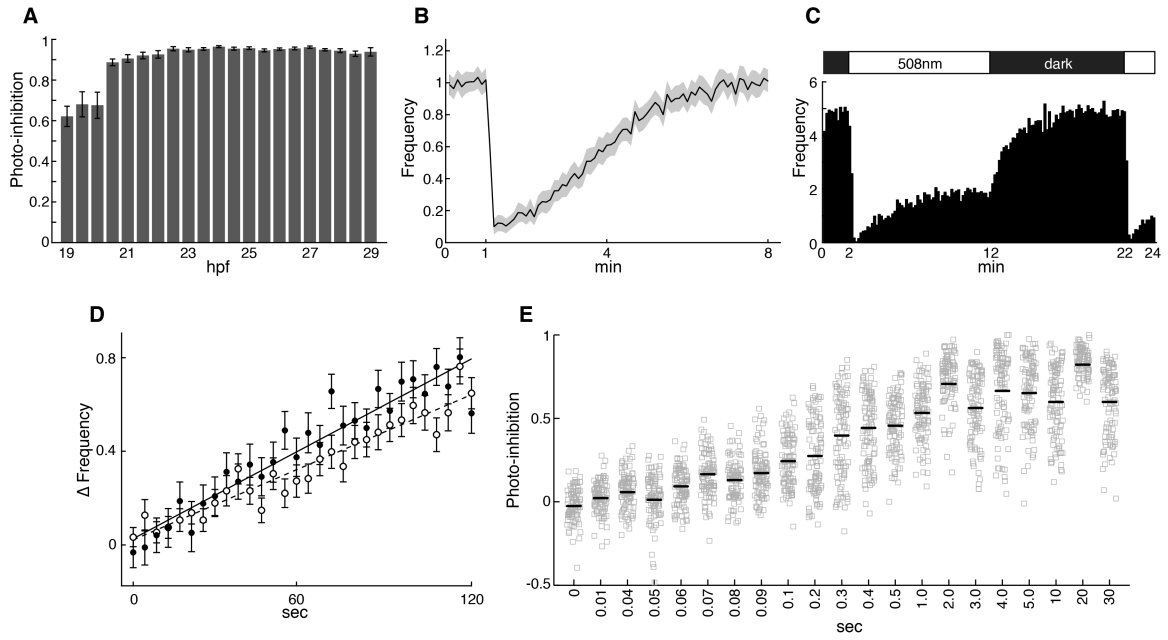

A. Mean photo-inhibition $-(Hz_{Light}-Hz_{Dark})/Hz_{Dark}$ for the ages sampled in Fig. 1E. *n* = 39-75. **B.** Photo-inhibitory response to a 2 sec light stimulus delivered at 1 min. Black line is the normalized mean coils/fish in bins of 6 sec. Shaded region represents the 95% confidence interval; *n* = 96. **C.** Peri-stimulus time histogram of coiling frequency during adaptation to light and dark, bin = 12 sec, *n* = 48. **D.** Recovery from photo-inhibition in the dark following 10 min of light (as in (C), filled circles), $R^2 = 0.91$ or a 2 sec flash (as in (B), open circles), $R^2 = 0.92$. Bin size = 4 sec; *n* = 96. **E.** Photo-inhibition as a function of flash duration. Hz_{Dark} calculated from 120 sec dark activity and Hz_{Light} measured from the first 60 sec after light onset. Gray squares are individual fish < 3 s.d. from each mean (black lines), *n* = 96. Inhibition by stimuli ≥ 60 msec are significantly above a control group without light treatment, one-way ANOVA with Dunnett *post hoc* test, $p < 0.001$.

Figure S2. Effects of light on neural activity through development.

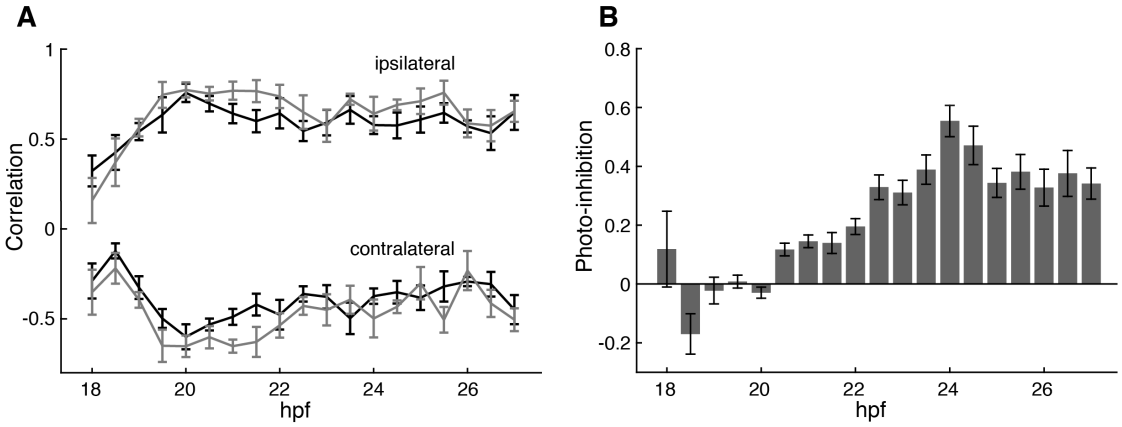

A. Mean pairwise correlations of active cells before (black) and after (gray) light stimulus. Two-tailed paired *t* test, Bonferroni adjusted p-value, $p > 0.05$ at all ages. *n* = 21-123 cells from 4-8 fish at each age. **B.** Mean photo-inhibition for the ages sampled in Fig 2C. *n* = 21-123 cells from 4-8 fish at each age.

Figure S3. FACS and RNA-Seq of spinal neurons.

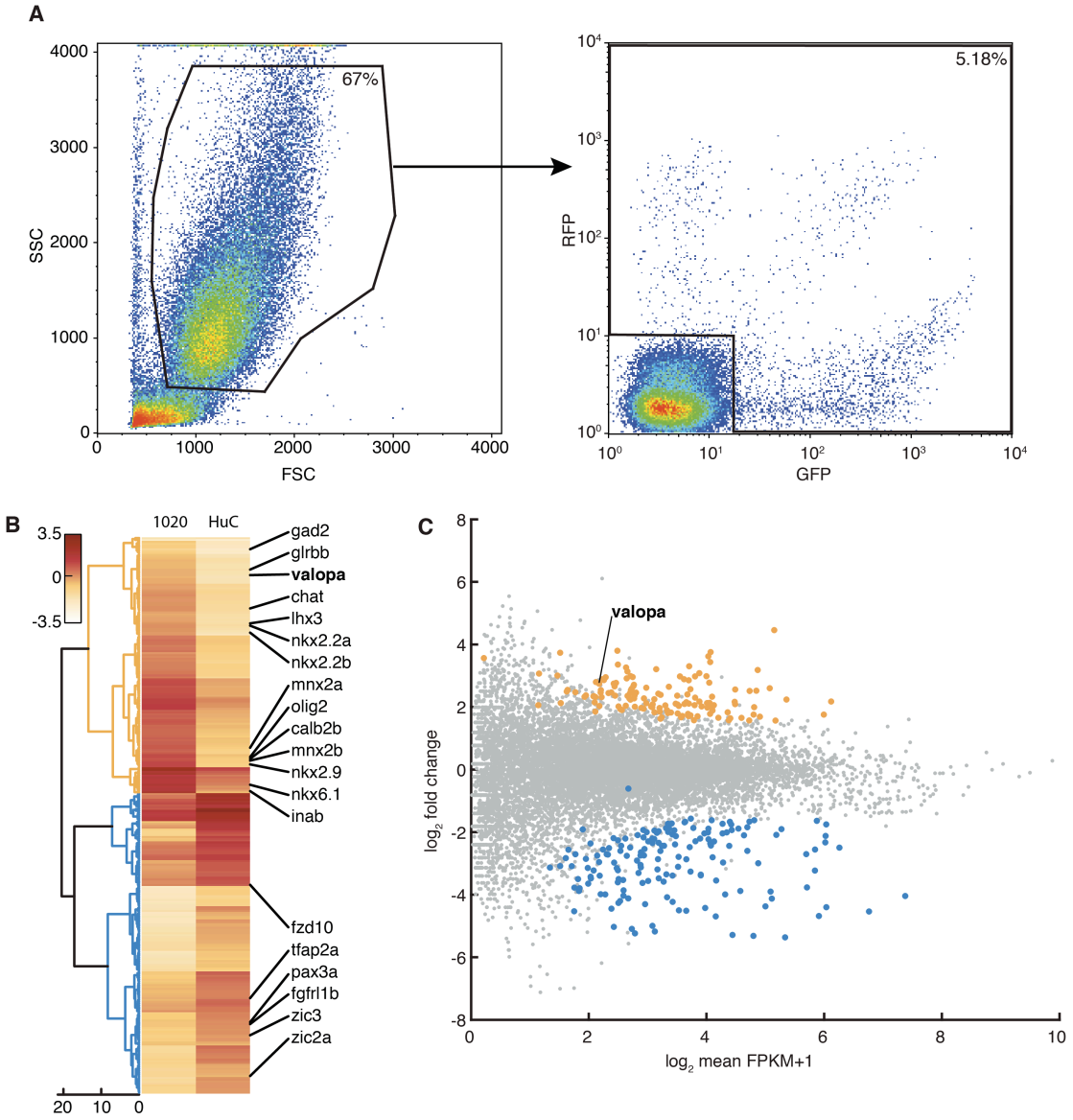

A. Left, representative flow cytometry dot plot of forward scatter and side scatter of cells dissociated from embryonic trunk and tail (see methods). Right, subgated red and green fluorescent positive cells from the 1020:Gal4^{+} population. *n* = 58 tails. **B.** Heatmap of the z-score of $\log_2$(FPKM+1) values from 300 differentially expressed genes. Columns represent the fluorescent sorted population of cells from each transgenic line. Colored branches of the dendrogram (Ward's method) correspond to marker color in (C). **C.** Scatter plot of $\log_2$ fold difference in expression of 11,910 transcripts as a function of the mean expression level. Orange and blue markers represent the genes displayed in the heat map in (B) and correspond to elevated expression in the 1020:Gal4^{+} and HuC:Gal4^{+} populations respectively.

Figure S4. VALopA couples to $Ga_{i/o}$ in *Xenopus* oocytes.

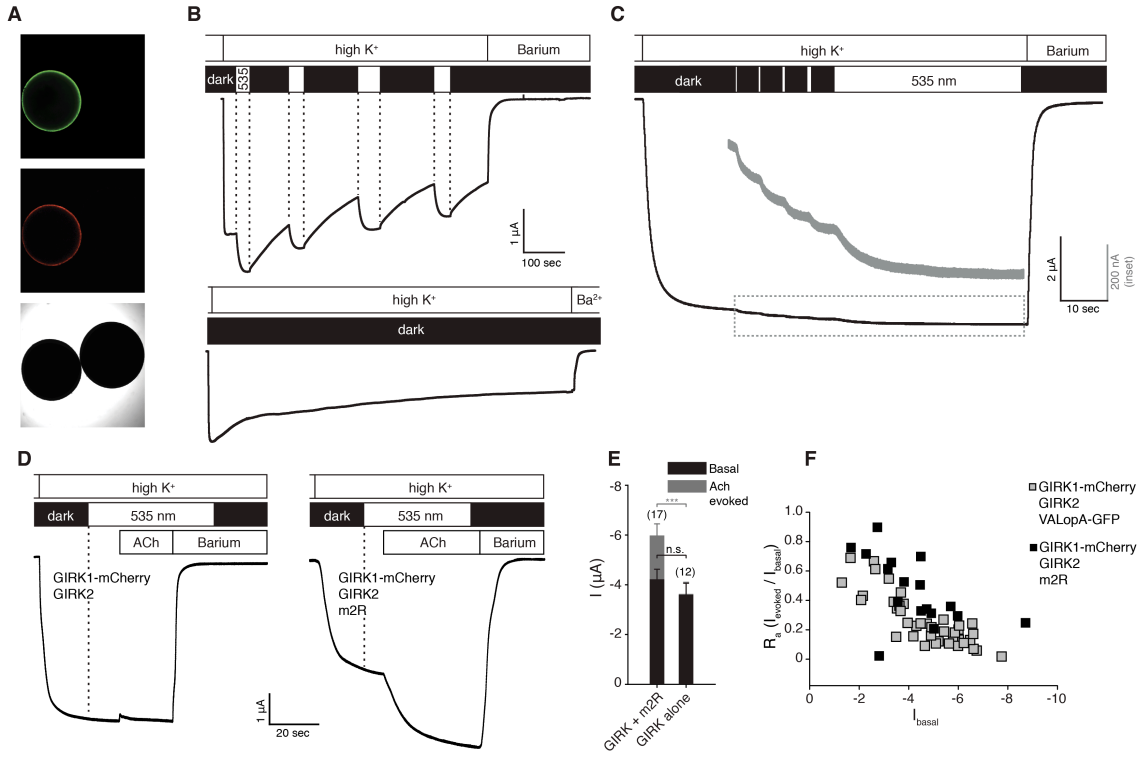

A. Membrane expression of $VALopA_{GFP}$ (green) and $GIRK1_{mCherry}$ (red) seen in a co-expressing oocyte, compared to no visible signal in an uninjected oocyte, which is only seen in transmitted light (bottom). **B.** Top, representative current in response to repeated photo-stimulation of $VALopA_{GFP}$ in an oocyte co-expressing $GIRK1_{mCherry}$ and GIRK2. Despite the relaxation of the basal current over the course of minutes, noticeable and repetitive currents can be evoked by light. Bottom, similar relaxation of the basal current is observed in an oocyte in high K^+ with no light stimulus. **C.** Representative photo-currents in response to incrementing light flash durations. Gray inset, zoom of the dashed box. Flash durations (in sequence) = 5, 10, 15 and 25 msec, $n = 6$. **D.** Representative currents showing basal and 10 µM acetylcholine-evoked currents in oocytes expressing $GIRK1_{mCherry}$ and GIRK2 (left) or $GIRK1_{mCherry}$, GIRK2, and acetylcholine muscarinic-2 receptor (m2R) (right). Light does not induce any response in these oocytes. **E.** Summary for the basal and acetylcholine-evoked currents, as in (D), for $GIRK1_{mCherry}$ and GIRK2 (GIRK alone) and $GIRK1_{mCherry}$, GIRK2, and m2R (GIRK + m2R). Two-tailed unpaired *t* test, *** $p < 0.001$. **F.** Negative relationship between the ratio of activation (I_{evoked}/I_{basal}) and basal current (I_{basal}) of GIRK. Oocytes expressing the GIRK channel and $VALopA_{GFP}$ ($n = 42$, Spearman's $r = 0.684$, $p < 0.01$) or m2R ($n = 17$, Spearman's $r = 0.789$, $p < 0.001$) show the prototypical negative correlation, as previously described for m2R. The inverse relationship is caused by having an increasingly large basal current at the

expense of the ability to further potentiate the channel, thus reducing the evoked current.

References

1. Peirson, S.N., Halford, S., and Foster, R.G. (2009). The evolution of irradiance detection: melanopsin and the non-visual opsins. Philos. Trans. R. Soc. Lond. B Biol. Sci. *364*, 2849–2865.
2. Fernandes, A.M., Fero, K., Driever, W., and Burgess, H.A. (2013). Enlightening the brain: linking deep brain photoreception with behavior and physiology. BioEssays *35*, 775–779.
3. Cheng, N., Tsunenari, T., and Yau, K.-W. (2009). Intrinsic light response of retinal horizontal cells of teleosts. Nature *460*, 899–903.
4. Nissilä , J., Mänttäri, S., Särkioja, T., Tuominen, H., Takala, T., Timonen, M., and Saarela, S. (2012). Encephalopsin (OPN3) protein abundance in the adult mouse brain. J. Comp. Physiol. A Neuroethol. Sens. Neural Behav. Physiol. *198*, 833–839.
5. Kojima, D., Torii, M., Fukada, Y., and Dowling, J.E. (2008). Differential expression of duplicated VAL-opsin genes in the developing zebrafish. J. Neurochem. *104*, 1364–1371.
6. Fernandes, A.M., Fero, K., Arrenberg, A.B., Bergeron, S.A., Driever, W., and Burgess, H.A. (2012). Deep brain photoreceptors control light-seeking behavior in zebrafish larvae. Curr. Biol. *22*, 2042–2047.
7. Kirkby, L.A., Sack, G.S., Firl, A., and Feller, M.B. (2013). A role for correlated spontaneous activity in the assembly of neural circuits. Neuron *80*, 1129–1144.
8. Ackman, J.B., Burbridge, T.J., and Crair, M.C. (2012). Retinal waves coordinate patterned activity throughout the developing visual system. Nature *490*, 219–225.
9. Penn, A.A., Riquelme, P.A., Feller, M.B., and Shatz, C.J. (1998). Competition in retinogeniculate patterning driven by spontaneous activity. Science *279*, 2108–2112.
10. Garaschuk, O., Linn, J., Eilers, J., and Konnerth, A. (2000). Large-scale oscillatory calcium waves in the immature cortex. Nat. Neurosci. *3*, 452–459.
11. Yu, Y.-C., He, S., Chen, S., Fu, Y., Brown, K.N., Yao, X.-H., Ma, J., Gao, K.P., Sosinsky, G.E., Huang, K., and Shi, S.H. (2012). Preferential electrical coupling regulates neocortical lineage-dependent microcircuit assembly. Nature *486*, 113–117.
12. Kleindienst, T., Winnubst, J., Roth-Alpermann, C., Bonhoeffer, T., and Lohmann, C. (2011). Activity-dependent clustering of functional synaptic inputs on developing hippocampal dendrites. Neuron *72*, 1012–1024.
13. Ben-Ari, Y., Cherubini, E., Corradetti, R., and Gaiarsa, J.L. (1989). Giant synaptic potentials in immature rat CA3 hippocampal neurones. J. Physiol. *416*, 303–325.
14. Kastanenka, K.V., and Landmesser, L.T. (2010). In vivo activation of channelrhodopsin-2 reveals that normal patterns of spontaneous activity are required for motoneuron guidance and maintenance of guidance molecules. J. Neurosci. *30*, 10575–10585.
15. Plazas, P.V., Nicol, X., and Spitzer, N.C. (2013). Activity-dependent competition regulates motor neuron axon pathfinding via PlexinA3. Proc. Natl. Acad. Sci.

USA *110*, 1524–1529.
16. Pineda, R.H., Svoboda, K.R., Wright, M.A., Taylor, A.D., Novak, A.E., Gamse, J.T., Eisen, J.S., and Ribera, A.B. (2006). Knockdown of Nav1.6a Na+ channels affects zebrafish motoneuron development. Development *133*, 3827–3836.
17. Gu, X., Olson, E.C., and Spitzer, N.C. (1994). Spontaneous neuronal calcium spikes and waves during early differentiation. J. Neurosci. *14*, 6325–6335.
18. Saint-Amant, L., and Drapeau, P. (2001). Synchronization of an embryonic network of identified spinal interneurons solely by electrical coupling. Neuron *31*, 1035–1046.
19. Saint-Amant, L. (2010). Development of motor rhythms in zebrafish embryos. Prog. Brain Res. *187*, 47–61.
20. Kokel, D., Dunn, T.W., Ahrens, M.B., Alshut, R., Cheung, C.Y.J., Saint-Amant, L., Bruni, G., Mateus, R., van Ham, T.J., Shiraki, T., et al. (2013). Identification of nonvisual photomotor response cells in the vertebrate hindbrain. J. Neurosci. *33*, 3834–3843.
21. Chhetri, J., Jacobson, G., and Gueven, N. (2014). Zebrafish—on the move towards ophthalmological research. Eye (Lond.) *28*, 367–380.
22. Pietri, T., Manalo, E., Ryan, J., Saint-Amant, L., and Washbourne, P. (2009). Glutamate drives the touch response through a rostral loop in the spinal cord of zebrafish embryos. Dev. Neurobiol. *69*, 780–795.
23. Tong, H., and McDearmid, J.R. (2012). Pacemaker and plateau potentials shape output of a developing locomotor network. Curr. Biol. *22*, 2285–2293.
24. Scott, E.K., Mason, L., Arrenberg, A.B., Ziv, L., Gosse, N.J., Xiao, T., Chi, N.C., Asakawa, K., Kawakami, K., and Baier, H. (2007). Targeting neural circuitry in zebrafish using GAL4 enhancer trapping. Nat. Methods *4*, 323–326.
25. Wyart, C., Del Bene, F., Warp, E., Scott, E.K., Trauner, D., Baier, H., and Isacoff, E.Y. (2009). Optogenetic dissection of a behavioural module in the vertebrate spinal cord. Nature *461*, 407–410.
26. Warp, E., Agarwal, G., Wyart, C., Friedmann, D., Oldfield, C.S., Conner, A., Del Bene, F., Arrenberg, A.B., Baier, H., and Isacoff, E.Y. (2012). Emergence of patterned activity in the developing zebrafish spinal cord. Curr. Biol. *22*, 93–102.
27. Akerboom, J., Chen, T.-W., Wardill, T.J., Tian, L., Marvin, J.S., Mutlu, S., Calderón, N.C., Esposti, F., Borghuis, B.G., Sun, X.R., et al. (2012). Optimization of a GCaMP calcium indicator for neural activity imaging. J. Neurosci. *32*, 13819–13840.
28. Ferreira, T., Wilson, S.R., Choi, Y.G., Risso, D., Dudoit, S., Speed, T.P., and Ngai, J. (2014). Silencing of odorant receptor genes by G protein βγ signaling ensures the expression of one odorant receptor per olfactory sensory neuron. Neuron *81*, 847–859.
29. Sato, K., Yamashita, T., Ohuchi, H., and Shichida, Y. (2011). Vertebrate ancient-long opsin has molecular properties intermediate between those of vertebrate and invertebrate visual pigments. Biochemistry 50, 10484–10490.
30. Reuveny, E., Slesinger, P.A., Inglese, J., Morales, J.M., Iñiguez-Lluhi, J.A., Lefkowitz, R.J., Bourne, H.R., Jan, Y.N., and Jan, L.Y. (1994). Activation of the

cloned muscarinic potassium channel by G protein beta gamma subunits. Nature *370*, 143–146.
31. Lüscher, C., and Slesinger, P.A. (2010). Emerging roles for G protein-gated inwardly rectifying potassium (GIRK) channels in health and disease. Nat. Rev. Neurosci. *11*, 301–315.
32. West, R.E., Jr., Moss, J., Vaughan, M., Liu, T., and Liu, T.Y. (1985). Pertussis toxin-catalyzed ADP-ribosylation of transducin. Cysteine 347 is the ADP-ribose acceptor site. J. Biol. Chem. *260*, 14428–14430.
33. Li, X., Gutierrez, D.V., Hanson, M.G., Han, J., Mark, M.D., Chiel, H., Hegemann, P., Landmesser, L.T., and Herlitze, S. (2005). Fast noninvasive activation and inhibition of neural and network activity by vertebrate rhodopsin and green algae channelrhodopsin. Proc. Natl. Acad. Sci. USA *102*, 17816–17821.
34. Crisp, S.J., Evers, J.F., and Bate, M. (2011). Endogenous patterns of activity are required for the maturation of a motor network. J. Neurosci. *31*, 10445–10450.
35. Guemez-Gamboa, A., Xu, L., Meng, D., and Spitzer, N.C. (2014). Non-cell-autonomous mechanism of activity-dependent neurotransmitter switching. Neuron *82*, 1004–1016.
36. Kusakabe, T., Kusakabe, R., Kawakami, I., Satou, Y., Satoh, N., and Tsuda, M. (2001). Ci-opsin1, a vertebrate-type opsin gene, expressed in the larval ocellus of the ascidian Ciona intestinalis. FEBS Lett. *506*, 69–72.
37. Inada, K., Horie, T., Kusakabe, T., and Tsuda, M. (2003). Targeted knockdown of an opsin gene inhibits the swimming behaviour photoresponse of ascidian larvae. Neurosci. Lett. *347*, 167–170.
38. Xiang, Y., Yuan, Q., Vogt, N., Looger, L.L., Jan, L.Y., and Jan, Y.N. (2010). Light-avoidance-mediating photoreceptors tile the Drosophila larval body wall. Nature *468*, 921–926.
39. Spence, R., Ashton, R., and Smith, C. (2007). Oviposition decisions are mediated by spawning site quality in wild and domesticated zebrafish, Danio rerio. Behaviour *144*, 953–966.
40. Engeszer, R.E., Patterson, L.B., Rao, A.A., and Parichy, D.M. (2007). Zebrafish in the wild: a review of natural history and new notes from the field. Zebrafish *4*, 21–40.

CHAPTER 4
Sensory Specialization of Primary Cilia on Motor Neurons
unpublished findings

LINKER STATEMENT

The findings presented in the previous chapter have a number of implications to consider for the zebrafish research community. For anyone studying behavior on the first day of development, lighting conditions must be standardized in order to compare their results across experiments or to findings in the literature. Similarly, researchers looking at processes affected by activity dependent development should also consider standardizing the lighting in incubators housing their developing larvae. As this is the third study since 2012 identifying a novel nonvisual behavior in zebrafish, and since there remain many extraretinal opsins without any known associated behavior, I suspect that additional photobehaviors will be discovered. This underscores the importance of proper controls in any calcium imaging experiments using 1-photon imaging or optogenetic experiments using visible light for stimulation. It is no longer enough to assume that using blind fish is sufficient for ruling out endogenously mediated light-driven effects..

Our work left a number of unanswered questions that we address in the next chapter. Namely, the identification of the cell types within the spinal cord that are intrinsically photosensitive and those that are developmentally sensitive to sustained illumination. We also satisfy the now-standard requirement to pair any morpholino phenotype with a null knockout. We have made the surprising finding that VALopA localizes to the primary cilium of spinal neurons and though these experiments are ongoing, the initial findings are reported here in this chapter.

Sensory Specialization of Primary Cilia on Motor Neurons

Drew Friedmann,[1] Amy Winans,[1] Tsung-Li Liu,[4] Tong Xiao,[1] Eric Betzig,[4] and Ehud Y. Isacoff[1,2,3]

[1]Department of Molecular and Cell Biology, University of California, Berkeley, Berkeley, CA 94720, USA
[2]Helen Wills Neuroscience Institute, University of California Berkeley, Berkeley, CA 94720, USA
[3]Physical Bioscience Division, Lawrence Berkeley National Laboratory, Berkeley, CA 94720, USA
[4]Janelia Research Campus, Howard Hughes Medical Institute, Ashburn, VA 20147, USA

Acknowledgements: We thank A. Schier for providing materials and methods for Cas9 mutagenesis in zebrafish, C. Stanley for cloning and preparation of hippocampal neurons, and C. Wyart for providing pkd2l1:Gal4 zebrafish. We also thank H. Aaron and J. Lee for all the efforts of the Berkeley Molecular Imaging Center. This work was supported by the NIH Nanomedicine Development Center for the Optical Control of Biological Function (2PN2EY01824) and the Human Frontier Science Program (RGP0013/2010).

Abstract

Spontaneous activity in zebrafish embryos is strongly inhibited by physiological levels of environmental light. Our previous research identified that ventral spinal expression of vertebrate ancient long opsin a (VALopA) is both necessary and sufficient for the inhibitory photobehavior. The strength of the inhibitory effect on ongoing spontaneous activity raises questions about the mechanism of action of VALopA. Here we identify motor neurons as a photosensitive population and demonstrate localization of VALopA to the primary cilium in these cells. Additionally, when ectopically expressed, VALopA localizes to motile cilia within the central canal at the ventral midline of the fish. Our previous work highlighted a developmentally photosensitive medial cell population with long-duration calcium events. Here we identify these cells as Kolmer Aghdur (KA) cells, a GABAergic 'proprioceptive' cell population known to synapse onto motor circuits and also shown to extend cilia into the central canal. Our ongoing experiments raise important questions about the role of the primary cilium in development, the sensory abilities of motor neurons, and the mechanism by which GPCR signaling in a small cellular compartment can strongly inhibit the cell's activity.

Introduction

The primary cilium of eukaryotic cells has generated far less interest than its motile counterpart. Initially described nearly 150 years ago (Kowalevsky, 1867), but not named for a century [1], there is still widespread disagreement over the role of this cellular compartment. The suggestion that primary cilia are merely vestigial has been handily disproved over the years, in particular by research on human disease states caused by improper cilia formation and function. These ciliopathies, including Joubert and Bardet-Biedl syndromes, are associated with mutations in over 40 different ciliary proteins [1, 2] and are rare when considered individually, but collectively have prevalence rates as high as 1 in 2000 people [3]. Cilia are present on most differentiated cell types in the body, including postmitotic neurons throughout the brain [4]. Though advances have been made in understanding the role and function of primary cilia in specialized locations within the nervous system—for example the ependymal cells lining ventricles and sensory cilia in rods, cones, and olfactory neurons—less is known about the cilia on other neurons [5, 6].

Considering the known role of cilia in sensory tissues, the prevailing hypothesis for cilia on other cell types is that they may be acting as an 'antenna' for sensing local cues. Support for this idea began with the identification of individual GPCRs that partition into the ciliary compartment, including the somatostatin receptor 3 (SSTR3) [7], the serotonin receptor 6 [8], and the downstream target adenylyl cyclase type 3 (AC3) [9]. Given that there is no known protein production within cilia, the specific localization of these proteins must be the result of targeted trafficking [10]. The transition zone from somatic membrane to ciliary membrane is a specialized structure adjacent to the basal body attachment point for the ciliary axoneme. It is here that vesicles are excluded from the cilia and diffusion is restricted

for both cytosolic and membrane proteins, with passage permitted only to some [11, 12].

The localization of specific receptors to cilia is often required for their proper function. For example, in the hypothalamus, the ciliary receptors MCHR1 and SSTR3 are known to regulate feeding behaviors and their mislocalization in the case of Bardet-Biedl syndrome may be the cause of the disease's obesity phenotype [13, 14]. Similarly, ciliary AC3 in the hypothalamus may participate in the same pathway, given that AC3-deficient mice are also obese [15]. Another common phenotype of ciliopathies, polydactyly, stems from improper or missing signals from the sonic hedgehog pathway, perhaps the best understood ciliary GPCR pathway [16]. The hedgehog receptor Patched localizes to the ciliary membrane and prevents the entrance of Smoothened until activation of the receptor [17]. The presence of Smoothened in the cilia triggers the activation of Gli transcription factors and the resultant expression of target genes [18]. In each of these pathways, and considering the size of the ciliary compartment, there is ample opportunity for cross talk and regulation by other GPCRs with shared signaling molecules. In fact, the lack of clarity surrounding the role for PKA in regulating the Smoothened-Gli interaction is in part due to competing regulation of cAMP levels by other ciliary GPCRs [19, 20].

In the spinal cord, hedgehog signaling is essential for determining the eventual patterning of cell types. For example, it controls the number of motor neurons, their location, as well as the ratio of neurons to glia and the timing of their relative appearances [21, 22]. Within this Shh-sensitive domain, the ventrally located KA cells are GABAergic, ciliated neurons that have received notable attention of late. These cells were named in 1987 for W. Kolmer and E. Agduhr [23]. They initially identified these cells in many vertebrate classes and they have since been found in frog, fish, mouse, and macaque [24]. These cells protrude into the central canal, an extension that is often described as a ciliary tuft, but is actually composed of microvilli and a single 9 + 2 cilium [25].

The role of KA cells on the first day of development has not yet been determined. In larvae however, extensive work has determined that these neurons likely play a proprioceptive role in which they sense tail motion by detecting fluid flow of the CSF within the central canal. KA cells exhibit calcium transients in response to a tail bend during swimming and to a passive deflection of the tail in a paralyzed animal [26]. These responses are abolished in fish mutant for the TRPP channel pkd2l1 [25]. These fish have a reduced tail beat frequency during escape responses, a similar behavioral phenotype to fish lacking synaptic transmission from KAs and supported by the finding that activation of these cells can drive swimming [26, 27]. The modulatory action of these cells is complicated by the fact that activation of KAs is also capable of suppressing ongoing swim activity. This effect derives from releasing GABA onto premotor excitatory interneurons (V0-v) which can silence downstream activity or elicit a rebound effect in an otherwise quiet network. However, the story is not yet complete, as blockade of GABA signaling does not completely abolish these behavioral responses [26].

Altogether, the purpose of primary cilia in the nervous system remains unclear. Cilia may specialize on different cell types, as evidenced by GPCR expression patterns and the unexpected motility of 9 + 0 cilia in the central canal. The importance of cilia in early signaling for cell fate determination also hampers the ability to study their role in mature cells as mutations affecting their formation lead to developmental defects. We show here that the endogenous opsin VALopA localizes to the primary cilium of cells within the spinal cord, further expanding the list of ciliary function in neurons. We hope that the optical control of this receptor can shed light on the function of GPCR signaling in this cellular compartment in both native and heterologous contexts.

Results and Discussion

Motor neurons express the nonvisual opsin VALopA

Our previous work highlighted the necessity and sufficiency for the nonvisual opsin VALopA in generating photoinhibition of spontaneous coiling behavior in zebrafish embryos [28]. Owing to the recent controversy in the zebrafish community surrounding the relative merits and drawbacks of morpholinos, we supplemented our previous knockdown experiments by generating genetic null knockouts at the VALopA locus [29, 30]. We targeted Cas9 to the first exon of the VALopA locus and screened these F0, mosaically mutant individuals for photoinhibitory behavior between 22 and 25 hpf, as described previously. The injected population of embryos showed reduced photoinhibition as compared to WT individuals, though it was not abolished in any fish (Fig 1A). We raised to adults the embryos with the lowest PI scores and upon incrossing these individuals, identified non-responsive VALopA null mutants (Fig 1B). Sequencing of these mutants revealed 19 separate mutations generated by non homologous end joining at the Cas9 target site (Fig 1C). Given the location of these mutations within a transmembrane helix [31], it is interesting to note that frame shifts, in-frame indels, and a combination of each all abolish the photoinhibitory response (Fig 1D).

Though we previously established that illumination of the spinal cord is sufficient for generating inhibition of neural activity, it was still an outstanding question as to which spinal cell types express VALopA. Single color in situ hybridization in a 22 hpf embryo confirms expression in cell bodies of the ventral spinal cord, as had been described previously [32](Fig 2A). We previously identified VALopA through its expression within the *olig2*-positive Gal4^{1020} enhancer trap pattern, and 2-color FISH for *valopa* displays overlap with the Gal4^{+} population (Fig 2B). However, some slightly more dorsal *valopa*-positive cell bodies do not dual-label, and given the spread of *valopa* positive somata along the dorsal-ventral axis, is apparent that a heterogeneous population of neurons expresses the opsin. Of note, *valopa* mRNA is also identified within a number of cell bodies co-labeled by the mnx1:Gal4 expression pattern at 24 hpf (Fig 2C). These data support the surprising possibility that motor neurons possess sensory capabilities.

One possibility for further dissecting the relative importance of the cell types expressing VALopA will be to rescue the opsin in a cell type specific manner. To this

end, we generated a transgenic line for expressing VALopA via the Gal4:UAS system. Like the transient rescue experiments described in the previous chapter, we used cerulean as a marker for transgenesis and assessed the photoinhibitory effect of light on coiling behavior. In a wildtype background, expression of VALopA with the $Gal4^{1020}$ driver increased by 20% the strength of photoinhibition in embryos exposed to a short, dim flash of light (Fig 1E). Though small in effect, it will be interesting to see how null mutant fish will react after these transgenes are introduced.

VALopA localizes to the primary cilium in zebrafish and mouse neurons

Due to the difficulty of generating successful knockin of reporters at endogenous loci in zebrafish (data not shown, A. Schier personal correspondence), we turned to expression of a mKate2 tagged VALopA molecule in order to visualize its intracellular localization. In mosaic expression within the $Gal4^{1020}$ pattern, the opsin strongly compartmentalizes to an individual ciliary projection on each cell expressing the transgene (Fig 3A). By using a bicistronic strategy to include a cytosolic cerulean marker, we were able to classify some of the individual cells by morphology and soma location (Fig 3B). Of note, we found VALopA-mKate2 positive, ventrally projecting cilia near the axon initial segment of primary motor neurons and ipsilateral interneurons suggesting that endogenous VALopA will also localize to cilia in these cells (Fig 3C-F). Cilia on these cells are short and difficult to resolve without the improved resolution and optical sectioning afforded by the lattice light sheet with adaptive optics (AO-LLS, with E. Betzig) (compare Fig 3C and 3E).

It is uncertain which other cell types within the $Gal4^{1020}$ pattern overlap with endogenous VALopA expression; however, every cell labeled with the cerulean marker traffics VALopA-mKate2 to a single cilium. For cells abutting the central canal, including likely radial glia precursors and KA neurons, these cilia extend into and across the canal (Fig 3A-B,G). Images of these VALopA labeled cilia appear identical to those made visible by acetylated tubulin staining and those previously documented by other labs (Fig 3H) [33, 34]. The clear experimental path forward from these results is outlined in the General Discussion chapter, as these experiments are new and ongoing.

Interestingly, some of these cilia in the central canal are motile and beat at frequencies as high as 30 Hz (Fig 4A-D). This motion has been shown to drive CSF fluid flow and may be a mixture of 9 + 2 motile cilia and 9 + 0 dynein-controlled monocilia [34]. Confocal imaging with frame rates of 20-60 ms is not sufficient to capture the full motion of these cilia; however, we were able to identify cilia on neighboring cells with distinct patterns of beating and pauses, suggesting that this motion is actively generated and not from passive fluid flow alone (Fig 4A-B). The faster frame rates (2.56 ms / frame) from light sheet imaging fully resolve the speed of ciliary beating (Fig 4C-D).

In a parallel line of experiments, we expressed GFP-tagged VALopA in primary mouse hippocampal neuron (HN) cultures where it also localizes to primary cilia (Fig 5A-B). Interestingly, expression in glia also reveals primary cilia, and in some cases, multiple cilia originating from the same location on the membrane (Fig

5C). Similarly, when ectopically expressed in the zebrafish, VALopA-mKate2 also reveals multiple cilia on a single early Müller glia cell in the retina (Fig 5D). In an alignment with bovine rhodopsin, VALopA shares a purported ciliary targeting sequence at the C-terminal tail of the protein [31, 35]. This VxPx motif is one of multiple proposed motifs for localization [36]. In our hippocampal expression system, mutations to this sequence (V374A and P376A) disrupted ciliary localization while still expressing protein on the cell membrane (Fig 5E-N). The level of signal remaining on the cilium is comparable to other small projections and would not be identifiable as a cilium without co-labeling with SSTR3-tdTomato. Mutation of another proposed motif, a pair of residues (FR) on the intracellular side of the seventh transmembrane helix [37], not only did not show ciliary localization, but expressed more weakly and not on the membrane (Fig 5O-S). Other reports suggest that this pair of residues is not for trafficking, but rather for proper folding [16]. To test the function of VALopA in this heterologous system, we coexpressed the opsin with GCaMP-6f (Fig 6A-B) [38]. Preliminary findings suggest that, like in zebrafish, 1-photon stimulation slows the rate of spontaneous activity as observed by 2-photon imaging (Fig 6C-D). This system could prove to be a useful optical tool for the study of GPCR signaling in primary cilia.

KA cells are sensitive to sustained illumination during development

In our previous work using calcium imaging in the spinal cord of the zebrafish, we observed a population of midline-contacting cells with long duration calcium events (Fig 7A-B) [28, 39]. These cells do not participate in the fast, correlated motor network in the lateral cord. Global suppression of activity in the spinal network increases the prevalence of these long-duration calcium events by an unknown mechanism. Without a promoter that labels this population, we had to use fast volumetric imaging in order to track calcium activity in individual projections as a way to calculate the morphology of these midline cells. We used light sheet imaging (diSPIM, [40]) to image spontaneous calcium activity within the $Gal4^{1020}$ line at 22 hpf and identified a rostrally projecting axon with a long calcium rise in synchrony with a midline cell body. Careful choice of z-position using traditional confocal imaging also revealed these rostral projections (Fig 7C,E). Taken together, the soma location, the small protrusion into the central canal, and the rostrally extending axon indicate that these cells are KA interneurons (Fig 7D-E).

Competing hypotheses for the increased frequency of calcium events in KA cells include (1) a developmental increase in their cell number in the two hours between the time of illumination and the time of GCaMP imaging, and (2) an increase in the frequency of events in these cells. This second hypothesis is better explained by considering that our previous results relied on 3-minute long recordings of calcium events. However, recordings over a longer time scale reveal that the inter-event interval can be as long as 6.5 minutes (Fig 7B). To determine if proliferation is present in this zone, we injected EdU into the trunk of embryos at 22 hpf and fixed them after a 15 minute pulse label. The fluorescence from GCaMP5 expression was sufficient to determine whether proliferating cells that incorporated EdU were within

the Gal4^{1020} expression domain. Results indicate that there is ongoing proliferation at the midline of the spinal cord and within the Gal4^{1020} pattern at 22 hpf (Fig 7F). This is in line with recent findings suggesting the developmentally late appearance of KAs as compared to other neurons [41]. Exposing these embryos to 508 nm LED illumination between 18-20 hpf shows a trend towards an increase in dual-labeled EdU^{+} and Gal4^{1020+} at 22 hpf (Fig 7G). A recently published Gal4 line that labels KAs will make it possible to test these two possibilities—cell number and event frequency—more accurately [26].

In initial experiments with this line, using pkd2l1:Gal4 driving GCaMP5, we recorded long duration calcium events with similar kinetics to those observed in our Gal4^{1020} GCaMP5 imaging. In particular, we observe long duration but discrete events in some cells (Fig 8A-B) and ongoing variable events in others (Fig 8C-D, compare to Fig 7B). It is possible that these two activity patterns reflect differences in the firing rates of dorsal and ventral pools of KA interneurons. However, it is unclear why we would see both activity patterns within the Gal4^{1020} pattern, as it is reported to only cover the *olig2*-positive, dorsal set of KAs [24]. We were also able to confirm the presence of rostrally projecting axons on most KA cells at 22-23 hpf (Fig 8E) and the presence of microvilli within the central canal that appear identical to tufts seen in the Gal4^{1020} GCaMP line (Fig 8F-G). However, these protrusions are much shorter than the VALopA-mKate2 positive cilia observed in previous experiments. This is similar to the comparison between the microvilli and the Arl13b-positive single cilium observed on these cells by Böhm, et al (2016). Fortuitously, we also captured a cell during mitosis, suggesting that the pkd2l1:Gal4 pattern also includes precursor cells and lending credence to the hypothesis that proliferative rates may control the eventual cell number in this population (Fig 8H-I).

The preliminary findings from this study are particularly important to the field of motor control and motor development. The recent finding that motor neurons can feed back into and influence the premotor network of interneurons has begun to flip the dogma surrounding these cells [42]. No longer are they being viewed as simple integrators of input with single output in the muscle. With the identification of a nonvisual opsin in the primary cilium of these cells, motor neurons must also now be considered as sensory *inputs* to a developing circuit. We've also begun to see a possibility for use of VALopA as a tool to control the G_i pathway, either in vivo in cells outside of the normal VALopA expression pattern or in heterologous systems like hippocampal cultures. In these cases, it will be important to determine if and how G-protein signaling in the cilium alters firing frequency, but VALopA may also prove useful in manipulating other GPCRs, like those in the hedgehog pathway, and their function in cilia during development.

Figure1. VALopA null mutants do not respond to light stimuli.

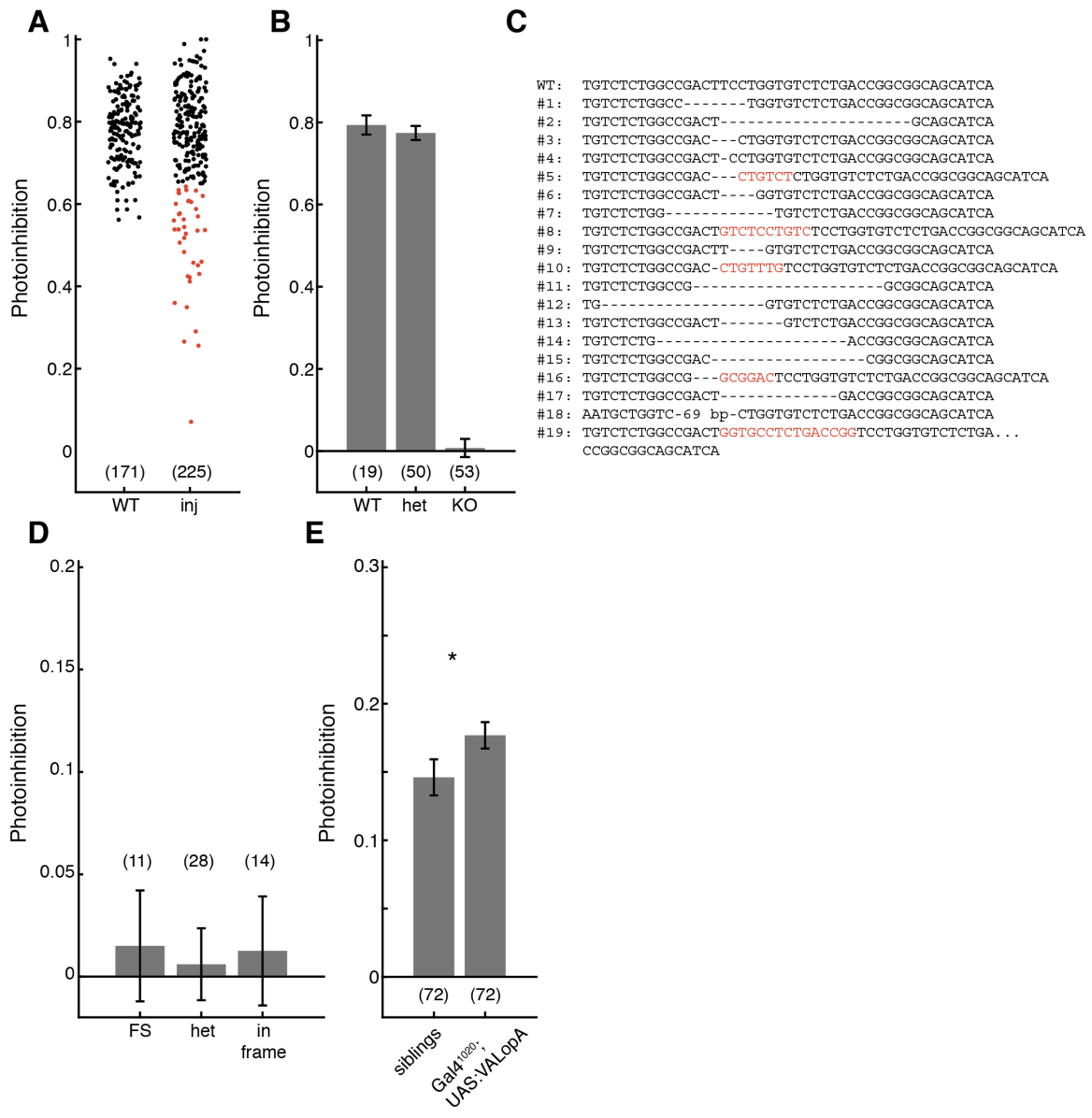

A. Photoinhibition ([Hz_{Light} – Hz_{Dark}] / Hz_{Dark}) scores for WT embryos as compared to embryos having received injection of Cas9 RNA and guide RNA targeting exon 1 of VALopA. Average of three movies per fish, *n* is displayed in the graphic. Red markers indicate the embryos which were raised to adults as putative founders. **B.** Photoinhibition scores from an incross of the F0 individuals described in (A). F1 fish were assayed as before, with an average of three movies per fish. Following behavioral testing, individuals were sequenced to determine genotype. **C.** 19 different mutant alleles identified within the F1 non-photosensitive population. Dashes represent deleted bases and red letters indicate inserted bases. **D.** Photoinhibition scores for the 53 mutant fish identified in (B) separated based on whether the

mutation induced a frame shift in the coding region. FS: 2 frame shift alleles; in frame: 2 in frame indels; het: one of each. *n* is displayed in the graphic. **E.** Photoinhibition scores from embryos WT at the VALopA locus and overexpressing VALopA within the $Gal4^{1020}$ pattern as compared to non-expressing sibling embryos. Dim light for only a 5 s stimulus was used. *n* is indicated in the graphic, t-test p = 0.047.

Figure 2. VALopA is expressed in primary motor neurons.

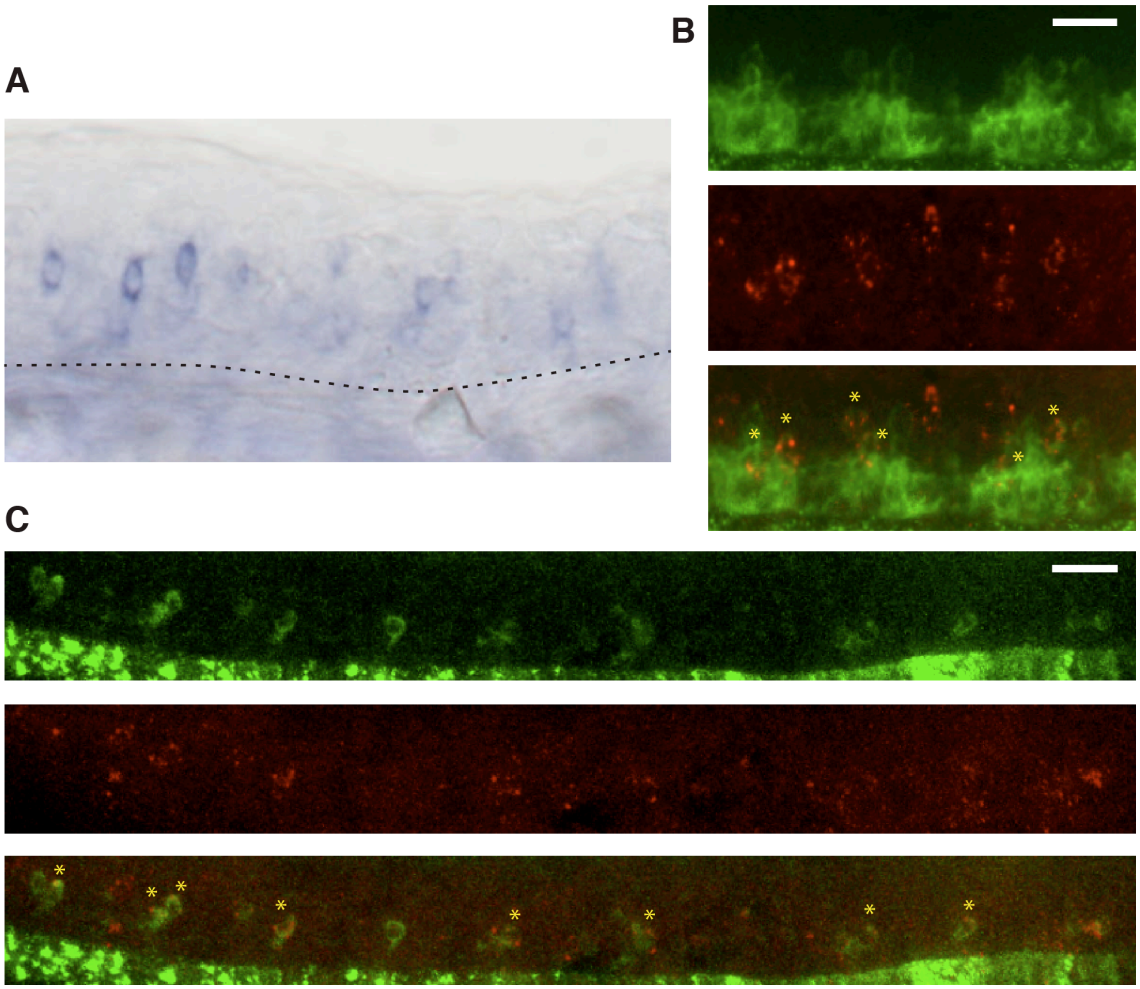

A. Single color *in situ* with antisense RNA probe for *valopa*. Rostral is to the left, notochord boundary is marked with a dashed line. **B.** Top, anti-GFP antibody labeling of Gal4^{1020}; UAS:CGaMP5 neurons in ventral spinal cord. Notochord boundary is at the bottom of the image. Middle, fluorescent *in situ* for *valopa*. Bottom, merged image. Yellow asterisks denote cells with clear dual labeling. Scale bar = 20 μm. **C.** Top, anti-GFP antibody labeling of mnx:Gal4; UAS:GCaMP5 motor neurons in ventral spinal cord. Non-specific signal from the notochors is visible at the bottom of the frame. Middle, fluorescent *in situ* for *valopa*. Bottom, merged image. Yellow asterisks denote cells with clear dual labeling. Scale bar = 20 μm.

Figure 3. VALopA localizes to primary cilia *in vivo*.

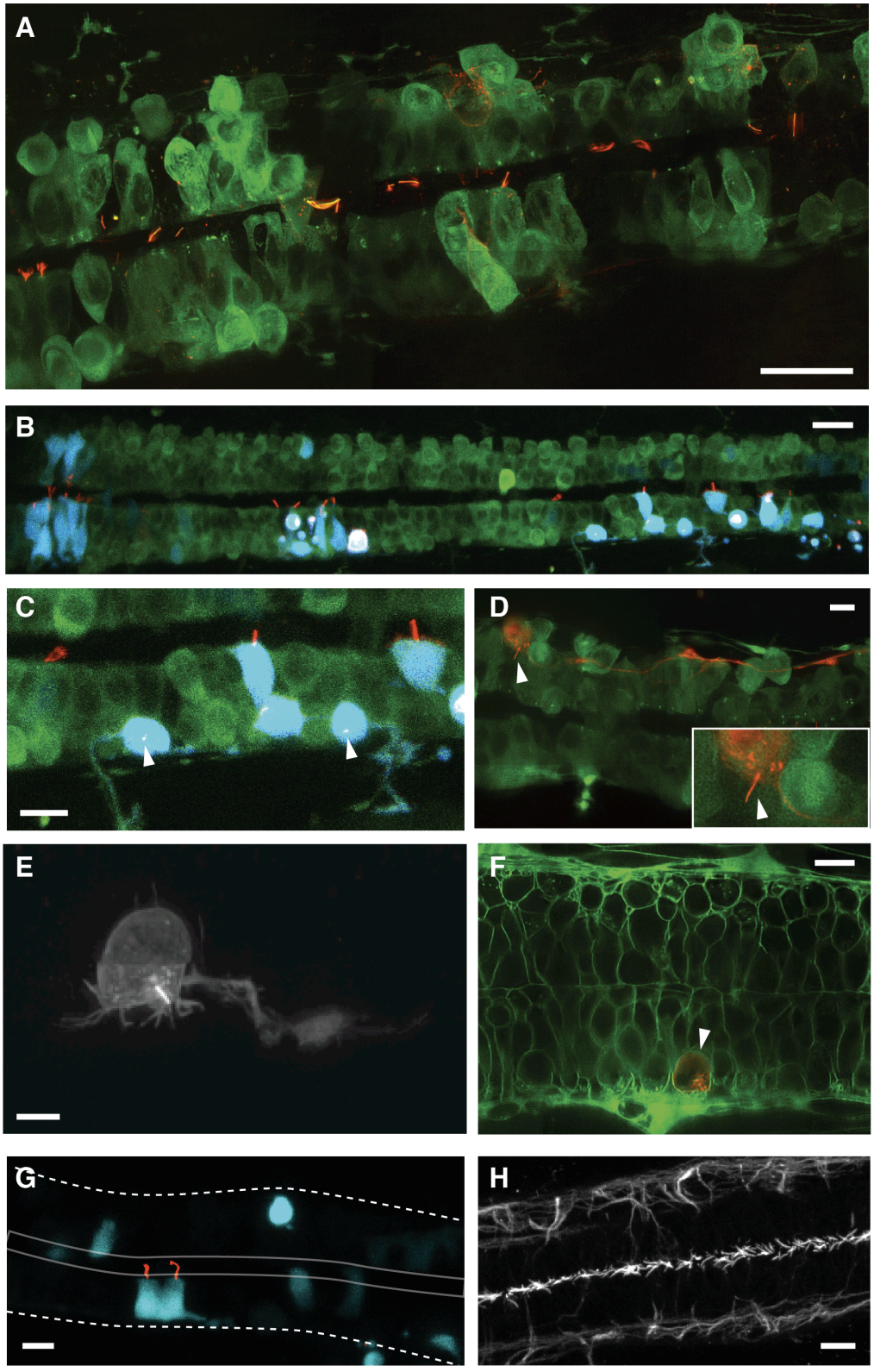

A. Dorsal view of ventral spinal neurons in a $Gal4^{1020}$ pattern. Stable transgenic expression of UAS:GCaMP5 (green) labels all $Gal4^{+}$ cells and transient expression of UAS:VALopA-mKate2 (red) labels a subset of these cells. Image is a partial z-stack taken by lattice light sheet with adaptive optics (AO-LLS). Scale bar = 20 μm, rostral direction is to the left in all images, all images are from 22-23 hpf embryos. **B.** Same as in (A) with the addition of a cerulean (blue) cytosilic marker for the cells transiently expressing UAS:VAlopA-mKate. Z-stack taken by confocal lambda scan (458, 488, 594 nm excitation) and linearly unmixed into the three channels in the image. Scale bar = 20 μm. **C.** Zoom from the image in (B). Arrowheads denote cilia located on the ventral side of two primary motor neurons. Scale bar = 10 μm. **D.** AO-LLS image of $Gal4^{1010}$;UAS:GCaMP5 and transient UAS:VALopA-mKate2 expression in a VeLD interneuron. Arrowhead highlights a primary cilium, zoom in inset. Scale bar = 10 μm. **E.** AO-LLS z-stack of UAS:VALopA-mKate2 expression in a primary motor neuron, highlighted in (F). Scale bar = 5 μm, gamma adjusted. **F.** Single optical section of an AO-LLS image of BODPIY-FL-C5-ceramide labeling in a $Gal4^{1020}$-positive embryo. Arrowhead highlights a UAS:VALopA-mKate2 transiently expressing neuron. Scale bar = 10 μm. **G.** Standard confocal image (458 and 594 nm excitation) of $Gal4^{1020}$ driving transient UAS:VAlopA-mKate2 and cytosolic cerulean in two KA neurons. Cerulean image consists of a z-stack while mKate2 image is a single optical section in order to reduce the motion artifact of the motile cilia. Spinal cord is bounded by dashed lines, central canal is marked by solid lines. Scale bar = 10μm. **H.** Anti-acetylated tubulin staining reveals cilia in the central canal and tracts of axons in the lateral spinal cord. Scale bar = 10 μm.

Figure 4. VALopA^{+} cilia in the central canal are motile.

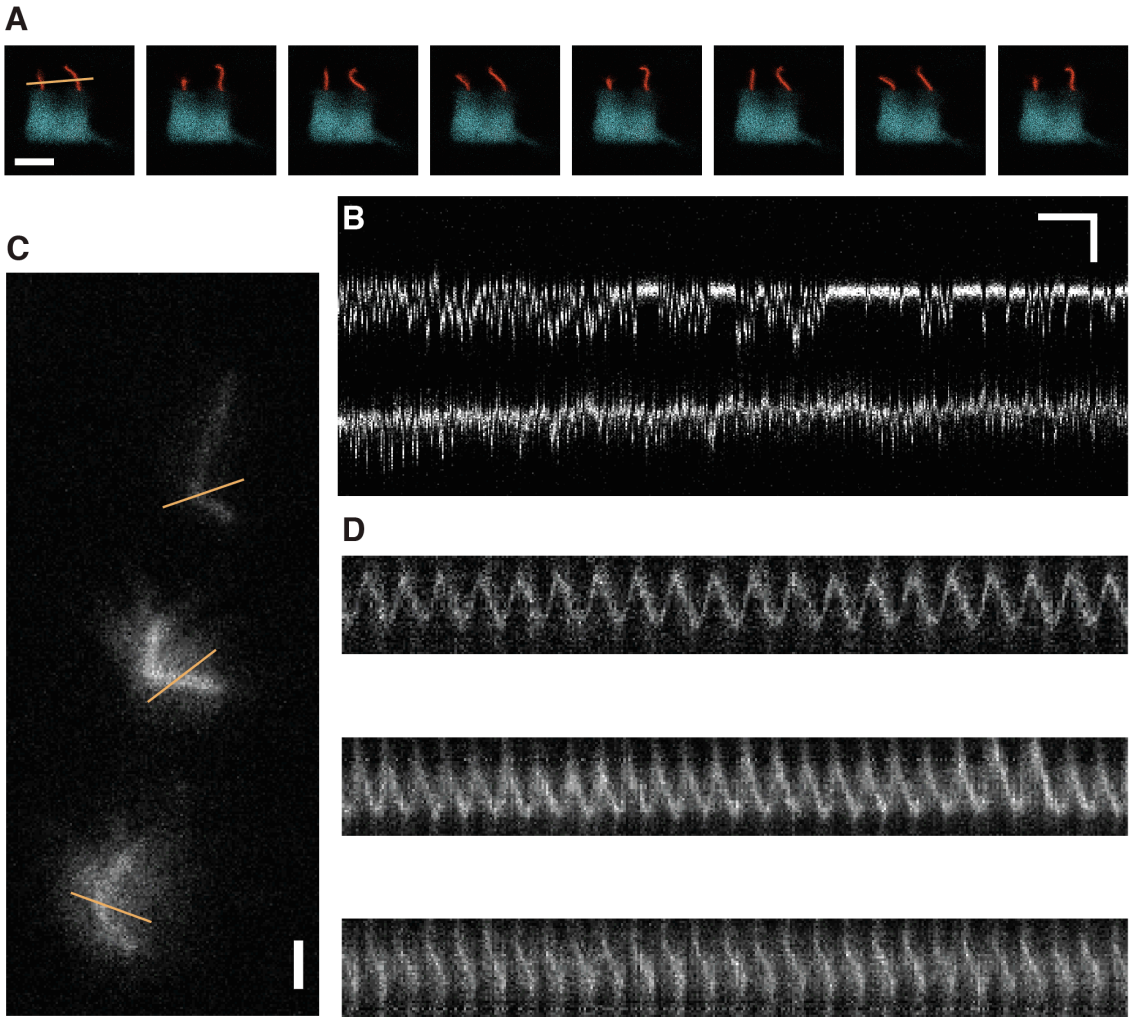

A. Still frames of KA interneurons within the Gal4^{1020} pattern expressing cytosolic cerulean and VALopA-mKate2. Simultaneously confocal imaging with 458 and 594 nm excitation wavelengths. Frames are 60.5 ms apart, Scale bar = 10 μm. **B.** Kymograph of ciliary motion from the cells imaged in (A), along the indicated line. Axes = 2 s, 2 μm. **C.** Single frame of three individual cilia projecting into the central canal from the same genetic background as (A). Imaged by lattice light sheet, only using 560 nm excitation. Scale bar = 2 μm. **D.** Kymographs calculated from the three individual cilia in (C). Frame rate = 2.56 ms, frequencies = 23.5, 30.1, and 30.5 Hz from top to bottom.

Figure 5. VALopA localizes to primary cilia in mouse hippocampal neurons.

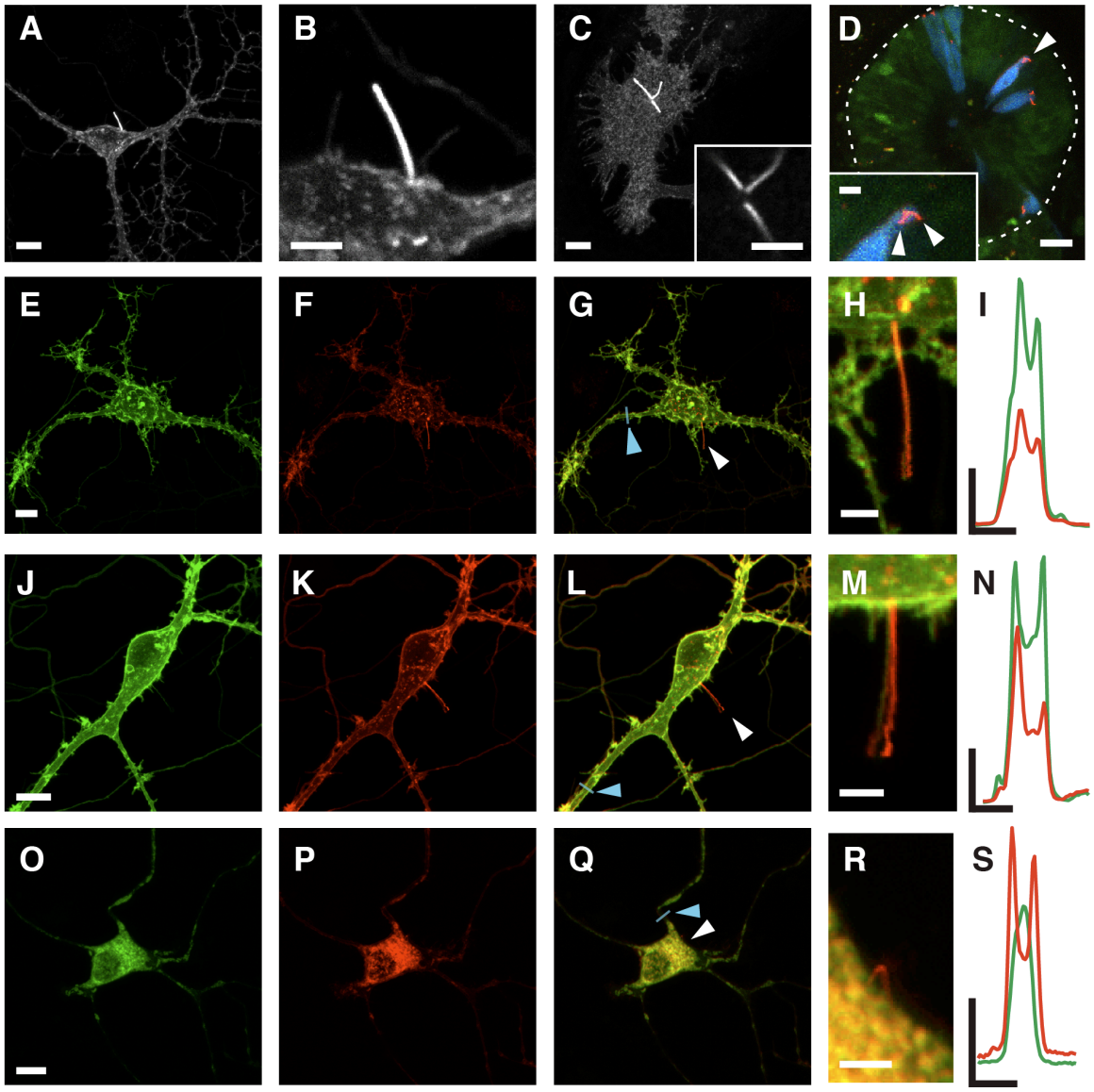

A. Confocal Z-stack of a 12 DIV mouse hippocampal neuron expressing VALopA-GFP fusion. Scale bar = 10 μm. **B.** Single optical section zoom image of the primary cilium from the cell in (A). Scale bar = 4 μm. **C.** Confocal z-stack of a glial cell from the same culture as (A), also expressing VALopA-GFP. Scale bar = 10 μm. Inset: Single optical section zoom image of multiple primary cilia originating in close proximity. Scale bar = 4 μm. **D.** Müller glia of a 24 hpf zebrafish retina expressing UAS:GCaMP5 and transient expression of UAS:VALopA-mKate2 with a cerulean marker. Dashed line marks the outer edge of the retina. Arrowhead marks a glial cell with two cilia, as seen in the inset. Scale bars = 20, 5 μm. **E.** Images taken as above, neuron expressing VALopA V374A-GFP fusion. Scale bar = 10 μm. **F.** Expression of SSTR3-tdTomato fusion within the same cell as (E). **G.** Merged image. White

arrowhead denotes the primary cilium seen in (H). Blue arrowhead denotes the 13-pixel wide region used to calculate the profile in (I). **H.** Zoom of the primary cilium highlighted in (G). Scale bar = 3 μm. **I.** Fluorescence intensity profile of a 13-pixel wide line across a dendrite of the cell in (G). Green and red lines represent VALopA V374A-GFP and SSTR3-tdTomato respectively. Axes = 3 μm, 4000 a.u. **J-N.** Same as (E-I), but with VALopA P376A-GFP. **O-S.** Same as (E-I), but with VALopA FR-AA-GFP.

Figure 6. VALopA inhibition of spontaneous activity in hippocampal neurons.

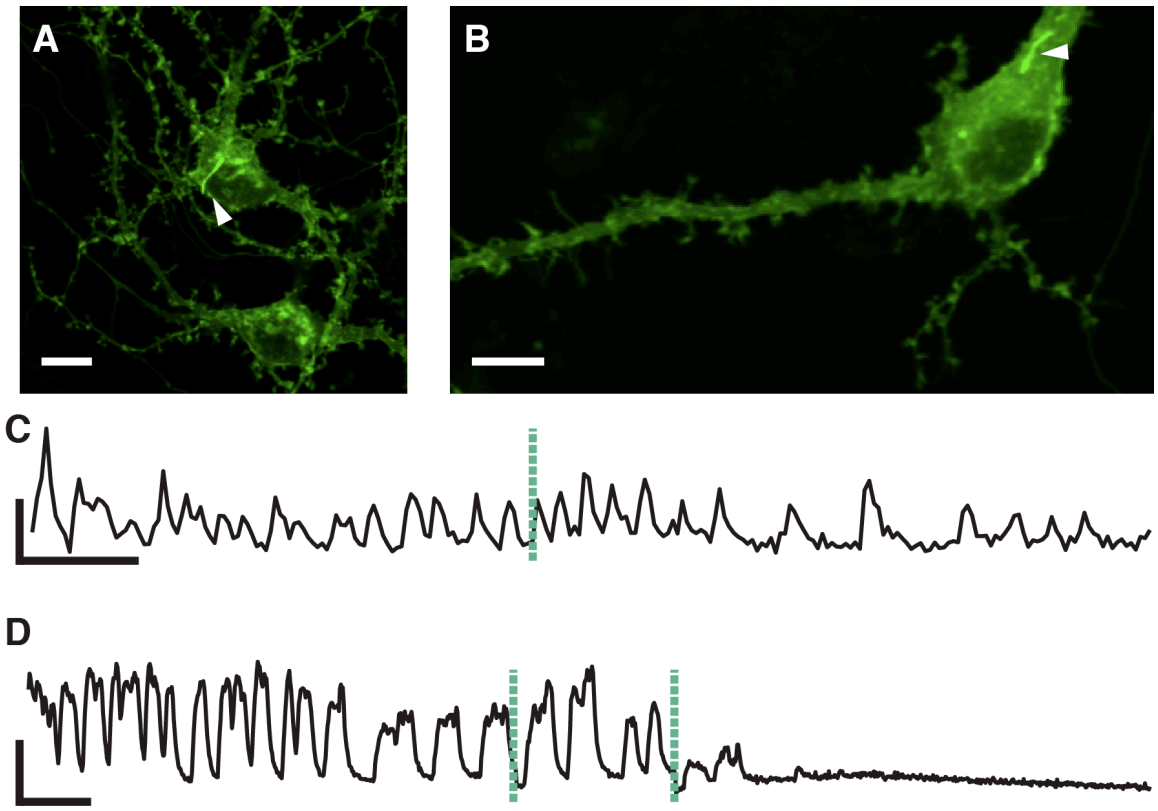

A,B. Confocal images takes of 12-13 DIV hippocampal neurons expressing VALopA-GFP fusion as well as GCaMP6f. Arrowhead denoted the heightened expression of VALopA-GFP in the primary cilium of each neuron. Scale bars = 10 μm. **C,D.** Fluorescence traces extracted from a region centered on the cell body of the neurons in (A) and (B) respectively. Movies were acquired by 2-photon imaging at 940 nm excitation. Green dashed lines indicate the location of 1-photon light stimuli, 600 ms in (C) and 1.3 s each in (D). Axes = 10 and 20 s; 20% and 50% dF/F respectively for (C) and (D).

Figure 7. Identification of KA morphology and activity within the Gal4^{1020} pattern.

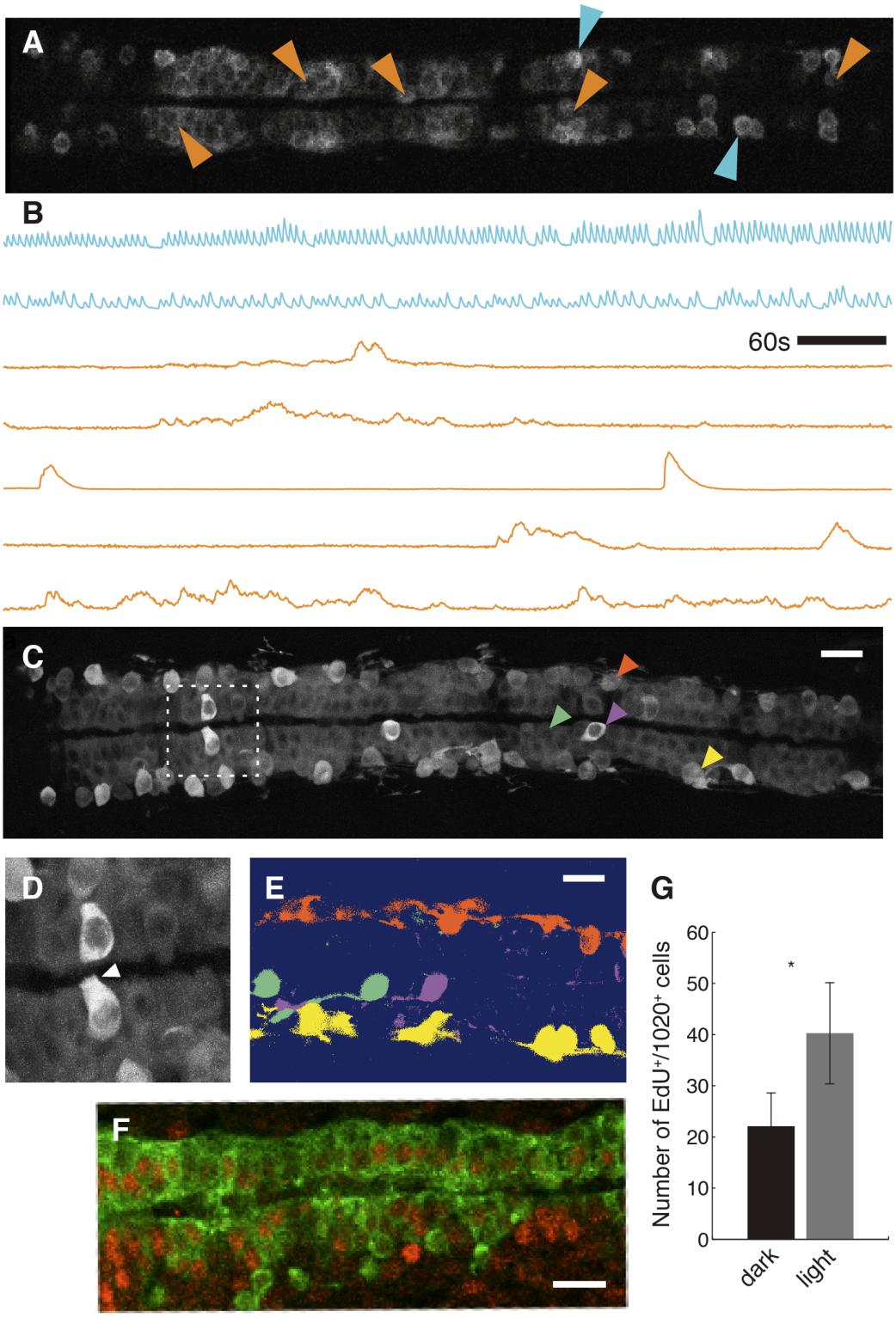

A. 2-photon single frame from calcium imaging of 22hpf Gal4^{1020}; UAS:GCaMP5 in ventral spinal neurons. Blue arrowheads mark two cell bodies within the motor circuit. Orange arrowheads mark midline-contacting KA neurons with long-duration calcium events. **B.** Individual traces from the cells marked in (A). **C.** 1-photon max projection of 23 hpf Gal4^{1020}; UAS:GCaMP5 acquired slowly. Active cells appear brighter than the basal fluorescence levels in neighboring neurons. Dashed box and arrowheads denote cells analyzed in (E). Scale bar = 20 μm. **D.** Zoom of the dashed region in (C). Arrowhead marks the characteristic protrusion into the central canal of a KA interneuron. **E.** Data collected in a timelapse of a single optical section in (C). Pixels are color-coded if they significantly correlated with the manually identified cells labeled in (C). Scale bar = 20 μm. **F.** Single optical section of a fixed 22 hpf embryo. Gal4^{1020}; UAS:GCaMP5 fluorescence overlaps with nuclei positive for EdU incorporation (Alexa 647). Scale bar = 20 μm. **G.** Number of double labeled (Gal4^{1020}; UAS:GCaMP5 and EdU) nuclei along 120 μm of spinal cord between somites 4 and 8. Groups 'dark' and 'light' reference the treatment received from 18-20 hpf. EdU pulse delivered by injection for 15 minutes at 22 hpf. n = 5, 4. t-test p = 0.039.

Figure 8. KA-specific Gal4 transgenic shows long-duration calcium events.

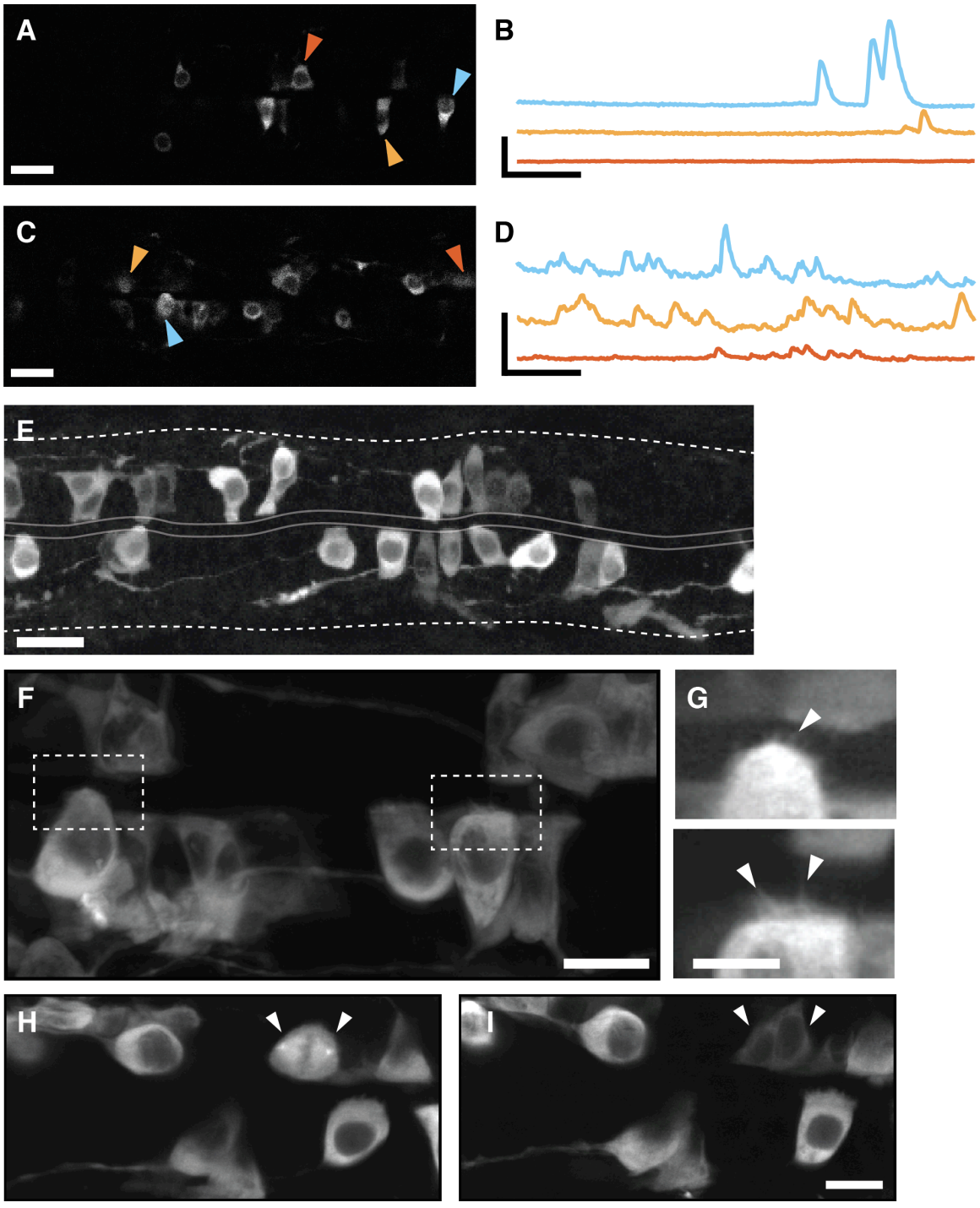

A. Single optical section, still frame from calcium imaging of dorsally-located KA cells within pkd2l1:Gal4; UAS:GCaMP5 embryos at 22.5 hpf. Arrowheads mark recorded cells. Scale bar = 20 μm **B.** Calcium traces from the identified cells in (A). Axes = 30 s and 200% dF/F. **C.** Same embryo and imaging location as in (A), but centered on

the ventral population of KA neurons. **D.** Calcium traces from the identified cells in (C). Axes = 30 s and 200% dF/F. **E.** Max projection of dorsal and ventral KA cells in a 22.5 hpf pkd2l1:Gal4; UAS:GCaMP5 embryo. Rostral direction is to the left. Dashed lines mark the boundary of the spinal cord, solid lines mark the central canal. Scale bar = 20 μm. **F.** Airy scan image of a 23 hpf embryo as in (E). Scale bar = 10 μm. **G.** Zoom of the two boxed regions in (F). Arrowheads mark microvilli projecting into the central canal. Gamma adjusted, scale bar = 5 μm. **H, I.** Airy scan images of KA neurons acquired 90 minutes apart. Arrowheads mark a cell during and after mitosis. Scale bar = 10 μm.

References

1. Acs, P., Bauer, P.O., Mayer, B., Bera, T., Macallister, R., Mezey, E., and Pastan, I. (2015). A novel form of ciliopathy underlies hyperphagia and obesity in Ankrd26 knockout mice. Brain Struct Funct *220*, 1511–1528.
2. Berbari, N.F., Lewis, J.S., Bishop, G.A., Askwith, C.C., and Mykytyn, K. (2008). Bardet-Biedl syndrome proteins are required for the localization of G protein-coupled receptors to primary cilia. Proc Natl Acad Sci USA *105*, 4242–4246.
3. Berbari, N.F., O'Connor, A.K., Haycraft, C.J., and Yoder, B.K. (2009). The primary cilium as a complex signaling center. Curr Biol *19*, R526–R535.
4. Bishop, G.A., Berbari, N.F., Lewis, J., and Mykytyn, K. (2007). Type III adenylyl cyclase localizes to primary cilia throughout the adult mouse brain. J Comp Neurol *505*, 562–571.
5. Borovina, A., Superina, S., Voskas, D., and Ciruna, B. (2010). Vangl2 directs the posterior tilting and asymmetric localization of motile primary cilia. Nat. Cell Biol. *12*, 407–412.
6. Böhm, U.L., Prendergast, A., Djenoune, L., Nunes Figueiredo, S., Gomez, J., Stokes, C., Kaiser, S., Suster, M., Kawakami, K., Charpentier, M., et al. (2016). CSF-contacting neurons regulate locomotion by relaying mechanical stimuli to spinal circuits. Nat Commun *7*, 10866.
7. Brailov, I., Bancila, M., Brisorgueil, M.J., Miquel, M.C., Hamon, M., and Vergé, D. (2000). Localization of 5-HT(6) receptors at the plasma membrane of neuronal cilia in the rat brain. Brain Res *872*, 271–275.
8. Chen, T.-W., Wardill, T.J., Sun, Y., Pulver, S.R., Renninger, S.L., Baohan, A., Schreiter, E.R., Kerr, R.A., Orger, M.B., Jayaraman, V., et al. (2013). Ultrasensitive fluorescent proteins for imaging neuronal activity. Nature *499*, 295–300.
9. Craige, B., Tsao, C.-C., Diener, D.R., Hou, Y., Lechtreck, K.-F., Rosenbaum, J.L., and Witman, G.B. (2010). CEP290 tethers flagellar transition zone microtubules to the membrane and regulates flagellar protein content. J. Cell Biol. *190*, 927–940.
10. Dale, N., Roberts, A., Ottersen, O.P., and Storm-Mathisen, J. (1987). The Development of a Population of Spinal Cord Neurons and their Axonal Projections Revealed by GABA Immunocytochemistry in Frog Embryos. Proc. Biol. Sci. *232*, 205–215.
11. Deretic, D., and Wang, J. (2012). Molecular assemblies that control rhodopsin transport to the cilia. Vision Res. *75*, 5–10.
12. Djenoune, L., Khabou, H., Joubert, F., Quan, F.B., Nunes Figueiredo, S., Bodineau, L., Del Bene, F., Burcklé, C., Tostivint, H., and Wyart, C. (2014). Investigation of spinal cerebrospinal fluid-contacting neurons expressing PKD2L1: evidence for a conserved system from fish to primates. Front Neuroanat *8*, 26.
13. Dutton, R., Yamada, T., Turnley, A., Bartlett, P.F., and Murphy, M. (1999). Sonic hedgehog promotes neuronal differentiation of murine spinal cord precursors and

collaborates with neurotrophin 3 to induce Islet-1. J Neurosci *19*, 2601–2608.
14. Fidelin, K., Djenoune, L., Stokes, C., Prendergast, A., Gomez, J., Baradel, A., Del Bene, F., and Wyart, C. (2015). State-Dependent Modulation of Locomotion by GABAergic Spinal Sensory Neurons. Curr Biol *25*, 3035–3047.
15. Friedmann, D., Hoagland, A., Berlin, S., and Isacoff, E.Y. (2015). A spinal opsin controls early neural activity and drives a behavioral light response. Curr Biol *25*, 69–74.
16. Händel, M., Schulz, S., Stanarius, A., Schreff, M., Erdtmann-Vourliotis, M., Schmidt, H., Wolf, G., and Höllt, V. (1999). Selective targeting of somatostatin receptor 3 to neuronal cilia. Neuroscience *89*, 909–926.
17. Hsiao, Y.-C., Tuz, K., and Ferland, R.J. (2012). Trafficking in and to the primary cilium. Cilia *1*, 4.
18. Kojima, D., Mano, H., and Fukada, Y. (2000). Vertebrate ancient-long opsin: a green-sensitive photoreceptive molecule present in zebrafish deep brain and retinal horizontal cells. J Neurosci *20*, 2845–2851.
19. Kojima, D., Torii, M., Fukada, Y., and Dowling, J.E. (2008). Differential expression of duplicated VAL-opsin genes in the developing zebrafish. J Neurochem *104*, 1364–1371.
20. Kok, F.O., Shin, M., Ni, C.-W., Gupta, A., Grosse, A.S., van Impel, A., Kirchmaier, B.C., Peterson-Maduro, J., Kourkoulis, G., Male, I., et al. (2015). Reverse genetic screening reveals poor correlation between morpholino-induced and mutant phenotypes in zebrafish. Dev Cell *32*, 97–108.
21. Kramer-Zucker, A.G., Olale, F., Haycraft, C.J., Yoder, B.K., Schier, A.F., and Drummond, I.A. (2005). Cilia-driven fluid flow in the zebrafish pronephros, brain and Kupffer's vesicle is required for normal organogenesis. Development *132*, 1907–1921.
22. Kumar, A., Wu, Y., Christensen, R., Chandris, P., Gandler, W., McCreedy, E., Bokinsky, A., Colón-Ramos, D.A., Bao, Z., McAuliffe, M., et al. (2014). Dual-view plane illumination microscopy for rapid and spatially isotropic imaging. Nat Protoc *9*, 2555–2573.
23. Mazelova, J., Astuto-Gribble, L., Inoue, H., Tam, B.M., Schonteich, E., Prekeris, R., Moritz, O.L., Randazzo, P.A., and Deretic, D. (2009). Ciliary targeting motif VxPx directs assembly of a trafficking module through Arf4. Embo J. *28*, 183–192.
24. Mukhopadhyay, S., and Rohatgi, R. (2014). G-protein-coupled receptors, Hedgehog signaling and primary cilia. Semin Cell Dev Biol *33*, 63–72.
25. Petracca, Y.L., Sartoretti, M.M., Di Bella, D.J., Marin-Burgin, A., Carcagno, A.L., Schinder, A.F., and Lanuza, G.M. (2016). The late and dual origin of cerebrospinal fluid-contacting neurons in the mouse spinal cord. Development *143*, 880–891.
26. Quinlan, R.J., Tobin, J.L., and Beales, P.L. (2008). Modeling ciliopathies: Primary cilia in development and disease. Curr. Top. Dev. Biol. *84*, 249–310.
27. Rohatgi, R., Milenkovic, L., and Scott, M.P. (2007). Patched1 Regulates Hedgehog Signaling at the Primary Cilium. Science *317*, 372–376.

28. Rosenbaum, J.L., and Witman, G.B. (2002). Intraflagellar transport. Nat. Rev. Mol. Cell Biol. *3*, 813–825.
29. Rossi, A., Kontarakis, Z., Gerri, C., Nolte, H., Hölper, S., Krüger, M., and Stainier, D.Y.R. (2015). Genetic compensation induced by deleterious mutations but not gene knockdowns. Nature *524*, 230–233.
30. Satir, P., Pedersen, L.B., and Christensen, S.T. (2010). The primary cilium at a glance. J Cell Sci *123*, 499–503.
31. Schou, K.B., Pedersen, L.B., and Christensen, S.T. (2015). Ins and outs of GPCR signaling in primary cilia. EMBO Rep. *16*, 1099–1113.
32. Song, J., Ampatzis, K., Björnfors, E.R., and Manira, El, A. (2016). Motor neurons control locomotor circuit function retrogradely via gap junctions. Nature *529*, 399–402.
33. Sorokin, S.P. (1968). Reconstructions of centriole formation and ciliogenesis in mammalian lungs. J Cell Sci *3*, 207–230.
34. Tadenev, A.L.D., Kulaga, H.M., May-Simera, H.L., Kelley, M.W., Katsanis, N., and Reed, R.R. (2011). Loss of Bardet-Biedl syndrome protein-8 (BBS8) perturbs olfactory function, protein localization, and axon targeting. Proc Natl Acad Sci USA *108*, 10320–10325.
35. Tong, C.K., Han, Y.-G., Shah, J.K., Obernier, K., Guinto, C.D., and Alvarez-Buylla, A. (2014). Primary cilia are required in a unique subpopulation of neural progenitors. Proc Natl Acad Sci USA *111*, 12438–12443.
36. Villanueva, H., Visbal, A.P., Obeid, N.F., Ta, A.Q., Faruki, A.A., Wu, M.-F., Hilsenbeck, S.G., Shaw, C.A., Yu, P., Plummer, N.W., et al. (2015). An essential role for Gα(i2) in Smoothened-stimulated epithelial cell proliferation in the mammary gland. Sci Signal *8*, ra92.
37. Wang, Z., Li, V., Chan, G.C.K., Phan, T., Nudelman, A.S., Xia, Z., and Storm, D.R. (2009). Adult type 3 adenylyl cyclase-deficient mice are obese. PLoS ONE *4*, e6979.
38. Warp, E., Agarwal, G., Wyart, C., Friedmann, D., Oldfield, C.S., Conner, A., Del Bene, F., Arrenberg, A.B., Baier, H., and Isacoff, E.Y. (2012). Emergence of patterned activity in the developing zebrafish spinal cord. Curr Biol *22*, 93–102.
39. Waters, A.M., and Beales, P.L. (2011). Ciliopathies: an expanding disease spectrum. Pediatr. Nephrol. *26*, 1039–1056.
40. Wyart, C., Del Bene, F., Warp, E., Scott, E.K., Trauner, D., Baier, H., and Isacoff, E.Y. (2009). Optogenetic dissection of a behavioural module in the vertebrate spinal cord. Nature *461*, 407–410.
41. Yu, K., McGlynn, S., and Matise, M.P. (2013). Floor plate-derived sonic hedgehog regulates glial and ependymal cell fates in the developing spinal cord. Development *140*, 1594–1604.
42. Østerlund, T., and Kogerman, P. (2006). Hedgehog signalling: how to get from Smo to Ci and Gli. Trends in Cell Biology *16*, 176–180.

CHAPTER 5

GENERAL DISCUSSION AND FUTURE EXPERIMENTS

General Discussion and Future Experiments

Here we have used the zebrafish to investigate the regulation of early spontaneous neural activity and behavior during the development of the spinal central pattern generator. The work shown includes a new role for spontaneous activity in network maturation, a novel means for environmental control over activity, and characterization of the sensory mechanism that regulates activity at the cellular and molecular levels. These findings fit into the research community's larger body of work on developing zebrafish, pattern generators, activity-dependent processes, and nonvisual photoreception. The most interesting implications of this work lie at the interfaces among these fields of study.

Activity Dependence in Development

The progression of spontaneous activity in the zebrafish spinal cord from uncorrelated and sporadic to strictly correlated and patterned is not unique to just this system. Similar progressions through these developmental phases of spontaneous activity are observed in retina, hippocampus, cortex, cerebellum, and other regions of the CNS (reviewed in (Kirkby et al., 2013)). In some of these systems, including retina, cortex, and spinal cord, coordinated activity arises first form electrical synapses that connect cells into a network. Experimental evidence in early zebrafish spinal cord shows these ipsilateral gap junctions among interneurons and motor neurons but also infers the presence of contralateral glycinergic synapses (Saint-Amant and Drapeau, 2001; Saint-Amant, 2010). Most experiments searching for activity-dependent processes differentiate between manipulations of global activity levels and restricted manipulation to alter intercellular competition. Electrical synapses that synchronize a network are a challenge to the latter.

The insufficiency of pharmacological blockers for gap junctions prohibits experiments that rely on disrupting or manipulating the pattern of cellular activity within a coupled network. Known blockers and uncouplers of gap junctions have extremely broad off-target effects and can be toxic at an effective concentration (Verselis and Srinivas, 2013). Additionally, owing to the genome duplication in zebrafish, there are a reported 37 individual connexin genes in contrast to the 20 mouse and 21 human connexins (Abascal and Zardoya, 2013; Eastman et al., 2006). Without knowing the list of which connexins can partner within a heteromeric hemichannel and which connexins can bridge two cells in a gap junction, knockout and dominant negative experiments are likely to only ever deliver negative results.

Without a means to disrupt patterns of correlated activity, we resorted to manipulating global activity levels. The effect we observed on the calcium activity of KA cells is interesting for a number of reasons. Though dorsal KA cells are included within the 1020:Gal4 / olig2^{+} expression domain and would also be manipulated by halorhodopsin in our early experiments, it is possible that the instigating signal is actually the decrease in activity in the lateral CPG network. We see the same effect on KAs by activating endogenous VALopA as our manipulation. Since our preliminary results indicate that VALopA expression predominantly covers motor neurons and lateral interneurons, this would support KA activity patterns changing in response to

global network activity levels. The mechanism by which this information is transferred from the CPG to KAs will be important to uncover. Transcriptome profiling of KAs from embryos raised in the light or raised in the dark could help determine the scaling mechanism by which these cells are altering their intrinsic activity patterns. The alternate hypothesis involving a change in proliferative rates would also appear in sequencing data as these precursors would be easily identifiable by genes involved in the cell cycle.

A number of reports highlighting the proliferative zone along the midline of the spinal cord suggest that these progenitors can easily switch the class of neurons or glia they generate (Batista et al., 2008). These comparisons often describe a push-pull between excitatory and inhibitory fates or neuronal and glial fates (Park et al., 2004; 2007). A number of signaling molecules, including canonical pathways like Notch and Shh, as well as network activity levels have been implicated in regulation of these progenitors and the fate of their output cells. Classic work by Nick Spitzer highlights "waves" of calcium along the midline of the cord during this proliferative stage (Gu et al., 1994). Together with known calcium signaling in precursors, it will be important to use the KA-specific transgenic fish line to differentiate between long-duration calcium transients in neurons and precursors.

Another question involving these immature neurons concerns the mechanism and timing with which these cells integrate into an existing network. Do they first extend a neuronal process any sync their activity? Or does the cell body migrate before becoming active? Interestingly, when blindly patching neurons of the spinal cord in embryonic zebrafish, 49% of cells were not identifiable by soma location or axonal trajectories but *were* spontaneously active (Saint-Amant and Drapeau, 2001). It may be that these unidentifiable cells exist in the continuum between classically defined cell types. For instance, it has been suggested that pacemaker IC cells are merely a subset of alx/chx10 interneurons that also encompass the CiD interneurons (Tong and McDearmid, 2012). As a result, defining more transcriptional markers in the cord at this age is likely to lead only to confusion. There is more hope in using new labeling tools like CaMPARI to identify these cells not by gene expression, but instead by function and activity (Fosque et al., 2015). The fate of these cells and whether their activity is important for development or behavior remains to be seen.

Endogenous photoregulation of neural activity

Studies of spontaneous activity in the early nervous system—including those in this thesis—highlight the simplicity of the circuit as a basic foundation that can be recruited by sensory circuitry *later* in development. This is the core argument against reflex theory: that neural activity and resultant motor behaviors can be generated from within the CNS and without canonical sensory inputs. But what if these inputs are non-canonical? Activity dependent programs purportedly rely on intrinsic genetic programs to generate activity, yet as shown here, it is possible to find environmental regulation of these networks before touch, vision, and other circuits mature. This finding chips away at the cornerstone of Hamburger's work in the 1960's. The claim that, in chick embryos, motor output begins before touch indicates activity before

sensation (Hamburger et al., 1965). While this likely remains true, we must be accepting of any potential environmental inputs as they are discovered.

This trajectory towards identification of further atypical signaling pathways is supported by discoveries in the developing zebrafish: the identification of two nonvisual behaviors and their upstream opsin (opn4 + dark photokinesis, VALopA + photoinhibition) and one behavior without a known photoreceptor (photomotor response) (Fernandes et al., 2012; Friedmann et al., 2015; Kokel et al., 2013). Similarly, there are other known behaviors in the early embryo with no known transduction mechanism. For example, spontaneous coiling frequency increases dramatically upon dechorionation, but it is not known if it is stimulated by pH, pressure, touch, ion concentration, or another input. With regards to light, there remain 18 other extraretinal opsins in the zebrafish genome, many of which are known to express in deep brain nuclei (Fernandes et al., 2013). Which, if any of these are important for behavior, circadian rhythms, or development is entirely unknown. Thankfully, the ease of generating knockouts with CRISPR/Cas9 will hopefully lead to the testing of each of these opsins in turn.

For each of these nonvisual behaviors, the most difficult question to answer is why they exist. Without crisp developmental phenotypes or experiments in natural conditions, experimenters are left with only ideas. For VALopA, we often suggest that photoinhibition is a predator avoidance mechanism akin to freezing behavior in mice. Egg laying is triggered by sunrise in the wild, and embryos are therefore 24 hours old at the following sunrise, depending on water temperature. They will have had 6 hours to freely coil their tail in darkness, but when suddenly made visible by the rising sun, ceasing or slowing their movement may help hide them from predation. VALopA certainly is active in this time window and is sensitive to light levels well below sunlight. The hypothesis that nonvisual behaviors are merely vestigial is not impossible; however, evolutionary arguments would suggest that such a dramatic effect on behavior would not persist if not maintained. At ages when the embryo remains in the chorion, one can certainly rule out place preference and escape behaviors, leaving the best remaining option that photoregulation of neural activity helps guide development.

We have shown an effect of sustained illumination on the patterns of activity within the KA cell population in ventral spinal cord. Though illumination leads to an increased prevalence of long duration calcium events within this cell type, we do not know how this would impact other aspects of development. It is possible that increasing the GABAergic signaling from this population helps drive excitation (GABA is excitatory in the embryonic chloride gradient) in the network following a sustained period of photoinhibition. This would be in line with findings that suggest regulation of levels of neural activity can homeostatically shift the development of an excitatory-inhibitory balance
(Borodinsky et al., 2004; Lin et al., 2008). Also suggestive of this hypothesis, we noticed a reduction in baseline (dark) coiling frequency in the VALopA knockdown and knockout embryos. Given that previous light exposure in wildtype individuals would lead to inhibition, it is possible that these animals experience a rebound-

triggered increase in coiling frequency when placed in total darkness (Fidelin et al., 2015; Warp et al., 2012). Animals lacking VALopA would not experience this rebound effect. In each of these scenarios, we assume that there is a developmental requirement for a predetermined coiling frequency. The rules governing this homeostatic setpoint for activity remain one of the most interesting and important questions in neuroscience.

Less direct evidence for the developmental role of VALopA in the spinal cord comes from the known expression timeline for the opsin. In line with the data we have presented here, previous work identified *valopa* RNA in the spinal cord at 24 hpf (Kojima et al., 2008). At later timepoints however, they observed an absence of *valopa* RNA at 48 hpf and persistent expression through larval stages in the brain. Other studies have identified expression of *valopa* in adult brain tissue in the pineal complex as well as in horizontal cells of the retina (Hang et al., 2014; Kojima et al., 2008). Interestingly but purely correlative, the brief 24 hour window for expression in the spinal cord overlaps with the duration of spontaneous coiling. By 2 dpf, the frequency of coiling drops to negligible rates until hatching. Future experiments will have to carefully observe KA and motor neuron development, connectivity, and electrical properties to search deeper for an effect of light and VALopA on development. The expression of VALopA and other opsins in brain tissue of larval fish may lead to the identification of new nonvisual behaviors in these individuals. Larval zebrafish exhibit a wide range of behaviors including spontaneous swimming, escape and avoidance, and hunting of prey(Kalueff et al., 2013; Portugues and Engert, 2009). Many of these are mediated by vision, but experiments with blind fish may identify generalized regulation of behavior by ambient light intensity.

Hopefully, future work on these nonvisual opsins in zebrafish can make connections to the evolutionary history of photodetection. The role for distributed photoreceptors in transparent marine organisms is readily apparent; however, it is less clear why opsins are expressed deep in the tissues of much more opaque animals like mice and humans. For example, neuropsin (OPN5) is expressed in the human brain and spinal cord though it has no known function in these tissues whereas in birds, this opsin is expressed in the lateral hypothalamus and directly senses light to regulate seasonal reproductive behaviors (Nakane et al., 2010; Tarttelin et al., 2003). Recently, OPN5 was identified in ganglion cells of the retina. In experiments with *rd1/rd1;Opn4*$^{-/-}$ mice lacking photoreceptors and melanopsin, it was surprisingly found that the molecular circadian clocks in retinal tissue persisted in wildtype, but not *Opn5*$^{-/-}$ retinas (Buhr et al., 2015). Other orphan opsins, including encephalopsin (OPN3) and RGR, are also expressed in retina, including in Müller glia, yet it is not known what their light-sensitive function may be in these cells (Peirson et al., 2009). Like OPN5, OPN3 is also expressed throughout the mammalian brain (Nissilä et al.). Some adventurous work has shown that ambient light is capable of penetrating brain tissue in humans and through the skull of the mouse (Chuong et al., 2014; Ganong et al., 1963). In fact, surprising results have identified a developmental effect of light on vasculature in mouse embryos (Rao et al., 2013). Given that this effect is dependent on melanopsin expression in the

embryo, but not the mother, it can be deduced that this light must penetrate the abdominal wall and activate opsins in the embryo.

Taken together, these findings have clear implications for the impact of light on behavior and development of many different organisms. Additionally, these findings raise concerns for imaging and optogenetic experiments that use visible light to stimulate or observe neural activity in tissues that are assumed to otherwise be light-insensitive. This is particularly true for whole brain imaging studies of fictive behavior in the larval zebrafish. Proper light-only controls are essential, and when possible, two-photon imaging techniques should be used as a comparison to confirm that patterns of activity are not altered by imaging with visible light. Zebrafish biologists studying early development and spontaneous activity would also be well served to standardize the lighting conditions in their laboratory housing and experimental chambers.

Motor neurons and cilia: shifting our perceptions

Recent research in the motor circuits of juvenile and adult zebrafish has begun to alter our view of motor neurons (Song et al., 2016). No longer are these cells viewed as passive integrators of command inputs that exit the domain of the nervous system before signaling to targets. With the identification of gap junctions that contact premotor V2a interneurons, results show that motor neuron activity can function as an ensemble with these interneurons and can regulate their synaptic release properties as well as the resultant rhythm generation. These electrical synapses also exist during early development—the new surprise is their persistence to adulthood.

Our recent discovery of an opsin in motor neurons has made the function of this cell type even less clear. With their known ability to signal back into the network at this age, these cells can now be perceived as sensory input neurons as well as outputs. Future work will have to examine the duration of VALopA's effect in these cells through development and how they communicate inhibition to other cells in the network. Though VALopA is a known GPCR, and we show it can couple though $G\alpha_i$ in a heterologous system, we do not yet know the signaling partners *in vivo*. Pharmacology experiments to test for blockers of photoinhibition are complicated by the presence of wholly intact skin. At 5 dpf, a common age for behavioral testing, the mouth of the larva is open and compounds in the water easily enter the internal environment of the fish. Before the mouth opens, only strongly lipophilic compounds can cross the skin. The increased permeability afforded by low concentrations of DMSO assists penetrance with variable success. Low throughput experiments with injected compounds show preliminary results in line with our findings in *Xenopus* oocytes and suggest that VALopA may couple to GIRK in the embryo. These experiments will be a priority for solving VALopA's cellular mechanism.

Ongoing experiments are addressing the necessity and sufficiency for localization of VALopA to specific cells and to the ciliary compartment. With the generation of a successful line of knockouts that completely lack any photoinhibitory response, we have a useful set of fish for testing various rescue experiments. We have recently generated a stable line for exogenous expression of VALopA under the

Gal4:UAS system and see increased photoinhibition in the wildtype background. Testing this UAS:VALopA line in the 1020, mnx1, and pkd2l1 Gal4 lines and in the background of the knockout, we will be able to determine which cell types of the ventral spinal cord are able to recapitulate natural photoinhibition.

Similarly, rescues in these same cell types with the VALopA V374A or P376A mutants will hopefully determine whether ciliary targeting of the opsin is required for efficient signaling. Using Cas9 and homologous recombination or the new Cas9-cytidine deaminase fusion to generate these mutations in the genome would also determine the necessity of ciliary VALopA *in vivo* (Gagnon et al., 2014; Komor et al., 2016). From these experiments, we also hope to learn more about ciliary function in general. Cilia are experiencing a small renaissance and recent publications have begun to address long-standing questions in the field. The presence of calcium signals in cilia has spurred many hypotheses. We have observed calcium signals in cilia paired in time with calcium transients in the cell body. Others have suggested that mechanical force generated by fluid flow could open calcium channels and lead to signaling (Zimmerman and Yoder, 2015). A recent set of experiments by the Clapham lab thoroughly tests this hypothesis and found no evidence for such signaling (Delling et al., 2016). Whether other GPCRs, including opsins, within this compartment can trigger calcium influx remains to be seen. In these motile cilia, we are also interested to determine if light impacts the frequency or mechanics of ciliary beating and are hoping that combinations of 2- and 1-photon imaging can give us this answer.

Perhaps the most interesting possibility for crosstalk with VALopA in these cells is the hedgehog pathway. Sonic hedgehog is released from the floor plate of the spinal cord and diffuses dorsally and laterally into the developing tissue. This generates a concentration gradient of the morphogen, and induces different cell types depending on the apparent local concentration of the molecule. Shh signals in the primary cilium of these cells and relies on the ciliary localization of downstream proteins in the pathway. This connection was first discovered in mutants for intraflagellar transport machinery that show reduced Shh signaling (Huangfu et al., 2003). The influence of PKA on blocking Gli transcription factors (an essential component of the Shh pathway) from the cilium suggests the possibility for crosstalk between $G_{i/a}$ GPCRs and Shh signals (Mukhopadhyay and Rohatgi, 2014). Future experiments in the fish will certainly look for light-dependent patterning changes, including the position and final number of primary and secondary motor neurons.

There is also potential for VALopA as a tool in heterologous systems. The localization of the opsin to cilia in mouse hippocampal neurons will potentially lead to optogenetic regulation of ciliary signals. We also hope to use these neurons to investigate how ciliary GPCR signaling can so strongly regulate spontaneous neural activity in the zebrafish by patching cilia in culture. In this vein, we are also developing *Drosophila* that express UAS:VALopA to determine if it remains functional in an invertebrate system. As a tool for manipulating neural activity, the extremely slow off kinetics of VALopA will preclude it from use in some scenarios. However, as many experiments with inhibition rely on chronic suppression of activity, these

kinetics will be an extremely useful property to produce long-lasting inhibition from just a short pulse of visible light.

REFERENCES

Abascal, F., and Zardoya, R. (2013). Evolutionary analyses of gap junction protein families. Biochim Biophys Acta *1828*, 4–14.

Ackman, J.B., Burbridge, T.J., and Crair, M.C. (2012). Retinal waves coordinate patterned activity throughout the developing visual system. Nature *490*, 219–225.

Adamantidis, A., Arber, S., Bains, J.S., Bamberg, E., Bonci, A., Buzsáki, G., Cardin, J.A., Costa, R.M., Dan, Y., Goda, Y., et al. (2015). Optogenetics: 10 years after ChR2 in neurons--views from the community. Nat Neurosci *18*, 1202–1212.

Airan, R.D., Thompson, K.R., Fenno, L.E., Bernstein, H., and Deisseroth, K. (2009). Temporally precise in vivo control of intracellular signalling. Nature *458*, 1025–1029.

Akerboom, J., Chen, T.-W., Wardill, T.J., Tian, L., Marvin, J.S., Mutlu, S., Calderón, N.C., Esposti, F., Borghuis, B.G., Sun, X.R., et al. (2012). Optimization of a GCaMP calcium indicator for neural activity imaging. J Neurosci *32*, 13819–13840.

Arendt, D., Tessmar-Raible, K., Snyman, H., Dorresteijn, A.W., and Wittbrodt, J. (2004). Ciliary photoreceptors with a vertebrate-type opsin in an invertebrate brain. Science *306*, 869–871.

Balice-Gordon, R.J., and Lichtman, J.W. (1994). Long-term synapse loss induced by focal blockade of postsynaptlc receptors. Nature *372*, 519–524.

Batista, M.F., Jacobstein, J., and Lewis, K.E. (2008). Zebrafish V2 cells develop into excitatory CiD and Notch signalling dependent inhibitory VeLD interneurons. Dev Biol *322*, 263–275.

Ben-Ari, Y., Cherubini, E., Corradetti, R., and Gaiarsa, J.L. (1989). Giant synaptic potentials in immature rat CA3 hippocampal neurones. J Physiol (Lond) *416*, 303–325.

Berlin, S., Carroll, E.C., Newman, Z.L., Okada, H.O., Quinn, C.M., Kallman, B., Rockwell, N.C., Martin, S.S., Lagarias, J.C., and Isacoff, E.Y. (2015). Photoactivatable genetically encoded calcium indicators for targeted neuronal imaging. Nat Meth *12*, 852–858.

Berndt, A., Lee, S.Y., Ramakrishnan, C., and Deisseroth, K. (2014). Structure-guided transformation of channelrhodopsin into a light-activated chloride channel. Science *344*, 420–424.

Bernhardt, R.R., Chitnis, A.B., Lindamer, L., and Kuwada, J.Y. (1990). Identification of spinal neurons in the embryonic and larval zebrafish. J Comp Neurol *302*, 603–

616.

Bill, B.R., Petzold, A.M., Clark, K.J., Schimmenti, L.A., and Ekker, S.C. (2009). A primer for morpholino use in zebrafish. Zebrafish *6*, 69–77.

Blackburn, P.R., Campbell, J.M., Clark, K.J., and Ekker, S.C. (2013). The CRISPR system--keeping zebrafish gene targeting fresh. Zebrafish *10*, 116–118.

Blankenship, A.G., and Feller, M.B. (2010). Mechanisms underlying spontaneous patterned activity in developing neural circuits. Nat Rev Neurosci *11*, 18–29.

Borodinsky, L.N., Belgacem, Y.H., and Swapna, I. (2012). Electrical activity as a developmental regulator in the formation of spinal cord circuits. Curr Opin Neurobiol 1–7.

Borodinsky, L.N., Root, C.M., Cronin, J.A., Sann, S.B., Gu, X., and Spitzer, N.C. (2004). Activity-dependent homeostatic specification of transmitter expression in embryonic neurons. Nature *429*, 523–530.

Brockerhoff, S.E., Hurley, J.B., Janssen-Bienhold, U., Neuhauss, S.C., Driever, W., and Dowling, J.E. (1995). A behavioral screen for isolating zebrafish mutants with visual system defects. Proc Natl Acad Sci USA *92*, 10545–10549.

Brown, T.G. (1914). On the nature of the fundamental activity of the nervous centres; together with an analysis of the conditioning of rhythmic activity in progression, and a theory of the evolution of function in the nervous system. J Physiol (Lond) *48*, 18–46.

Brown, T.G. (1911). The Intrinsic Factors in the Act of Progression in the Mammal. Proceedings of the Royal Society of London. Series B, Containing Papers of a Biological Character *84*, 308–319.

Buffelli, M., Busetto, G., Cangiano, L., and Cangiano, A. (2002). Perinatal switch from synchronous to asynchronous activity of motoneurons: link with synapse elimination. Proc Natl Acad Sci USA *99*, 13200–13205.

Buhr, E.D., Yue, W.W.S., Ren, X., Jiang, Z., Liao, H.-W.R., Mei, X., Vemaraju, S., Nguyen, M.-T., Reed, R.R., Lang, R.A., et al. (2015). Neuropsin (OPN5)-mediated photoentrainment of local circadian oscillators in mammalian retina and cornea. Proc Natl Acad Sci USA *112*, 13093–13098.

Bullock, T.H. (1961). The Origins of Patterned Nervous Discharge. Behaviour *17*, 48–59.

Busetto, G., Buffelli, M., Tognana, E., Bellico, F., and Cangiano, A. (2000). Hebbian mechanisms revealed by electrical stimulation at developing rat neuromuscular junctions. J Neurosci *20*, 685–695.

Buss, R.R., Bourque, C.W., and Drapeau, P. (2002). Membrane Properties Related to the Firing Behavior of Zebrafish Motoneurons. J Neurophysiol *89*, 657–664.

Cassone, V.M. (1998). Melatonin's role in vertebrate circadian rhythms. Chronobiol. Int. *15*, 457–473.

Chen, T.-W., Wardill, T.J., Sun, Y., Pulver, S.R., Renninger, S.L., Baohan, A., Schreiter, E.R., Kerr, R.A., Orger, M.B., Jayaraman, V., et al. (2013). Ultrasensitive fluorescent proteins for imaging neuronal activity. Nature *499*, 295–300.

Chhetri, R.K., Amat, F., Wan, Y., Höckendorf, B., Lemon, W.C., and Keller, P.J. (2015). Whole-animal functional and developmental imaging with isotropic spatial resolution. Nat Meth *12*, 1171–1178.

Chuong, A.S., Miri, M.L., Busskamp, V., Matthews, G.A.C., Acker, L.C., Sørensen, A.T., Young, A., Klapoetke, N.C., Henninger, M.A., Kodandaramaiah, S.B., et al. (2014). Noninvasive optical inhibition with a red-shifted microbial rhodopsin. Nat Neurosci *17*, 1123–1129.

Coghill, G.E. (1929). Anatomy and the Problem of Behaviour (Cambridge, England: Cambridge University Press).

Collin, S.P., Davies, W.L., Hart, N.S., and Hunt, D.M. (2009). The evolution of early vertebrate photoreceptors. Philos. Trans. R. Soc. Lond., B, Biol. Sci. *364*, 2925–2940.

Cowley, K.C., and Schmidt, B.J. (1995). Effects of inhibitory amino acid antagonists on reciprocal inhibitory interactions during rhythmic motor activity in the in vitro neonatal rat spinal cord. J Neurophysiol *74*, 1109–1117.

Davis, G.W. (2013). Homeostatic signaling and the stabilization of neural function. Neuron *80*, 718–728.

Deisseroth, K. (2011). Optogenetics. Nat Meth *8*, 26–29.

Delling, M., Indzhykulian, A.A., Liu, X., Li, Y., Xie, T., Corey, D.P., and Clapham, D.E. (2016). Primary cilia are not calcium-responsive mechanosensors. Nature *531*, 656–660.

Dhande, O.S., Hua, E.W., Guh, E., Yeh, J., Bhatt, S., Zhang, Y., Ruthazer, E.S., Feller, M.B., and Crair, M.C. (2011). Development of single retinofugal axon arbors in normal and β2 knock-out mice. J Neurosci *31*, 3384–3399.

Downes, G.B., and Granato, M. (2006). Supraspinal input is dispensable to generate glycine-mediated locomotive behaviors in the zebrafish embryo. J Neurobiol *66*, 437–451.

Drapeau, P., Ali, D.W., Buss, R.R., and Saint-Amant, L. (1999). In vivo recording from identifiable neurons of the locomotor network in the developing zebrafish. J. Neurosci. Methods *88*, 1–13.

Drapeau, P., Saint-Amant, L., Buss, R.R., Chong, M., McDearmid, J.R., and Brustein, E. (2002a). Development of the locomotor network in zebrafish. Prog Neurobiol *68*, 85–111.

Drapeau, P., Saint-Amant, L., Buss, R.R., Chong, M., McDearmid, J.R., and Brustein, E. (2002b). Development of the locomotor network in zebrafish. Prog Neurobiol *68*, 85–111.

Easter, S.S., and Nicola, G.N. (1996). The development of vision in the zebrafish (Danio rerio). Dev Biol *180*, 646–663.

Eastman, S.D., Chen, T.H.-P., Falk, M.M., Mendelson, T.C., and Iovine, M.K. (2006). Phylogenetic analysis of three complete gap junction gene families reveals lineage-specific duplications and highly supported gene classes. Genomics *87*, 265–274.

Eisen, J.S. (1991a). Motoneuronal development in the embryonic zebrafish. Development *Suppl 2*, 141–147.

Eisen, J.S. (1991b). Determination of primary motoneuron identity in developing zebrafish embryos. Science *252*, 569–572.

Eisen, J.S., and Smith, J.C. (2008). Controlling morpholino experiments: don't stop making antisense. Development *135*, 1735–1743.

Eklof-Ljunggren, E., Haupt, S., Ausborn, J., Dehnisch, I., Uhlen, P., Higashijima, S.-I., and Manira, El, A. (2012). Origin of excitation underlying locomotion in the spinal circuit of zebrafish. Proceedings of the National Academy of Sciences *109*, 5511–5516.

Ekström, P., and Meissl, H. (2003). Evolution of photosensory pineal organs in new light: the fate of neuroendocrine photoreceptors. Philos. Trans. R. Soc. Lond., B, Biol. Sci. *358*, 1679–1700.

Elias, L.A.B., Wang, D.D., and Kriegstein, A.R. (2007). Gap junction adhesion is necessary for radial migration in the neocortex. Nature *448*, 901–907.

Favero, M., Busetto, G., and Cangiano, A. (2012). Spike timing plays a key role in synapse elimination at the neuromuscular junction. Proc Natl Acad Sci USA *109*, E1667–E1675.

Favero, M., Cangiano, A., and Busetto, G. (2014). Hebb-based rules of neural plasticity: are they ubiquitously important for the refinement of synaptic connections

in development? Neuroscientist *20*, 8–14.

Fernandes, A.M., Fero, K., Arrenberg, A.B., Bergeron, S.A., Driever, W., and Burgess, H.A. (2012). Deep brain photoreceptors control light-seeking behavior in zebrafish larvae. Curr Biol *22*, 2042–2047.

Fernandes, A.M., Fero, K., Driever, W., and Burgess, H.A. (2013). Enlightening the brain: linking deep brain photoreception with behavior and physiology. Bioessays *35*, 775–779.

Fetcho, J.R., Cox, K.J., and O'Malley, D.M. (1998). Monitoring activity in neuronal populations with single-cell resolution in a behaving vertebrate. Histochem. J. *30*, 153–167.

Fidelin, K., Djenoune, L., Stokes, C., Prendergast, A., Gomez, J., Baradel, A., Del Bene, F., and Wyart, C. (2015). State-Dependent Modulation of Locomotion by GABAergic Spinal Sensory Neurons. Curr Biol *25*, 3035–3047.

Fosque, B.F., Sun, Y., Dana, H., Yang, C.-T., Ohyama, T., Tadross, M.R., Patel, R., Zlatic, M., Kim, D.S., Ahrens, M.B., et al. (2015). Neural circuits. Labeling of active neural circuits in vivo with designed calcium integrators. Science *347*, 755–760.

Foster, R.G., Provencio, I., Hudson, D., Fiske, S., De Grip, W., and Menaker, M. (1991). Circadian photoreception in the retinally degenerate mouse (rd/rd). J Comp Physiol A *169*, 39–50.

Foster, R.G., and Hankins, M.W. (2002). Non-rod, non-cone photoreception in the vertebrates. Progress in Retinal and Eye Research *21*, 507–527.

Friedmann, D., Hoagland, A., Berlin, S., and Isacoff, E.Y. (2015). A spinal opsin controls early neural activity and drives a behavioral light response. Curr Biol *25*, 69–74.

Fukada, Y., and Okano, T. (2002). Circadian clock system in the pineal gland. Mol Neurobiol *25*, 19–30.

Gagnon, J.A., Valen, E., Thyme, S.B., Huang, P., Ahkmetova, L., Pauli, A., Montague, T.G., Zimmerman, S., Richter, C., and Schier, A.F. (2014). Efficient mutagenesis by Cas9 protein-mediated oligonucleotide insertion and large-scale assessment of single-guide RNAs. PLoS ONE *9*, e98186.

Ganong, W.F., Sheperd, Wall, J.R., van Brunt, E.E., and Clegg, M.T. (1963). Penetration of light into the brain of mammals. Endocrinology *72*, 962–963.

Garaschuk, O., Linn, J., Eilers, J., and Konnerth, A. (2000). Large-scale oscillatory calcium waves in the immature cortex. Nat Neurosci *3*, 452–459.

García-Fernández, J.M., Cernuda-Cernuda, R., Davies, W.I.L., Rodgers, J., Turton, M., Peirson, S.N., Follett, B.K., Halford, S., Hughes, S., Hankins, M.W., et al. (2015). The hypothalamic photoreceptors regulating seasonal reproduction in birds: a prime role for VA opsin. Front Neuroendocrinol *37*, 13–28.

Garm, A., and Bielecki, J. (2008). Swim pacemakers in box jellyfish are modulated by the visual input. J. Comp. Physiol. a Neuroethol. Sens. Neural. Behav. Physiol. *194*, 641–651.

Goulding, M. (2009). Circuits controlling vertebrate locomotion: moving in a new direction. Nat Rev Neurosci *10*, 507–518.

Gradinaru, V., Thompson, K.R., and Deisseroth, K. (2008). eNpHR: a Natronomonas halorhodopsin enhanced for optogenetic applications. Brain Cell Bio *36*, 129–139.

Granato, M., van Eeden, F.J., Schach, U., Trowe, T., Brand, M., Furutani-Seiki, M., Haffter, P., Hammerschmidt, M., Heisenberg, C.P., Jiang, Y.J., et al. (1996). Genes controlling and mediating locomotion behavior of the zebrafish embryo and larva. Development *123*, 399–413.

Grillner, S., and Jessell, T.M. (2009). Measured motion: searching for simplicity in spinal locomotor networks. Curr Opin Neurobiol *19*, 572–586.

Gu, X., Olson, E.C., and Spitzer, N.C. (1994). Spontaneous neuronal calcium spikes and waves during early differentiation. J Neurosci *14*, 6325–6335.

Guemez-Gamboa, A., Xu, L., Meng, D., and Spitzer, N.C. (2014). Non-Cell-Autonomous Mechanism of Activity-Dependent Neurotransmitter Switching. Neuron *82*, 1004–1016.

Haffter, P., Granato, M., Brand, M., Mullins, M.C., Hammerschmidt, M., Kane, D.A., Odenthal, J., van Eeden, F.J., Jiang, Y.J., Heisenberg, C.P., et al. (1996). The identification of genes with unique and essential functions in the development of the zebrafish, Danio rerio. Development *123*, 1–36.

Halford, S., Pires, S.S., Turton, M., Zheng, L., González-Menéndez, I., Davies, W.L., Peirson, S.N., García-Fernández, J.M., Hankins, M.W., and Foster, R.G. (2009). VA opsin-based photoreceptors in the hypothalamus of birds. Curr Biol *19*, 1396–1402.

Halpern, M.E., Rhee, J., Goll, M.G., Akitake, C.M., Parsons, M., and Leach, S.D. (2008). Gal4/UAS transgenic tools and their application to zebrafish. Zebrafish *5*, 97–110.

Hamburger, V. (1963). Some Aspects of the Embryology of Behavior. Quarterly Review of Biology *38*, 342–365.

Hamburger, V., and Balaban, M. (1963). Observations and experiments on spontaneous rhythmical behavior in the chick embryo. Dev Biol *6*, 533–545.

Hamburger, V., Balaban, M., Oppenheim, R., and Wenger, E. (1965). Periodic motility of normal and spinal chick embryos between 8 and 17 days of incubation. J. Exp. Zool. *159*, 1–13.

Hang, C.Y., Kitahashi, T., and Parhar, I.S. (2014). Localization and characterization of val-opsin isoform-expressing cells in the brain of adult zebrafish. J Comp Neurol *522*, 3847–3860.

Hanson, M.G., and Landmesser, L.T. (2004). Normal patterns of spontaneous activity are required for correct motor axon guidance and the expression of specific guidance molecules. Neuron *43*, 687–701.

Hengen, K.B., Lambo, M.E., Van Hooser, S.D., Katz, D.B., and Turrigiano, G.G. (2013). Firing rate homeostasis in visual cortex of freely behaving rodents. Neuron *80*, 335–342.

Higashijima, S.-I., Mandel, G., and Fetcho, J.R. (2004a). Distribution of prospective glutamatergic, glycinergic, and GABAergic neurons in embryonic and larval zebrafish. J Comp Neurol *480*, 1–18.

Higashijima, S.-I., Schaefer, M., and Fetcho, J.R. (2004b). Neurotransmitter properties of spinal interneurons in embryonic and larval zebrafish. J Comp Neurol *480*, 19–37.

Huangfu, D., Liu, A., Rakeman, A.S., Murcia, N.S., Niswander, L., and Anderson, K.V. (2003). Hedgehog signalling in the mouse requires intraflagellar transport proteins. Nature *426*, 83–87.

Huberman, A.D., Feller, M.B., and Chapman, B. (2008). Mechanisms underlying development of visual maps and receptive fields. Annu Rev Neurosci *31*, 479–509.

Ihara, K., Umemura, T., Katagiri, I., Kitajima-Ihara, T., Sugiyama, Y., Kimura, Y., and Mukohata, Y. (1999). Evolution of the archaeal rhodopsins: evolution rate changes by gene duplication and functional differentiation. J Mol Biol *285*, 163–174.

Inada, K., Horie, T., Kusakabe, T., and Tsuda, M. (2003). Targeted knockdown of an opsin gene inhibits the swimming behaviour photoresponse of ascidian larvae. Neurosci Lett *347*, 167–170.

Jablonski, A.M., and Kalb, R.G. (2013). GluA1 promotes the activity-dependent development of motor circuitry in the developing segmental spinal cord. Ann N Y Acad Sci *1279*, 54–59.

Jinek, M., Chylinski, K., Fonfara, I., Hauer, M., Doudna, J.A., and Charpentier, E. (2012). A Programmable Dual-RNA-Guided DNA Endonuclease in Adaptive Bacterial Immunity. Science *337*, 816–821.

Kalueff, A.V., Gebhardt, M., Stewart, A.M., Cachat, J.M., Brimmer, M., Chawla, J.S., Craddock, C., Kyzar, E.J., Roth, A., Landsman, S., et al. (2013). Towards a comprehensive catalog of zebrafish behavior 1.0 and beyond. Zebrafish *10*, 70–86.

Kastanenka, K.V., and Landmesser, L.T. (2010). In vivo activation of channelrhodopsin-2 reveals that normal patterns of spontaneous activity are required for motoneuron guidance and maintenance of guidance molecules. J Neurosci *30*, 10575–10585.

Kawakami, K., Takeda, H., Kawakami, N., Kobayashi, M., Matsuda, N., and Mishina, M. (2004). A transposon-mediated gene trap approach identifies developmentally regulated genes in zebrafish. Dev Cell *7*, 133–144.

Keller, P.J., and Ahrens, M.B. (2015). Visualizing whole-brain activity and development at the single-cell level using light-sheet microscopy. Neuron *85*, 462–483.

Kiehn, O. (2011). Development and functional organization of spinal locomotor circuits. Curr Opin Neurobiol *21*, 100–109.

Kiehn, O., and Tresch, M.C. (2002). Gap junctions and motor behavior. Trends Neurosci *25*, 108–115.

Kimmel, C.B., Ballard, W.W., Kimmel, S.R., Ullmann, B., and Schilling, T.F. (1995). Stages of embryonic development of the zebrafish. Dev Dyn *203*, 253–310.

Kimura, Y. (2006). alx, a Zebrafish Homolog of Chx10, Marks Ipsilateral Descending Excitatory Interneurons That Participate in the Regulation of Spinal Locomotor Circuits. J Neurosci *26*, 5684–5697.

Kirkby, L.A., Sack, G.S., Firl, A., and Feller, M.B. (2013). A role for correlated spontaneous activity in the assembly of neural circuits. Neuron *80*, 1129–1144.

Kleindienst, T., Winnubst, J., Roth-Alpermann, C., Bonhoeffer, T., and Lohmann, C. (2011). Activity-dependent clustering of functional synaptic inputs on developing hippocampal dendrites. Neuron *72*, 1012–1024.

Knogler, L.D., Ryan, J., Saint-Amant, L., and Drapeau, P. (2014). A hybrid electrical/chemical circuit in the spinal cord generates a transient embryonic motor behavior. J Neurosci *34*, 9644–9655.

Knöpfel, T., Gallero-Salas, Y., and Song, C. (2015). Genetically encoded voltage

indicators for large scale cortical imaging come of age. Curr Opin Chem Biol *27*, 75–83.

Kojima, D., Torii, M., Fukada, Y., and Dowling, J.E. (2008). Differential expression of duplicated VAL-opsin genes in the developing zebrafish. J Neurochem *104*, 1364–1371.

Kok, F.O., Shin, M., Ni, C.-W., Gupta, A., Grosse, A.S., van Impel, A., Kirchmaier, B.C., Peterson-Maduro, J., Kourkoulis, G., Male, I., et al. (2015). Reverse genetic screening reveals poor correlation between morpholino-induced and mutant phenotypes in zebrafish. Dev Cell *32*, 97–108.

Kokel, D., Dunn, T.W., Ahrens, M.B., Alshut, R., Cheung, C.Y.J., Saint-Amant, L., Bruni, G., Mateus, R., van Ham, T.J., Shiraki, T., et al. (2013). Identification of nonvisual photomotor response cells in the vertebrate hindbrain. J Neurosci *33*, 3834–3843.

Komor, A.C., Kim, Y.B., Packer, M.S., Zuris, J.A., and Liu, D.R. (2016). Programmable editing of a target base in genomic DNA without double-stranded DNA cleavage. Nature.

Korf, B., Rollag, M., and Korf, H.-W. (1989). Ontogenetic development of S-antigen- and rodopsin immunoreactions in retinal and pineal photoreceptors of Xenopus laevis in relation to the onset of melatonin-dependent color-change mechanisms. Cell Tissue Res *258*, 319–329.

Kwan, K.M., Fujimoto, E., Grabher, C., Mangum, B.D., Hardy, M.E., Campbell, D.S., Parant, J.M., Yost, H.J., Kanki, J.P., and Chien, C.-B. (2007). The Tol2kit: a multisite gateway-based construction kit for Tol2 transposon transgenesis constructs. Dev Dyn *236*, 3088–3099.

Li, W.-C. (2011). Generation of locomotion rhythms without inhibition in vertebrates: the search for pacemaker neurons. Integr. Comp. Biol. *51*, 879–889.

Li, W.-C., Roberts, A., and Soffe, S.R. (2009). Locomotor rhythm maintenance: electrical coupling among premotor excitatory interneurons in the brainstem and spinal cord of young Xenopus tadpoles. J Physiol (Lond) *587*, 1677–1693.

Lin, Y., Bloodgood, B.L., Hauser, J.L., Lapan, A.D., Koon, A.C., Kim, T.-K., Hu, L.S., Malik, A.N., and Greenberg, M.E. (2008). Activity-dependent regulation of inhibitory synapse development by Npas4. Nature *455*, 1198–1204.

Lupo, G., Harris, W.A., and Lewis, K.E. (2006). Mechanisms of ventral patterning in the vertebrate nervous system. Nat Rev Neurosci *7*, 103–114.

Mahoney, R.E., Rawson, J.M., and Eaton, B.A. (2014). An age-dependent change in

the set point of synaptic homeostasis. J Neurosci *34*, 2111–2119.

Malenka, R.C., and Bear, M.F. (2004). LTP and LTD: an embarrassment of riches. Neuron *44*, 5–21.

Mano, H., Kojima, D., and Fukada, Y. (1999). Exo-rhodopsin: a novel rhodopsin expressed in the zebrafish pineal gland. Brain Res Mol Brain Res *73*, 110–118.

Marek, K.W., Kurtz, L.M., and Spitzer, N.C. (2010). cJun integrates calcium activity and tlx3 expression to regulate neurotransmitter specification. Nat Neurosci *13*, 944–950.

Max, M., McKinnon, P.J., Seidenman, K.J., Barrett, R.K., Applebury, M.L., Takahashi, J.S., and Margolskee, R.F. (1995). Pineal opsin: a nonvisual opsin expressed in chick pineal. Science *267*, 1502–1506.

Mendelson, B. (1986a). Development of reticulospinal neurons of the zebrafish. I. Time of origin. J Comp Neurol *251*, 160–171.

Mendelson, B. (1986b). Development of reticulospinal neurons of the zebrafish. II. Early axonal outgrowth and cell body position. J Comp Neurol *251*, 172–184.

Moly, P.K., Ikenaga, T., Kamihagi, C., Islam, A.F.M.T., and Hatta, K. (2014). Identification of initially appearing glycine-immunoreactive neurons in the embryonic zebrafish brain. Dev Neurobiol *74*, 616–632.

Montoro, R.J., and Yuste, R. (2004). Gap junctions in developing neocortex: a review. Brain Res Brain Res Rev *47*, 216–226.

Mukhopadhyay, S., and Rohatgi, R. (2014). G-protein-coupled receptors, Hedgehog signaling and primary cilia. Semin Cell Dev Biol *33*, 63–72.

Muto, A., Ohkura, M., Abe, G., Nakai, J., and Kawakami, K. (2013). Real-time visualization of neuronal activity during perception. Curr Biol *23*, 307–311.

Muto, A., Ohkura, M., Kotani, T., Higashijima, S.-I., Nakai, J., and Kawakami, K. (2011). Genetic visualization with an improved GCaMP calcium indicator reveals spatiotemporal activation of the spinal motor neurons in zebrafish. Proc Natl Acad Sci USA *108*, 5425–5430.

Myers, P.Z., Eisen, J.S., and Westerfield, M. (1986). Development and axonal outgrowth of identified motoneurons in the zebrafish. J Neurosci *6*, 2278–2289.

Nakai, J., Ohkura, M., and Imoto, K. (2001). A high signal-to-noise Ca(2+) probe composed of a single green fluorescent protein. Nat Biotechnol *19*, 137–141.

Nakane, Y., Ikegami, K., Ono, H., Yamamoto, N., Yoshida, S., Hirunagi, K., Ebihara,

S., Kubo, Y., and Yoshimura, T. (2010). A mammalian neural tissue opsin (Opsin 5) is a deep brain photoreceptor in birds. Proc Natl Acad Sci USA *107*, 15264–15268.

Nathans, J., and Hogness, D.S. (1983). Isolation, sequence analysis, and intron-exon arrangement of the gene encoding bovine rhodopsin. Cell *34*, 807–814.

Neuhauss, S.C., Biehlmaier, O., Seeliger, M.W., Das, T., Kohler, K., Harris, W.A., and Baier, H. (1999). Genetic disorders of vision revealed by a behavioral screen of 400 essential loci in zebrafish. J Neurosci *19*, 8603–8615.

Nissilä, J., Mänttäri, S., Särkioja, T., Tuominen, H., Takala, T., Timonen, M., and Saarela, S. Encephalopsin (OPN3) protein abundance in the adult mouse brain. J Comp Physiol A *198*, 833–839.

O'Leary, T., Williams, A.H., Franci, A., and Marder, E. (2014). Cell types, network homeostasis, and pathological compensation from a biologically plausible ion channel expression model. Neuron *82*, 809–821.

Ohkura, M., Matsuzaki, M., Kasai, H., Imoto, K., and Nakai, J. (2005). Genetically encoded bright Ca2+ probe applicable for dynamic Ca2+ imaging of dendritic spines. Anal. Chem. *77*, 5861–5869.

Ono, H., Nakao, N., and Yoshimura, T. (2009). Identification of the photoperiodic signaling pathway regulating seasonal reproduction using the functional genomics approach. Gen. Comp. Endocrinol. *163*, 2–6.

Palmer, A.E., and Tsien, R.Y. (2006). Measuring calcium signaling using genetically targetable fluorescent indicators. Nat Protoc *1*, 1057–1065.

Panda, S., Sato, T.K., Castrucci, A.M., Rollag, M.D., DeGrip, W.J., Hogenesch, J.B., Provencio, I., and Kay, S.A. (2002). Melanopsin (Opn4) requirement for normal light-induced circadian phase shifting. Science *298*, 2213–2216.

Parichy, D.M. (2015). Advancing biology through a deeper understanding of zebrafish ecology and evolution. Elife *4*, e05635.

Park, H.-C., Shin, J., and Appel, B. (2004). Spatial and temporal regulation of ventral spinal cord precursor specification by Hedgehog signaling. Development *131*, 5959–5969.

Park, H.-C., Shin, J., Roberts, R.K., and Appel, B. (2007). An olig2 reporter gene marks oligodendrocyte precursors in the postembryonic spinal cord of zebrafish. Dev Dyn *236*, 3402–3407.

Park, W.-M., Wang, Y., Park, S., Denisova, J.V., Fontes, J.D., and Belousov, A.B. (2011). Interplay of chemical neurotransmitters regulates developmental increase in

electrical synapses. J Neurosci *31*, 5909–5920.

Peirson, S.N., Halford, S., and Foster, R.G. (2009). The evolution of irradiance detection: melanopsin and the non-visual opsins. Philos. Trans. R. Soc. Lond., B, Biol. Sci. *364*, 2849–2865.

Penn, A.A., Riquelme, P.A., Feller, M.B., and Shatz, C.J. (1998). Competition in retinogeniculate patterning driven by spontaneous activity. Science *279*, 2108–2112.

Personius, K., Chang, Q., Bittman, K., Panzer, J., and Balice-Gordon, R. (2001). Gap junctional communication among motor and other neurons shapes patterns of neural activity and synaptic connectivity during development. Cell Commun Adhes *8*, 329–333.

Pietri, T., Manalo, E., Ryan, J., Saint-Amant, L., and Washbourne, P. (2009). Glutamate drives the touch response through a rostral loop in the spinal cord of zebrafish embryos. Dev Neurobiol *69*, 780–795.

Pineda, R.H., Svoboda, K.R., Wright, M.A., Taylor, A.D., Novak, A.E., Gamse, J.T., Eisen, J.S., and Ribera, A.B. (2006). Knockdown of Nav1.6a Na+ channels affects zebrafish motoneuron development. Development *133*, 3827–3836.

Plazas, P.V., Nicol, X., and Spitzer, N.C. (2013). Activity-dependent competition regulates motor neuron axon pathfinding via PlexinA3. Proc Natl Acad Sci USA *110*, 1524–1529.

Porter, M.L., Blasic, J.R., Bok, M.J., Cameron, E.G., Pringle, T., Cronin, T.W., and Robinson, P.R. (2012). Shedding new light on opsin evolution. Proc. Biol. Sci. *279*, 3–14.

Portugues, R., and Engert, F. (2009). The neural basis of visual behaviors in the larval zebrafish. Curr Opin Neurobiol *19*, 644–647.

Pozo, K., and Goda, Y. (2010). Unraveling mechanisms of homeostatic synaptic plasticity. Neuron *66*, 337–351.

Rao, S., Chun, C., Fan, J., Kofron, J.M., Yang, M.B., Hegde, R.S., Ferrara, N., Copenhagen, D.R., and Lang, R.A. (2013). A direct and melanopsin-dependent fetal light response regulates mouse eye development. Nature *494*, 243–246.

Reuss, S. (2010). Pineal ribbon synapses: regulated by the gland's central innervation. Neuro Endocrinol. Lett. *31*, 761–765.

Reynolds, A., Brustein, E., Liao, M., Mercado, A., Babilonia, E., Mount, D.B., and Drapeau, P. (2008). Neurogenic role of the depolarizing chloride gradient revealed by global overexpression of KCC2 from the onset of development. J Neurosci *28*, 1588–

1597.

Roeder, K.D., Tozian, L., and Weiant, E.A. (1960). Endogenous nerve activity and behaviour in the mantis and cockroach. Journal of Insect Physiology *4*, 45–62.

Rossi, A., Kontarakis, Z., Gerri, C., Nolte, H., Hölper, S., Krüger, M., and Stainier, D.Y.R. (2015). Genetic compensation induced by deleterious mutations but not gene knockdowns. Nature *524*, 230–233.

Saint-Amant, L., and Drapeau, P. (1998). Time course of the development of motor behaviors in the zebrafish embryo. J Neurobiol *37*, 622–632.

Saint-Amant, L., and Drapeau, P. (2000). Motoneuron activity patterns related to the earliest behavior of the zebrafish embryo. J Neurosci *20*, 3964–3972.

Saint-Amant, L., and Drapeau, P. (2001). Synchronization of an embryonic network of identified spinal interneurons solely by electrical coupling. Neuron *31*, 1035–1046.

Saint-Amant, L. (2006). Development of motor networks in zebrafish embryos. Zebrafish *3*, 173–190.

Saint-Amant, L. (2010). Development of motor rhythms in zebrafish embryos. Prog. Brain Res. *187*, 47–61.

Sato, K., Yamashita, T., Ohuchi, H., and Shichida, Y. (2011). Vertebrate Ancient-Long Opsin Has Molecular Properties Intermediate between Those of Vertebrate and Invertebrate Visual Pigments. Biochemistry *50*, 10484–10490.

Schier, A.F., Neuhauss, S.C., Harvey, M., Malicki, J., Solnica-Krezel, L., Stainier, D.Y., Zwartkruis, F., Abdelilah, S., Stemple, D.L., Rangini, Z., et al. (1996). Mutations affecting the development of the embryonic zebrafish brain. Development *123*, 165–178.

Schmidt, T.M., Chen, S.-K., and Hattar, S. (2011). Intrinsically photosensitive retinal ganglion cells: many subtypes, diverse functions. Trends Neurosci *34*, 572–580.

Selverston, A.I. (2010). Invertebrate central pattern generator circuits. Philos. Trans. R. Soc. Lond., B, Biol. Sci. *365*, 2329–2345.

Sherrington, C.S. (1910). Flexion-reflex of the limb, crossed extension-reflex, and reflex stepping and standing. J Physiol (Lond) *40*, 28–121.

Sherrington, C.S. The Integrative Action of the Nervous System (New Haven, CT: Yale University Press).

Shimamura, T., Hiraki, K., Takahashi, N., Hori, T., Ago, H., Masuda, K., Takio, K., Ishiguro, M., and Miyano, M. (2008). Crystal structure of squid rhodopsin with

intracellularly extended cytoplasmic region. J Biol Chem *283*, 17753–17756.

Silver, R., Witkovsky, P., Horvath, P., Alones, V., Barnstable, C.J., and Lehman, M.N. (1988). Coexpression of opsin- and VIP-like-immunoreactivity in CSF-contacting neurons of the avian brain. Cell Tissue Res *253*, 189–198.

Song, J., Ampatzis, K., Björnfors, E.R., and Manira, El, A. (2016). Motor neurons control locomotor circuit function retrogradely via gap junctions. Nature *529*, 399–402.

Stafford, B.K., Sher, A., Litke, A.M., and Feldheim, D.A. (2009). Spatial-temporal patterns of retinal waves underlying activity-dependent refinement of retinofugal projections. Neuron *64*, 200–212.

Streisinger, G., Walker, C., Dower, N., Knauber, D., and Singer, F. (1981). Production of clones of homozygous diploid zebra fish (Brachydanio rerio). Nature *291*, 293–296.

Takahashi, J.S., and Menaker, M. (1982). Entrainment of the circadian system of the house sparrow: A population of oscillators in pinealectomized birds. J Comp Physiol A *146*, 245–253.

Tarttelin, E.E., Bellingham, J., Hankins, M.W., Foster, R.G., and Lucas, R.J. (2003). Neuropsin (Opn5): a novel opsin identified in mammalian neural tissue. FEBS Lett. *554*, 410–416.

Tian, L., Hires, S.A., Mao, T., Huber, D., Chiappe, M.E., Chalasani, S.H., Petreanu, L., Akerboom, J., McKinney, S.A., Schreiter, E.R., et al. (2009). Imaging neural activity in worms, flies and mice with improved GCaMP calcium indicators. Nat Meth *6*, 875–881.

Todd, K.L., Kristan, W.B., and French, K.A. (2010). Gap junction expression is required for normal chemical synapse formation. J Neurosci *30*, 15277–15285.

Tong, H., and McDearmid, J.R. (2012). Pacemaker and plateau potentials shape output of a developing locomotor network. Curr Biol *22*, 2285–2293.

Turrigiano, G.G., Leslie, K.R., Desai, N.S., Rutherford, L.C., and Nelson, S.B. (1998). Activity-dependent scaling of quantal amplitude in neocortical neurons. Nature *391*, 892–896.

Turrigiano, G. (2012). Homeostatic synaptic plasticity: local and global mechanisms for stabilizing neuronal function. Cold Spring Harb Perspect Biol *4*, a005736.

Turrigiano, G.G., and Nelson, S.B. (2004). Homeostatic plasticity in the developing nervous system. Nat Rev Neurosci *5*, 97–107.

Verselis, V.K., and Srinivas, M. (2013). Connexin channel modulators and their mechanisms of action. Neuropharmacology *75*, 517–524.

Vigh, B., Manzano, M.J., Zádori, A., Frank, C.L., Lukáts, A., Röhlich, P., Szél, A., and Dávid, C. (2002). Nonvisual photoreceptors of the deep brain, pineal organs and retina. Histol. Histopathol. *17*, 555–590.

Vladimirov, N., Mu, Y., Kawashima, T., Bennett, D.V., Yang, C.-T., Looger, L.L., Keller, P.J., Freeman, J., and Ahrens, M.B. (2014). Light-sheet functional imaging in fictively behaving zebrafish. Nat Meth *11*, 883–884.

Wada, Y., Okano, T., Adachi, A., Ebihara, S., and Fukada, Y. (1998). Identification of rhodopsin in the pigeon deep brain. FEBS Lett. *424*, 53–56.

Warp, E., Agarwal, G., Wyart, C., Friedmann, D., Oldfield, C.S., Conner, A., Del Bene, F., Arrenberg, A.B., Baier, H., and Isacoff, E.Y. (2012). Emergence of patterned activity in the developing zebrafish spinal cord. Curr Biol *22*, 93–102.

Weissman, T.A., Riquelme, P.A., Ivic, L., Flint, A.C., and Kriegstein, A.R. (2004). Calcium waves propagate through radial glial cells and modulate proliferation in the developing neocortex. Neuron *43*, 647–661.

Wietek, J., and Prigge, M. (2016). Enhancing Channelrhodopsins: An Overview. Methods Mol. Biol. *1408*, 141–165.

Wilson, D.M. (1961). The central nervous control of flight in a locust. J. Exp. Biol. *38*, 471–490.

Wyart, C., Del Bene, F., Warp, E., Scott, E.K., Trauner, D., Baier, H., and Isacoff, E.Y. (2009). Optogenetic dissection of a behavioural module in the vertebrate spinal cord. Nature *461*, 407–410.

Xiang, Y., Yuan, Q., Vogt, N., Looger, L.L., Jan, L.Y., and Jan, Y.N. (2010). Light-avoidance-mediating photoreceptors tile the Drosophila larval body wall. Nature *468*, 921–926.

Yu, Y.-C., He, S., Chen, S., Fu, Y., Brown, K.N., Yao, X.-H., Ma, J., Gao, K.P., Sosinsky, G.E., Huang, K., et al. (2012). Preferential electrical coupling regulates neocortical lineage-dependent microcircuit assembly. Nature *486*, 113–117.

Zelenchuk, T.A., and Brusés, J.L. (2011). In vivo labeling of zebrafish motor neurons using an mnx1 enhancer and Gal4/UAS. Genesis *49*, 546–554.

Zhang, L.I., Tao, H.W., Holt, C.E., Harris, W.A., and Poo, M. (1998). A critical window for cooperation and competition among developing retinotectal synapses. Nature *395*, 37–44.

Zimmerman, B.L., and Tso, M.O. (1975). Morphologic evidence of photoreceptor differentiation of pinealocytes in the neonatal rat. J. Cell Biol. *66*, 60–75.

Zimmerman, K., and Yoder, B.K. (2015). SnapShot: Sensing and Signaling by Cilia. Cell *161*, 692–2.e1.

Zuker, C.S., Cowman, A.F., and Rubin, G.M. (1985). Isolation and structure of a rhodopsin gene from D. melanogaster. Cell *40*, 851–858.

An essential role for Gα(i2) in Smoothened-stimulated epithelial cell proliferation in the mammary gland.

Appendix A

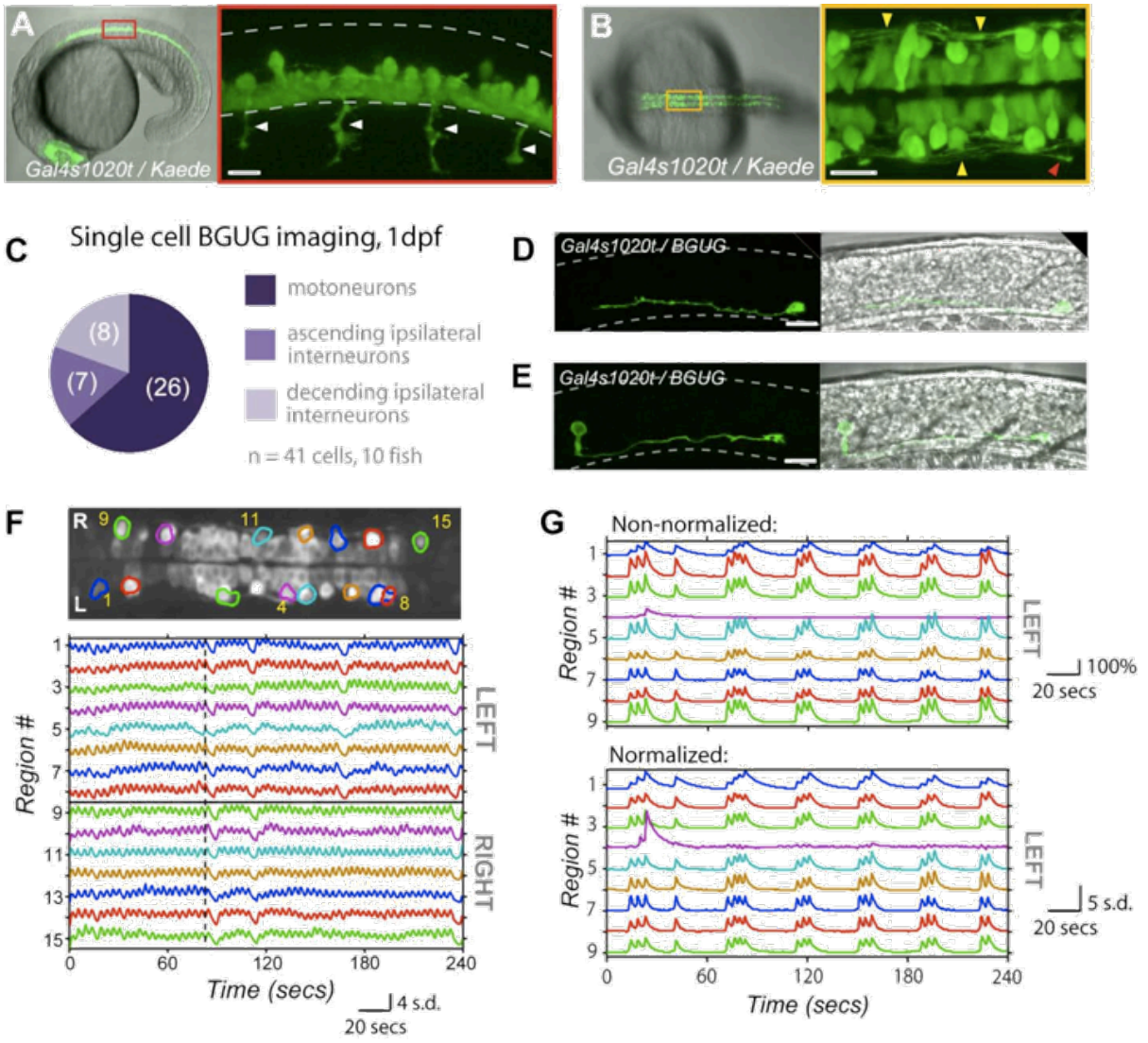

Figure S1. The *Gal4s1020t* Line Targets Ventral Spinal Neurons of the Motor System at 1 dpf which Display Locomotor-Like Patterns of Activity, Related to Figure 1

(A) Lateral view of *Gal4s1020t* expression pattern in a 20 hpf *Gal4s1020t*/*UAS:Kaede* embryo. (*left*) Low magnification showing entire embryo. (*right*) Zoomed view of red boxed area showing the ventral location of cell bodies and motoneuron axons (arrows) extending out of the cord.

(B) Low (*left*) and high magnification (*right*) dorsal views of 20 hpf *Gal4s1020t*/*UAS:Kaede* embryo show lateral processes (yellow arrows) with a descending growth cone in view (red arrow).

(C-E) Using the BGUG transgenic line[1], we stochastically expressed GFP in 1-10% of the *Gal4s1020t* population to identify the morphology of cells targeted at 1 dpf. As

at 5 dpf[2], GFP expression at 1 dpf was found in motoneurons (63%), whose axons can be seen in A (arrows), and ascending ipsilateral interneurons, presumed to be KA interneurons, (17%), an example of which can be seen in (D) at 1 dpf. We also found expression in descending ipsilateral interneurons, presumed to be VeLDs (20%), an example of which (E) shows their characteristic large cell body located in the middle of the cord along the dorsal/ventral axis in a 1 dpf embryo.

(B) GCaMP3 activity in an example embryo at 20.5 hpf. (*top*) Dorsal view of GCaMP3 baseline fluorescence with active regions circled (rostral left; imaged area somites 4-8). (*bottom*) Normalized intensity traces for active regions (identified on the y-axis) for the left and right sides of the cord. This fish shows very short periods of correlated quiescence between the left and right sides, with long sustained bursts alternating between the left and right sides. Dotted vertical line emphasizes alternation, passing through event peaks for left-sided cells and troughs for the right.

(C) Shows nine cells from Fig. 1 before normalization (*top*), where traces are plotted as$\Delta F/F$ (%), and after normalization by zscore (*bottom*), where traces are plotted as standard deviation (s.d.) for comparison. Scale bar=20 μm for B, D, E and F. Dotted lines in A, C and D outline approximate border of spinal cord. Rostral to left.

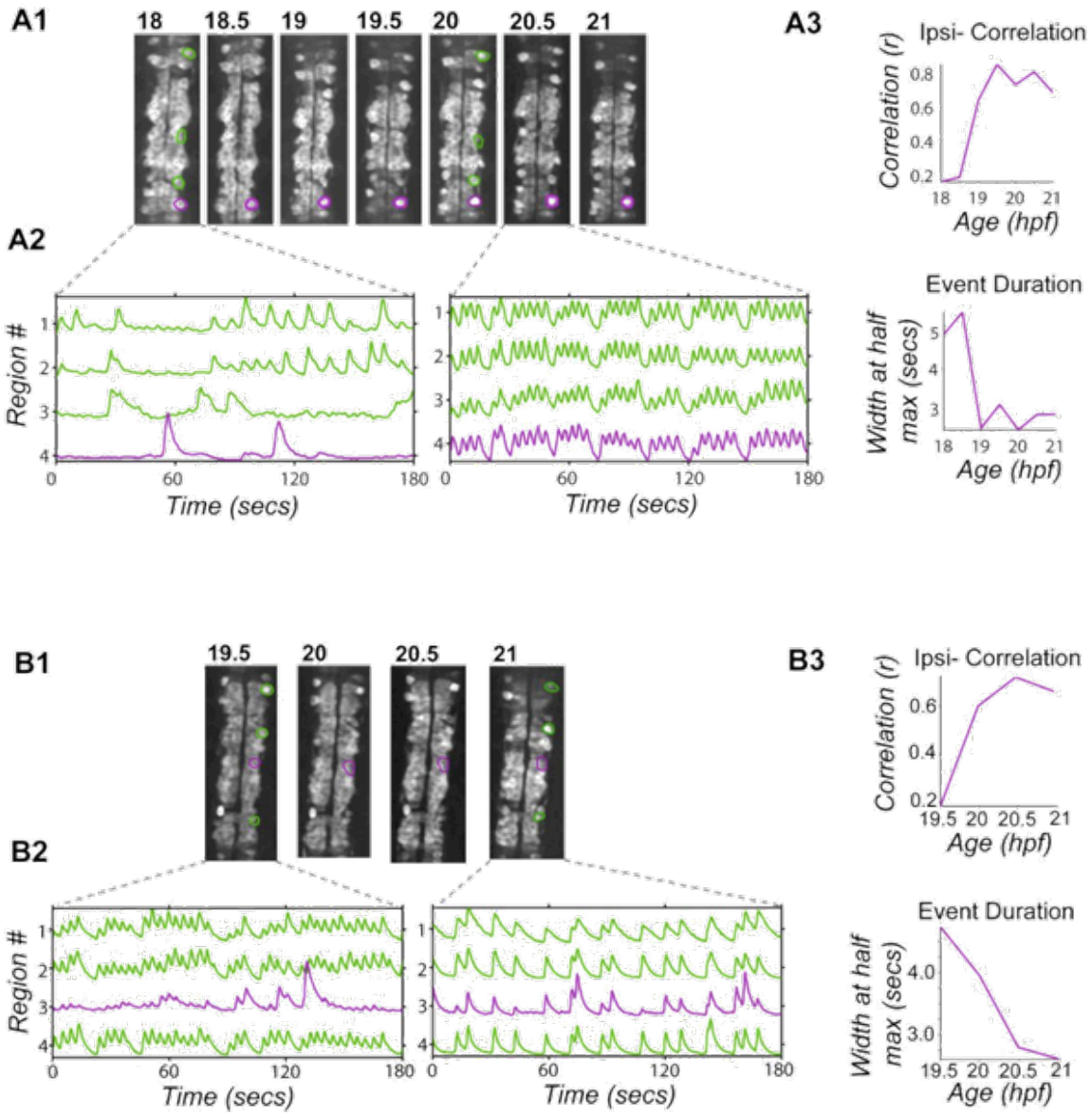

Figure S2. Early and Late Onset Neurons Show Increases in Correlation and Decreases in Event Duration through Development, Related to Figure 2

Single cells with detected activity onset at 18 hpf (A) and 19.5 hpf (B) tracked through consecutive time lapse movies until 21 hpf.

(*1*) Baseline GCaMP3 fluorescence with tracked cells (purple) and other active ipsilateral cells (green) circled.

(*2*) Normalized intensity traces (plotted as standard deviation) for tracked cells (purple) and other active ipsilateral cells (green) showing uncorrelated activity at early time points and correlated activity at later time points.

(*3*) Correlation of tracked cells versus other ipsilateral cells increased through development for both example cells, as seen in the pooled population data (Fig. 2C).

Event duration was calculated as the width at half maximum for the fitted event kernel and decreased for both examples. Rostral, up.

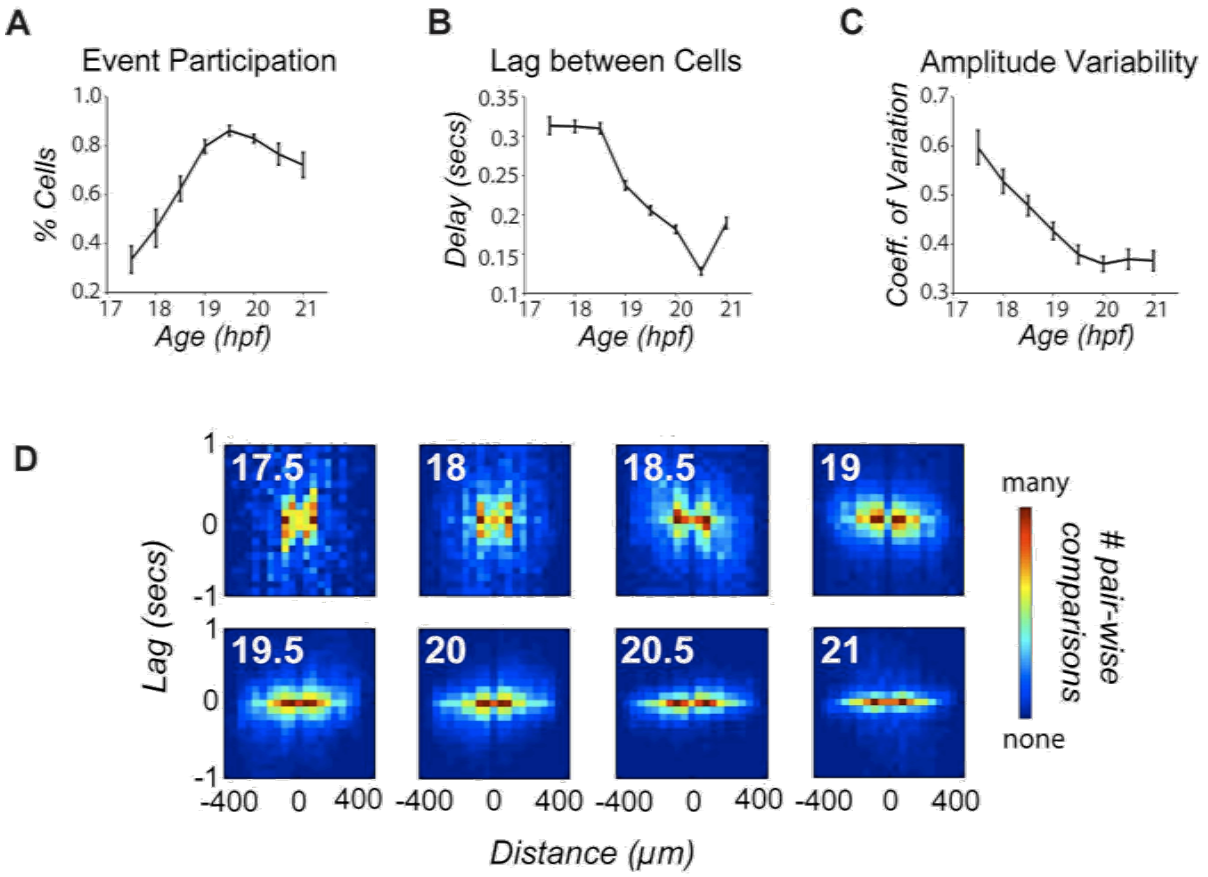

Figure S3. Synchronized Groups Contain More Cells and Are More Accurately Time-Locked at Later Stages in Development, Related to Figure 3

(A) The percentage of active ipsilateral cells in the field of view participating in a synchronous event (defined as having a calcium event within 1 second of an event peak, see *Experimental Procedures*) increases until 19.5 hpf and was significantly different between 18 and 20 hpf (18 hpf, 46 ± 7.6%; 20 hpf, 83 ± 1.7%; P = 0.002, paired Student's *t* test; n = 9 fish).

(B) For cells participating in synchronous events, the temporal lag between event start times between cells decreases until 20.5 hpf, with significant differences between 18 and 20 hpf (18 hpf, 0.31 ± 0.15 sec, n = 385 events; 20 hpf, 0.18 ± 0.09 sec, n = 360 events; $P < 10^{-10}$, unpaired Student's *t* test).

(C) The variability of amplitude, calculated as the coefficient of variation within events from a given cell, decreases from 17.5 to 20 hpf, and was significantly different between 18 and 20 hpf (18 hpf, coefficient of variation = 0.528 ± 0.024, n = 121 cells; 20 hpf, coefficient of variation = 0.360 ± 0.015, n = 189 cells, $P < 10^{-8}$, unpaired Student's *t* test).

(D) Two-dimensional histograms plotting the relative rostral-caudal pair-wise distance between cells in correlated groups against the temporal lag between the same cells (n = 9 fish for 18-21 hpf; n = 4 fish at 17.5 hpf). Individual pixels represent the number

of cell pairs (with high values in red) that were part of a correlated group and had a given distance between them (x-axis) and temporal lag (y-axis). Correlated groups were defined as two or more cells having pair-wise correlation coefficients greater than 0.5. Histogram data was normalized within each age group and ranged from zero to between 36 and 878 pair-wise comparisons. Error bars=s.e.m.

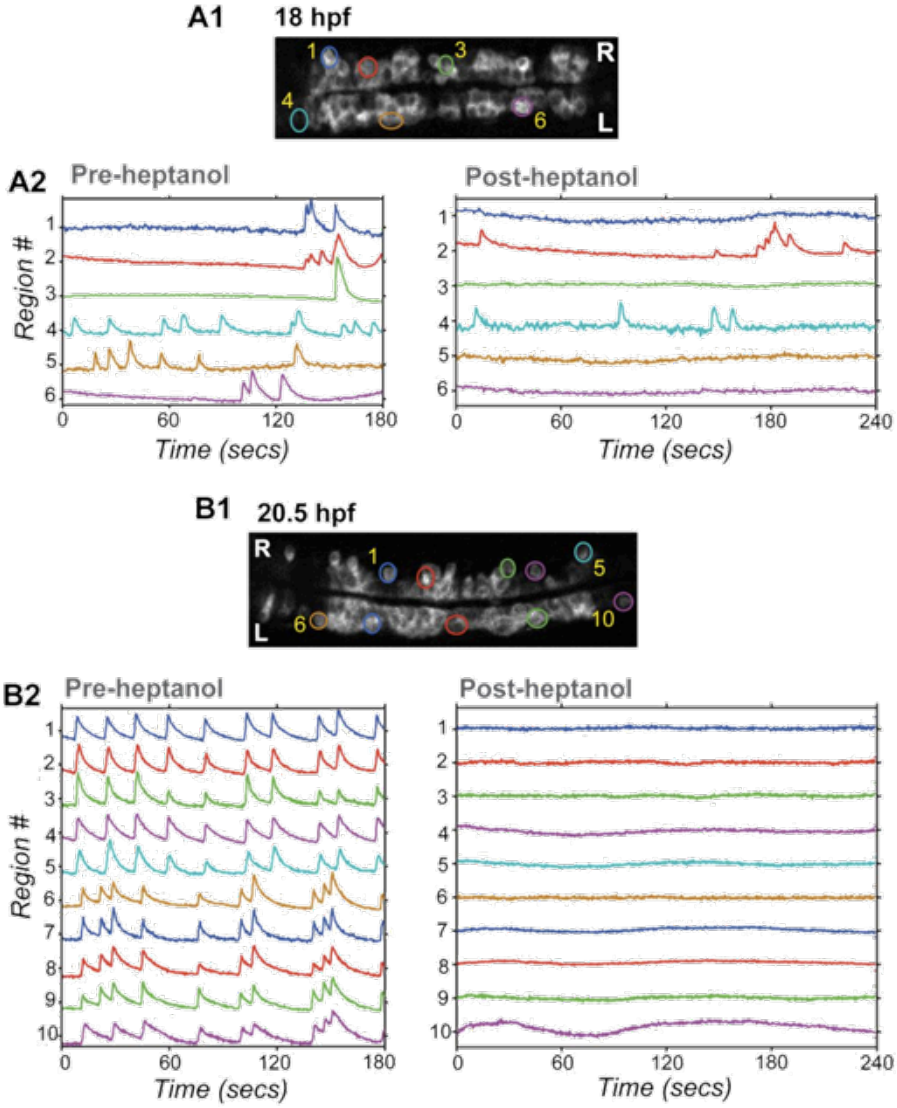

Figure S4. Gap Junction Blocker Heptanol Has Little Effect on Substantial Fraction of Cells in Younger Embryos, But Profoundly Blocks Activity in Older Embryos, Related to Figure 4

GCaMP3 population activity before and after heptanol treatment in an 18 (A) and 20.5 (B) hpf embryo.

(D) Baseline GCaMP3 fluorescence images with cells active in pre-heptanol movies circled.

(E) GCaMP3 intensity traces (ΔF/F) for these regions before (*left*) and after (*right*) 2mM heptanol treatment shows that some cells remained spontaneously active during gap junction block in the younger embryo (A2; cells 2 and 4), but no cells were active after heptanol treatment in the older embryo (B2).

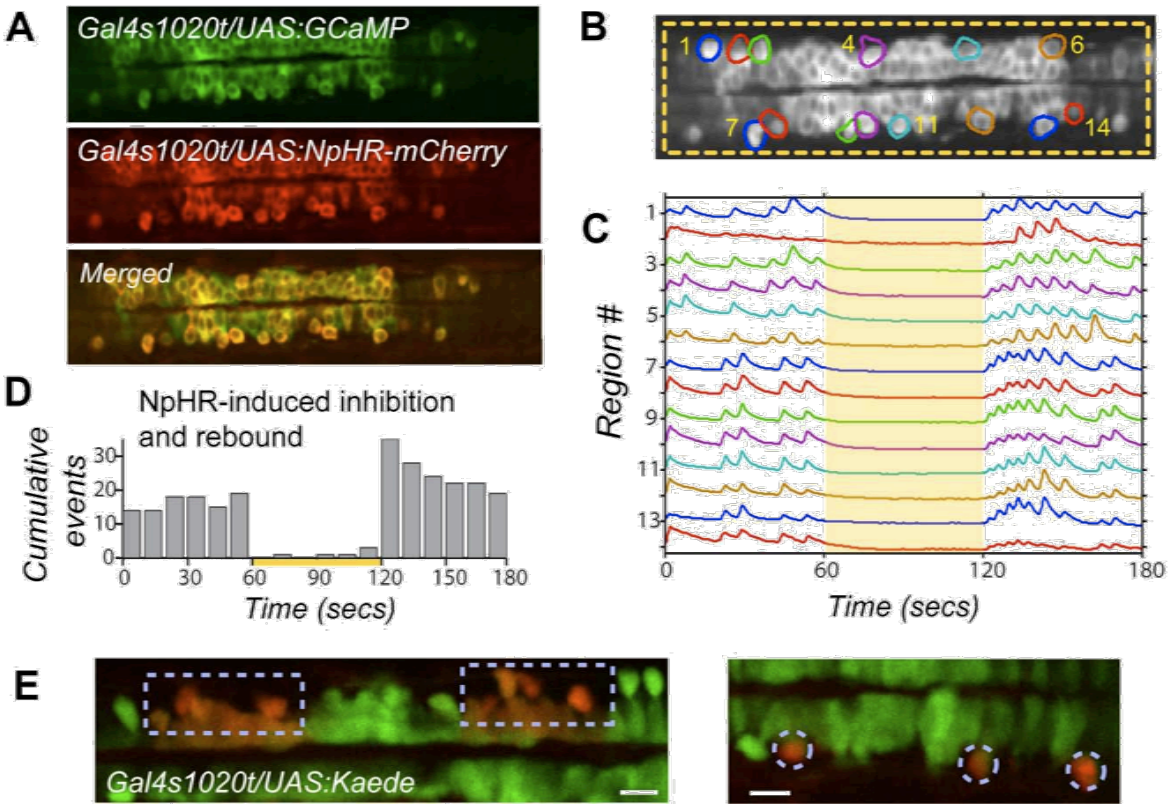

Figure S5. Activation of the Light-Driven Chloride Pump Halorhodopsin Robustly Inhibits Spontaneous Events and Causes Rebound Excitation, Related to Figures 4 and 5

(A) *Gal4s1020t/ UAS:GCaMP3/ UAS:NpHR-mCherry* fish express GCaMP3 and NpHR in the same spinal neurons.

(B) Full field illumination (yellow dashed box) with 19mW/mm^2 593nm light is targeted to NpHR-expressing spinal neurons while simultaneously imaging population activity with GCaMP3.

(C) Spontaneous events in active regions, plotted as standard deviation, are eliminated during application of yellow light (yellow bar) in a 19 hpf fish.

(D) Tallied events across several fish (n=6) shows effective inhibition when yellow light is on (yellow bar) and there is an increase in activity above baseline at light offset.

(E) Accurate light targeting with the digital micro-mirror device is confirmed with the restricted photo-conversion of Kaede. Illumination with blue light (380nm) switches the fluorescence emission of Kaede from green to red[22]. Cells within illuminated region (boxed areas on left, single cells circled on right) convert to red while adjacent cells remain green. Though the wavelength used for NpHR activation is longer (593nm) and may scatter a little differently, we used a similar light power

(15.2mW/mm^2 for Kaede; 19mW/mm^2 for NpHR) and exposure time (1 min). Scale bars=20μm.

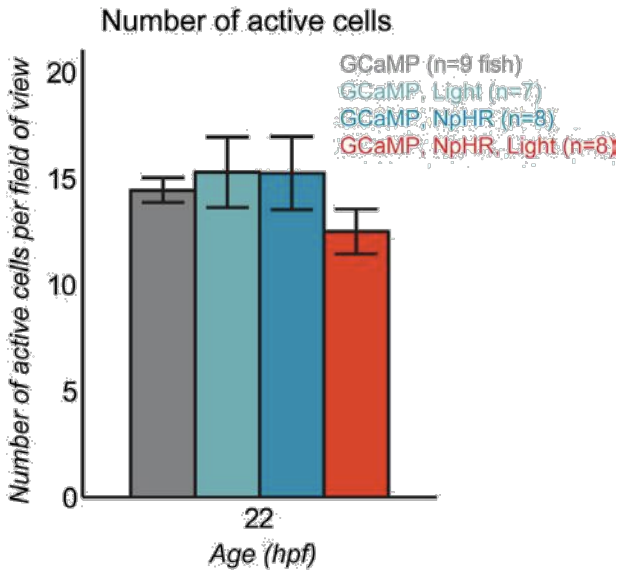

Figure S6. Experimental Fish Expressing NpHR and Receiving One Hour Light Manipulation Have the Same Number of Spontaneously Active Cells as Control Groups, Related to Figure 7

The total number of active cells in the field of view during a 3 minute movies was tallied for experimental fish (GCaMP, NpHR, Light) and the three control groups: i) NpHR-negative fish without yellow/blue light (GCaMP), ii) NpHR-negative fish with yellow/blue light (GCaMP, Light), and iii) NpHR-positive fish without yellow/blue light (GCaMP, NpHR). There was no significant difference between the four groups at 22 hpf (one- way ANOVA, P=0.40), though we did see a slight reduction in the number of cells in GCaMP, NpHR, Light fish. This reduction could be accounted for by the relatively lower frequency of long duration, uncorrelated events, making cells with these events less probable to detect. Bars=s.e.m.

Supplemental Experimental Procedures

Embryo Preparation and GCaMP Imaging

Embryos of the Tubingen genetic background were raised in E3 embryo medium at 28.5ºC until 60% epiboly, and at 25ºC thereafter to delay development for experimentation. GCaMP positive progeny of *UAS:GCaMP3* and *Gal4s1020t* fish were mounted in 1.4% agar and paralyzed with
injections of 750μg/ml $\propto$-bungarotoxin (Invitrogen) into the tail once before imaging (at 17-17.5 hpf). Embryos were aged by somite counting and were in a 28.5ºC heated chamber for time-lapse experiments (including NpHR rebound experiments, Fig. 5) so that they could develop at a normal rate. NpHR functional connectivity experiments (Fig. 4, 5) were performed at room temperature. Morphology images of *UAS:Kaede/ Gal4s1020t* fish were taken on a Zeiss 510 Meta confocal microscope. Functional imaging was performed on a 3i Marianas system (Intelligent Imaging Innovations) with a spinning disk confocal (Yokagawa) mounted on a Zeiss microscope and using a 488nm laser and 20x water- immersion objective (numerical aperture = 1.0). For time-lapse experiments, 4 minute movies were acquired every half hour at 4 Hz. Imaging was acquired at 2 Hz for all NpHR experiments to reduce potential activation of NpHR by imaging light.

Photomanipulation of Activity

Photostimulation of NpHR and Kaede was accomplished through a digital micro- mirror device (DMD) illumination system (Photonic Instruments) coupled to the imaging microscope. Activating light was provided by a Xenon lamp (Sutter Instruments) filtered to 573-613nm and was 19mW/mm^2 at the sample. Spatial and temporal control of the yellow light was achieved through integration software (Intelligent Imaging Innovations). NpHR experiments were performed on *UAS:NpHR-mCherry/ UAS:GCaMP3/ Gal4s1020t* fish displaying both red and green fluorescence. For functional connectivity experiments (Fig. 4), the experimental protocol consisted of 1 minute NpHR activation with yellow light to the targeted region (e.g. single cell, two somite section or two somite-sized light control off of cord) followed by 1 minute of rest while calcium activity was simultaneously imaged at 2 Hz. Experimental epochs were preceded and followed by 2 minute baseline periods for frequency normalization of individual cells. Single cell manipulations were restricted to CaP primary motoneurons for consistency. For bilateral rebound excitation experiments (Fig. 5), light was applied in 15 second intervals with 15 seconds of rest in between and repeated four times per embryo per time point. For chronic manipulation of activity (Fig. 6A), 9.5 seconds of 19mW/mm^2 593 nm light alternated with 500 msec of yellow/blue light using a double bandpass filter for 410 nm and 568 nm to provide continuous yellow light illumination and pulses of blue light for re-sensitization of NpHR. GCaMP3 movies were taken during light manipulation to test effectiveness of inhibition.

Analysis of Calcium Imaging Movies

All analysis for time-lapse and NpHR experiments was performed using Matlab (Mathworks).

ROI and Time-Course Extraction

Drift during image acquisition was corrected using the DIPimage package (www.diplib.org) for all time-lapse and NpHR movies. The CellSort toolbox[3] was used to automatically detect active cell bodies, identified as contiguous pixel islands, each with a distinctive time course response. ROIs that were redundant (i.e. corresponding to the same cell) were manually merged; ROIs corresponding to axons or moving cells were manually removed. Traces plotted in Figs. 1, 4 and 7 and Figs. S1F, S2 and S5 were normalized by taking the zscore of the ΔF/F values (plots display these standard deviation values) to best visualize event contours in all cells. All other traces shown are ΔF/F. See *Fig. S1G* for a comparison of traces pre- and post-normalization.

Event Detection and Characterization

Each intensity trace was scanned for instances when the rise in fluorescence over a 1-s interval exceeded an empirically determined threshold. The resulting estimated timing and amplitudes of the events were used to initialize a parameterized model of the trace, which was subsequently refined using a nonlinear, least -squares fitting algorithm (*lsqnonlin*, Matlab) . The model consisted of three components: a cubic spline that accounted for any slow drifts in baseline; a double exponential kernel to match each cell's unique, stereotyped calcium transient (Fig. 1B, E); and the timing and amplitude of each event detected as described above. The convergence of the resulting fits was manually verified. Events were identified as spurious if the estimated magnitude was exceeded by its confidence interval. The amplitudes and timings of all remaining events encoded the time course of a cell's activity (Fig 1C, F) and were used for all subsequent analysis.

Characterization of Synchronous Events

To identify time-coupled events in a given movie, binary traces encoding the occurrence of events in all cells were filtered with a 2-second wide Gaussian window and summed. Peaks in the resulting trace that exceeded an empirically-determined threshold were marked as "synchronous" events. Cells were identified as participating in an event when they were active within 1 second of a peak (in other words, synchrony allowed for a little temporal jitter between cells). For these time-coupled cells, lag times between when a particular cell was active and the event peak were determined. The response amplitudes of *n* cells during *m* population events (0 if a cell was inactive during the event) were compiled into an *n* x *m* matrix. This was used to calculate an *n* x *n* correlation matrix, resulting in correlations across events (Figs. 2C, 3, 6C and for *Figs. S2 and S3*). In contrast, the correlations presented in Fig. 2A, B were calculated for the entire activity trace, using the idealized traces filtered with a 1-second wide Gaussian. To identify correlated ensembles of cells within a network for Fig. 3 and *Fig. S3*, cell pairs were marked as belonging to the

same group if their correlation across synchronous events was greater than 0.2 for Fig. 3 or 0.5 for *Fig. S3*. Separate groups were then identified using the *components* function within the Matlab mesh partitioning toolbox[4].

NpHR Experiments

For the analysis of NpHR functional connectivity experiments, frequency in the first 30 s after yellow light on and off was compared to average frequency for pre- and post-experiment baseline epochs in paired Student's t tests. For NpHR rebound bilateral excitation experiments, synchronous events were determined as described above and left/right lag was determined by calculating the temporal difference between the first synchronous event (two or more cells) on the left versus the right side of the cord after light offset. Ipsilateral correlation for Fig. 6C was calculated as in Fig. 2C.

Statistical Analysis

For chronic Halorhodopsin experiments, the effect of group (GCaMP, GCaMP/Light, GCaMP/NpHR, and GCaMP,NpHR,Light) on frequency x amplitude (Fig. 6B), mean correlation (Fig. 6C), mean event width (Fig. 7C), mean cell distance to midline (Fig. 7D), and number of active cells (*Fig. S6*) was tested with one-way ANOVAs at each time point. Time points with significant effects of group ($p<0.05$) were further analyzed with a post-hoc comparison test with Bonferroni correction (at alpha = 0.05 and 0.01) to identify which group pairs were significantly different from one another. For all other analyses, statistical significance between mean data was calculated using the unpaired and paired two-tailed Student's *t* test.

Supplemental References

(C) Scott, E.K. *et al.* (2007) Targeting neural circuitry in zebrafish using GAL4 enhancer trapping. *Nat. Methods*, 4:323-326.

(D) Wyart, C. et al. (2009) Optogenetic dissection of a behavioural module in the vertebrate spinal cord. *Nature,* 461:407-410.

(E) Mukamel, E.A., Nimmerjahn, A. & Schnitzer, M.J. (2009) Automated analysis of cellular signals from large-scale calcium imaging data. *Neuron,* 63:747-760.

(F) Gilbert, J., Miller, G. & Shang-Hua Teng. (1995) Geometric mesh partitioning: implementation and experiments. *Parallel Processing Symposium, 1995. Proceedings., 9th International* 418-427.

Appendix B

Supplemental Experimental Procedures

Embryo collection and behavior

All animal care and experiments were in accordance with the University of California at Berkeley Animal Care and Use Committee guidelines. Embryos were collected in E3 embryo medium and raised at 28.5° C at least until 60% epiboly after which some fish were lowered to 25° C in order to delay development for proper timing of experiments. All coiling behavior experiments used wiltype AB embryos between 22 and 25 hours post fertilization (hpf) unless otherwise noted. Individual fish were loaded into single wells of a clear bottomed 384-well plate and positioned above two LED arrays (940 nm and 508 nm, Mouser) [S2]. Green light stimulus was measured to be 13.2 $\mu W/mm^2$ (PM100D, SF150C, THOR Labs). Fish were dark adapted for 10 minutes before starting each experiment and videos began >10 minutes apart unless otherwise noted. Video was collected through a 650 nm longpass IR filter (Edmund Optics) at 10 frames per second with a Fire-I 980b camera (Unibrain). Coiling behavior for each fish was analyzed by calculating the number of pixels changing in value (above background) between frames of the movie. Wavelength testing was accomplished using a polychrome V (Till Photonics) with a configurable exit aperture to modulate intensity. Fitted curve and λ_{max} were calculated using a universal template for visual pigment absorbance [S3]. Stimuli, video synchronization, and behavioral analysis were coordinated with MATLAB software.

Transgenic fish

The GCaMP5 open reading frame was PCR amplified using the primers 5'-ATATATGGAT CCTCACGTTA CTAGTATGGG TTCTC-3' and 5'-ATATATGCGG CCGCTCACAA AGATCCTCTA GACTTCG-3' and inserted into the BamHI and NotI sites in the Tol2 Kit Gateway PME-MCS plasmid [S4]. This middle element was combined with a 5' element containing a 10x UAS repeat, a 3' element containing the SV40 polyadenalation sequence, and the destination vector pDestTol2pA2. The resulting plasmid was injected into single cell stage embryos at a concentration of 25 ng/μl along with RNA for the Tol2 transposase at a concentration of 25 ng/μl and phenol red for visualization. Embryos with strong expression were raised and screened for transmission of the gene. One founder was selected and crossed to the transgenic line *Et(–0.6hsp70l:Gal4-VP16)s1020t* (a.k.a. *Gal4s1020t*) and the resulting embryos carrying both genes raised to adults.

GCaMP imaging and analysis

Fish expressing GCaMP5 were mounted in 1.4% agarose and paralyzed with a tail injection of 0.7 mg/ml α-bungarotoxin (Invitrogen). Embryo age was determined by somite counting and embryos were contained in a heated chamber (28.5° C) (Warner Instruments) for the duration of the timelapse experiments. All other

experiments were conducted at room temperature using 24-26 hpf embryos. Calcium imaging was performed using a Zeiss Axio Examiner Z1 upright LSM 780 microscope with either a Spectra Physics/Newport MaiTai HP (920 nm, 180 fs pulse width) infrared laser or an argon laser (488 nm). Signal was collected using a 20x 1.0 NA W Plan Apo water dipping objective (Carl Zeiss) and a transmitted photomultiplier tube or a GaAsP detector. Argon and helium lasers and an ultraviolet diode were used for photic stimulation with reported laser powers measured at the sample location (PM100D, SF150C, THOR Labs). Stimulation consisted of 10 scans of the imaging area (500 msec/scan, pixel dwell time = 3.15 μsec, 2.9 mW/pixel for 561 nm stimulations). Embryos were dark adapted for >8 minutes before each movie. Control of the microscope and lasers was accomplished using Zen (2010) software. All imaging was performed at 2 Hz to reduce the potential for heating by the infrared laser. Movie analysis and peak detection were accomplished using ImageJ and MATLAB (Mathworks) software. ROI detection, event detection and characterization, and subsequent analyses were performed as previously outlined [S5].

Chronic Illumination

Embryos were prepared as in the GCaMP timelapse experiments. Starting at 17.5-18 hpf, paralyzed embryos were held in a heated stage (Warner Instruments) at 28.5° C above the 508 nm LED array as described in the behavioral experiments. Simultaneously, movies were recorded as described in the timelapse experiments with additional paralyzed sibling dark-adapted embryos, at 18 hpf and also in a heated stage. After two hours of steady illumination, movies were recorded from all fish in the dark until 22 hpf. Analysis of imaging, correlations, and event widths were as described previously [S5].

FACS and RNASeq

In order to increase sample size, embryos from crosses between 1020:Gal4$^+$ animals and transgenic lines carrying mCherry, YFP, GCaMP, and Kaede reporters were grouped together. Eggs were temperature staged to group individuals at 20 hpf. The following protocol was based on previous work [S6]. Embryos were dechorionated and tails were dissected free at the level of the third somite (± a small margin of error) and kept in Ringer's on ice. In total, 151 tails from 1020:Gal4$^+$ embryos and 85 tails from HuC:Gal4$^+$ embryos were used. Tails were transferred into 1.2 ml of protease solution containing 0.25% trypsin, 1 mM EDTA pH 8.0, and 2.7 mg collagenase type II (from a 100 mg/ml stock in HBSS) in 1x PBS and incubated at 28.5° C for 15 minutes. Protease activity was stopped with 0.2 ml solution containing 30% calf serum and 6 mM $CaCl_2$ in 1x PBS. Cells were manually triturated to dissociate tissue and gently pelleted at 4° C. Cells were washed once with 0.35 ml chilled suspension media containing 1% calf serum, 0.8 mM $CaCl_2$, 50 U/ml penicillin, and 0.05 mg/ml streptomycin in DMEM without phenol red. After pelleting the cells and removing the wash, the samples were resuspended in a total volume of 800 μl of suspension media and passed through a 40 μm cell strainer. Maximum time allowed from the first dissection to the start of sorting was two hours. With the UC Berkeley

Flow Cytometry Core, cells were sorted using a Beckman-Coulter MoFlo High Speed Sorter equipped with Innova I-70 and Innova I-90 lasers (Coherent). Samples were gated on the forward scatter and side scatter dot plot to select the probable cellular fraction and subgated on fluorescence in the red and green channels. Fluorescent positive and negative populations were sorted and collected into 1 ml Trizol and stored at -80° C. Approximately 31,000 cells from 1020:Gal4^{+} embryos and 78,000 cells from HuC:Gal4^{+} embryos were used for RNA isolation.

With the UC Berkeley Functional Genomics Laboratory, total RNA was extracted and quality checked with a Bioanalyzer 2100 (Agilent). Samples were poly(A)+ selected using oligo(dT)25 magnetic beads (Life Technologies). cDNA libraries were prepared using PrepX SPIA RNA-Seq and ILM DNA Library kits (IntegenX, Inc.). Quality control was again conducted with a Bioanalyzer 2100 (Agilent) before sequencing with an Illumina HiSeq 2000. Positive and negative FACS-purified samples were all sequenced yielding 28-48 million 100 bp paired-end reads per library. Reads were mapped to the zebrafish genome version Zv9 [S7] (downloaded from the University of California, Santa Cruz) using TopHat v1.4.0. Reads were joined into transcripts using Cufflinks v2.1.1 to generate fragments per kilobase of transcript per million mapped reads (FPKM) values. Transcripts were compared between samples using Cuffdiff and the Zv9 reference genome [S8]. The top 300 genes, as ranked by the false discovery rate adjusted p-value were selected for further analysis.

Morpholino and rescue

The splice-blocking morpholino against VALopA (TTTGTGAAGA CCTTTCTGAG TTTGC) [S9] and the scrambled control morpholino (CCTTTTATAC AGTTCTTACC TACAA) (GeneTools) were injected into single cell eggs at a concentration of 0.5 mM in a volume of 1 nl containing phenol red to visualize the injection. The rescue construct was made by subcloning the VALopA (AB035276) coding region from pcDNA3.1 [S10] with the primers 5'-CATGGCGCGC CACCATGGA GGCGTCCTC CGCGGCC-3' and 5'-GACACGCGT TTACATGGG ACACACTTT GTTCTC-3' into the AscI and MluI sites of a modified pDestTol2pA2 vector containing a 10x UAS promoter and SV40 polyA [S4]. The mCeurlean coding region and a BGH polyA were PCR amplified together and an e1b region with a Kozak sequence were added next to the mCeurlean start codon. The primers used to amplify were 5'-TCCACACGAA TTCCTGCCAC CATGGTGAGC AAGGGCGAGG AG-3' and 5'-TCAATCGATC CATAGAGCCC ACCGCATCCC CAGCATGCCT GCTATTG-3' and e1b added with the primer 5'-AAAATCGATT CGACTCTAGA GGGTATATAA TGGATCCCAT CGCGTCTCAG CCTCACTTTG AGCTCCTCCA CACGAATTC-3'. The resulting PCR product was inserted into pDestTol2pA2 in the 3' to 5' direction at the ClaI site on the 5' side of the UAS promoter [S11]. For rescue experiments, the morpholino against VALopA at 0.5mM was co-injected with the rescue construct at 12.5 ng/μl at the single cell stage. Embryos were staged at 25° C overnight and behavior was assayed between 22-24 hpf. Embryos were removed individually from each well, dechorionated, and mounted in 2% agar. Images were

collected through a 5x air objective on the same microscope used for GCaMP experiments, using identical settings for each image. Fluorescence was quantified as the total sum of pixel intensities within the spinal cord above background and was then grouped into low, intermediate, and high bins with evenly spaced thresholds.

cDNA constructs and oocyte electrophysiology

The cDNAs used in this study were obtained or prepared using standard PCR-based procedures. Clones were inserted into high expression oocyte vectors containing 5'- and 3'-untranslated sequences of *Xenopus* β-globin: pGEM-HE, or its derivative pGEM-HJ. Rat GIRK1 (U01071), mouse GIRK2–1 (U11859), human $G\alpha_{i3}$ (J03198), human muscarinic-2 receptor (m2R) (X15264), *Danio rerio* VALopA (AB035276) and the catalytic subunit of pertussis toxin, (PTX-S1) (M13223), were used for mRNA production for oocyte expression and as the basis for modifications. GIRK1 fused to CFP at the C-terminus ($GIRK1_{CFP}$) [S12], GIRK2, and $G\alpha_{i3}$ in pGEM-HJ, were kindly provided by Nathan Dascal, Tel Aviv University. PTX-S1 in pGEM-HE was kindly provided by Eitan Reuveny, Weizmann Institute, Israel.

In $GIRK1_{CFP}$, we have replaced the CFP, located between XbaI and HindIII restriction sites, with mCherry ($GIRK_{mCherry}$). VALopA was subcloned into pGEM-HE between restriction sites BamHI and XbaI and fused to a C- terminal GFP ($VALopA_{GFP}$). Pertussis-toxin (PTX)-insensitive $G\alpha_{i3}$ was created using PCR, by mutating the cysteine at position 351 (4th position from the C-terminus) to isoleucine, C351I [S12].

Xenopus oocytes were prepared and injected with RNA, as described previously [S13]. Briefly, linearized cDNA-containing vectors were used to transcribe cRNA in vitro using the appropriate RNA polymerase, as described by the manufacturer (mMessage mMachine, Ambion, Austin, TX, USA). All oocytes were injected with 50 nl cRNAs for GIRK1 (1.0 ng), GIRK2 (1.0 ng), m2R (0.5 ng), VALopA (1-2.0 ng), PTX-S1 (0.2 ng) and $G\alpha_{i3}$ (*wt* and C351I) (0.5 ng). Cells were then incubated in ND96 (in mM): 96 NaCl, 2 KCl, 1.8 $CaCl_2$, 1 $MgCl_2$, 50 mg/ml gentamicin, 2.5 Na^+-pyruvate, and 5 HEPES, pH 7.6 at 18-20° C for 3-4 days.

A Nikon Diaphot inverted microscope with a 20x 0.75 NA fluorescence objective (Nikon) was used with a Dagan CA-1 amplifier (Dagan Corporation), illuminated with a 150 W Xenon lamp. Excitation light was filtered through HQ:TRITC excitation filter (535/50 nm, Chroma Technology). Whole-cell currents were measured using standard two-electrode voltage clamp procedures at RT [S14]. During the recordings, cells were constantly perfused with ND96 (low K^+) solution and quickly switched to a high K^+ solution (24 mM K^+, isotonically replacing NaCl in ND96, as described previously [S15]) to reveal the channel's basal activity. Then, receptor-dependent evoked currents were induced by applying 10 μM acetylcholine (for m2R) or light (for VALopA), while the cells were exposed to the high K^+ solution. To block the channel, 5 mM Ba^{2+} in high K^+ was used.

Statistical analysis

Results are shown as mean ± s.e.m. Multiple group comparison was performed using one-way analysis of variance (ANOVA) followed by Tukey or

Dunnett pairwise analysis and two group comparisons were done using two-tailed *t* test or paired *t* test, when applicable (MATLAB 2010 and SigmaPlot 2011). In instances where individual measurements >3 s.d. from the mean were excluded, no more than 3 data points were removed from each independent group. Correlations between two parameters were examined using Spearman test. Asterisks indicate statistically significant differences as follows, adjusted p-values used when applicable: * $p < 0.05$; ** $p < 0.01$; *** $p < 0.001$.

Supplemental References

S1. Peleg, S., Varon, D., Ivanina, T., Dessauer, C. W., and Dascal, N. (2002). G(alpha)(i) controls the gating of the G protein-activated K(+) channel, GIRK. Neuron *33*, 87–99.

S2. Levitz, J., Pantoja, C., Gaub, B., Janovjak, H., Reiner, A., Hoagland, A., Schoppik, D., Kane, B., Stawski, P., Schier, A. F., et al. (2013). Optical control of metabotropic glutamate receptors. Nat Neurosci *16*, 507–516.

S3. Govardovskii, V. I., Fyhrquist, N., Reuter, T., Kuzmin, D. G., and Donner, K. (2000). In search of the visual pigment template. Vis. Neurosci. *17*, 509–528.

S4. Kwan, K. M., Fujimoto, E., Grabher, C., Mangum, B. D., Hardy, M. E., Campbell, D. S., Parant, J. M., Yost, H. J., Kanki, J. P., and Chien, C.-B. (2007). The Tol2kit: a multisite gateway-based construction kit for Tol2 transposon transgenesis constructs. Dev Dyn *236*, 3088–3099.

S5. Warp, E., Agarwal, G., Wyart, C., Friedmann, D., Oldfield, C. S., Conner, A., Del Bene, F., Arrenberg, A. B., Baier, H., and Isacoff, E. Y. (2012). Emergence of patterned activity in the developing zebrafish spinal cord. Curr Biol *22*, 93–102.

S6. Ferreira, T., Wilson, S. R., Choi, Y. G., Risso, D., Dudoit, S., Speed, T. P., and Ngai, J. (2014). Silencing of odorant receptor genes by G protein βγ signaling ensures the expression of one odorant receptor per olfactory sensory neuron. Neuron *81*, 847–859.

S7. Flicek, P., Amode, M. R., Barrell, D., Beal, K., Brent, S., Carvalho-Silva, D., Clapham, P., Coates, G., Fairley, S., Fitzgerald, S., et al. (2011). Ensembl 2012. Nucleic Acids Research *40*, D84–D90.

S8. Trapnell, C., Roberts, A., Goff, L., Pertea, G., Kim, D., Kelley, D. R., Pimentel, H., Salzberg, S. L., Rinn, J. L., and Pachter, L. (2012). Differential gene and transcript expression analysis of RNA-seq experiments with TopHat and Cufflinks. Nat Protoc *7*, 562–578.

S9. Kokel, D., Dunn, T. W., Ahrens, M. B., Alshut, R., Cheung, C. Y. J., Saint-Amant, L., Bruni, G., Mateus, R., van Ham, T. J., Shiraki, T., et al. (2013). Identification of nonvisual photomotor response cells in the vertebrate hindbrain. J Neurosci *33*, 3834–3843.

S10. Kojima, D., Torii, M., Fukada, Y., and Dowling, J. E. (2008). Differential expression of duplicated VAL-opsin genes in the developing zebrafish. J Neurochem *104*, 1364–1371.

S11. Paquet, D., Bhat, R., Sydow, A., Mandelkow, E.-M., Berg, S., Hellberg, S.,

Fälting, J., Distel, M., Köster, R. W., Schmid, B., et al. (2009). A zebrafish model of tauopathy allows in vivo imaging of neuronal cell death and drug evaluation. J. Clin. Invest. *119*, 1382–1395.

S12. Berlin, S., Tsemakhovich, V. A., Castel, R., Ivanina, T., Dessauer, C. W., Keren-Raifman, T., and Dascal, N. (2011). Two distinct aspects of coupling between Gα(i) protein and G protein-activated K+ channel (GIRK) revealed by fluorescently labeled Gα(i3) protein subunits. Journal of Biological Chemistry *286*, 33223–33235.

S13. Kohout, S. C., Bell, S. C., Liu, L., Xu, Q., Minor, D. L., and Isacoff, E. Y. (2010). Electrochemical coupling in the voltage-dependent phosphatase Ci-VSP. Nat. Chem. Biol. *6*, 369–375.

S14. Dascal, N. (2001). Voltage clamp recordings from Xenopus oocytes. Curr Protoc Neurosci *Chapter 6*, Unit 6.12.

S15. Berlin, S., Keren-Raifman, T., Castel, R., Rubinstein, M., Dessauer, C. W., Ivanina, T., and Dascal, N. (2010). G alpha(i) and G betagamma jointly regulate the conformations of a G betagamma effector, the neuronal G protein-activated K+ channel (GIRK). Journal of Biological Chemistry *285*, 6179–6185.